

This manuscript is a non-peer reviewed preprint submitted to EarthArXiv

Estimating Stability Constants and Entropy for Reactions Between Aqueous Metal Ions and Monovalent Oxygen-Bearing Ligands: Applications to Hydrothermal Metal-Organic Acid Systems

Apar Prasad^{1*}, Everett L. Shock^{1,2}

¹School of Molecular Sciences

²School of Earth and Space Exploration

*Corresponding author: Apar Prasad (aprasal1@asu.edu)

Arizona State University

551 E University Drive

Tempe, AZ 85281, USA

Abstract- Linear free energy relations were obtained from existing experimental data and used to estimate stability constants for over 16,000 metal complexes with monovalent oxygen-bearing ligands comprising 75 metal species and 220 ligands. Similar relationships for metal-ligand entropy of association were also obtained which facilitate computation of stability constants from 0 to 125°C for over 6000 metal-ligand complexes. Our inventory for monovalent oxygen-bearing ligands includes carboxylic acids, phenols, alkyl alcohols, substituted alcohols and inorganic ligands with a special emphasis on geobiologically prevalent ligands like lactate, pyruvate, ascorbate and borate. Methods were also devised to estimate metal-ligand stability constants and complexation entropy if only the pK_a of the ligand were known. The slopes and intercepts of these linear free energy relations can be explained by ligand denticity and metal ionic radius, as well as inductive and steric effects, thus providing chemical foundations for these estimation strategies. The stability constant estimates derived from this work were applied to model the speciation of metals and hexanoic acid in two hypothetical hydrothermal mixing fluids representative of the Rainbow and Lau vent fields. This enabled prediction of the distribution of biologically relevant chemical species across key state variables of the chemical system, including temperature, pH, and chemical composition when no stability constant information is available. We further explore the implications of these findings in the areas of metal transport in terrestrial and extra-terrestrial aqueous systems, deep-sea biology, origin and evolution of life, and environmental chemistry and biology.

Keywords- Thermodynamics, aqueous chemistry, metal ions, ligands, metal-ligand complexes, organic, inorganic, carboxylic acids, phenols, alcohols, equilibrium constant, stability constant, extropy, complexation reaction, linear free energy relationships, pK_a, periodic table, van't Hoff

equation, metal speciation, metal bioavailability, hydrothermal systems, hexanoic acid, siderophore, petrobactin, metal transport, organic transport, deep-sea biology, origin and evolution of life, environmental chemistry, environmental biology, mathematical modeling

1. Introduction

From the naturally occurring lactic acid to the artificially synthesized epilepsy drug valproic acid, low molecular mass ligands are integral parts of modern biochemistry, environmental geochemistry, and geobiology. Similarly, many metal ions like calcium, iron, copper and zinc are integral to the functioning of cellular processes while others like cadmium and lead can be toxic even at low concentrations. Almost all organic ligands bond with metal ions via their oxygen, nitrogen or S atoms affecting bioavailability through metal speciation, which is a direct function of metal-ligand thermodynamic properties. However, the thermodynamic measurements for such complexes are far from complete and in order to better understand metal bioavailability, there is a pressing need for alternatives to protracted experimental measurements that may be expensive and time-consuming. This motivated us to estimate stability constants (log K_{ML}) and standard entropy changes (ΔS°_{ML}) at 25°C and 1 bar for metal complexation reactions with monovalent oxygen-bearing (O⁻) ligands. These estimates facilitate metal speciation calculations for systems like microbial growth media and all aqueous geochemical and geobiological systems at the biologically relevant temperature range up to 125°C.

The highly electronegative nature of oxygen predisposes it to take up the negative charge on the ligand following the loss of a proton akin to a weak acid or strong alcohol. We have focused on monovalent oxygen ligands here as such molecules are generally seen in high abundance on Earth's aqueous systems and are likely to be of biological relevance. Ligands like lactate, ascorbate and phosphate are integral components of blood plasma and many microbial growth media (Sunda and Guillard, 1976; Lentner, 1981; Jackson and Byrne, 1996; Kim et al., 2012). Other O⁻ ligands like silicate, bicarbonate and acetate are commonly found in hot springs,

hydrothermal vents and oilfield brines (Willey et al., 1975; Shock, 1998; Amend et al. 2003, Shock and Canovas 2010). Studying such ligands may also be useful in the context of metal association with polymeric ligands like proteins and humic substances which may have monovalent acidic or phenolic side-chains.

We developed ligand-specific linear free energy relations (LFER) and analogous entropy correlations to estimate stability constants and entropy of association for metal complexes of monovalent oxygen ligands using corresponding thermodynamic properties of metal-acetate or metal-hydroxide complexes. A linear relationship was also obtained between the protonation constant (pK_a) and protonation entropy for several monovalent oxygen ligands like carboxylates and phenols. These relationships enabled the estimation of metal-ligand stability constants from 0-125°C within 1 log unit when only the ligand pK_a is known.

We compiled our dataset of experimental measurements from original papers while critically evaluating the data. As suggested from the title of this work, our estimation strategy is based on chemical properties of the electron-donating atom of the ligand. While some previous work has alluded to this strategy (Hancock and Marsicano, 1976; 1978; and Hancock, 1997), we chose to use the best proxy ligand for which most data was available. This approach was picked on observing that the predictive ability of correlations decreased as the ligands differed on moving from the negatively charged oxygen to other parts of the ligand, thus revealing a simple chemical basis. Our work also shows that some of the previously held notions about denticity may need revision and explain why different estimation strategies need to be employed for different O- ligands.

Equilibrium speciation calculations are routinely used to determine the elemental distribution of a system and due to the limitations of analytical techniques (Levina et al., 2017,

Bonito et al. 2024), they are often the only option available. Such simulations are particularly accurate in studying complex formation and protonation as these processes are extremely fast and hence equilibrium can be reached within seconds (Tipping, 2002). Thus, our estimates of equilibrium constants of these complexation reactions can be directly applied to study metal or ligand speciation in any aqueous system within 0 to 125°C, i.e., the whole biosphere

2. Definitions and data evaluation

The reactions studied in this work can be generalized by the following equation:

$$M^{y+} + L^{-} = ML^{y-1}$$
 (Eqn. 1)

where M refers to the metal ion of charge y+ and L indicates the monovalent O^- ligand. Each such reaction has a corresponding overall standard state equilibrium constant, K_{ML} , and entropy change of the reaction, ΔS°_{ML} .

The standard state equilibrium constant (generally given in the logarithmic form as log K_{ML}) is generally obtained upon measuring the stoichiometric constants over multiple concentrations and extrapolating to zero ionic strength (I). Many scientific investigations, however, report stoichiometric constants at a single ionic strength (generally 0.15 or 0.7 for applications in blood or seawater respectively). We extrapolated these data to zero ionic strength using the B-dot equation which is an extended Debye-Hückel equation (Helgeson, 1969). While the B-dot equation was primarily devised to deal with inorganic species, we found that the equation worked extremely well for organic species when extrapolating data at $I \le 0.5$ and occasionally for higher ionic strength. It should be noted that this is the same equation employed by the equilibrium speciation software EQ3/6 (Wolery, 2010). Thus, no extrapolation errors would be made upon using the modified equilibrium constant at the original ionic strength with

EQ3/6 or other codes that employ the B-dot equation Reports that explicitly defined the terms and conditions were preferred over ill-defined reports and those with extreme disparity of data were discarded in accordance with the guidelines as outlined in Martell & Smith, 1974, 1977; Smith & Martell 1975,1982, 1989; Pettit, 1984; Kiss et al., 1991; Berthon, 1995.

Standard states

In aqueous thermodynamics, the standard state refers to unit activity of the solute in a hypothetical one molal solution referenced to infinite dilution. In terms of the parameters reported in experiments, this state refers to an ionic strength of zero. As such a state is impossible to measure experimentally, standard state thermodynamic properties are either obtained upon extrapolating a series of low concentration solutions to infinite dilution or using theoretical approaches like the B-dot equation.

3. Methodology

3.1 Estimation strategy for stability constants

Numerous researchers have developed multiple LFERs to estimate metal-ligand stability constants. These relations are built on assumptions that the metal-ligand interaction is a function of the ligand pK_a (Irving and Rossotti, 1956; Carbonaro & Di Toro, 2007; Carbonaro et al., 2011; Atalay et al., 2013), the electrostatic potential of the metal ion as determined by the ratio of charge² to ionic radius (Davies, 1951), ligand electronegativity (Van Uitert et al., 1953) or Gibbs energy of metal ion formation (Shock & Koretsky, 1993; 1995; Prapaipong et al., 1999). However, these correlations are far from perfect and often have serious outliers or limited applicability. Thus, there is a need to create a set of LFERs with greater accuracy and extended applicability.

The correlations in earlier models reveal that metal-ligand thermodynamic properties are complex functions of several factors including: the type of ligand electron-donor atom, ligand denticity, chelate-ring size, ligand preorganization, inductive effects, steric effects, metal ionic radius, metal coordination number and the charge of metal or ligand. The majority of these factors can be attributed to the ligand, which suggests that ligand-based correlations may yield estimation methods of lower uncertainty. Consideration of multiple estimation strategies revealed that correlating properties of metal complexes for a ligand with those of a structurally similar proxy ligand minimizes variability among estimated thermodynamic properties. Thus, our strategy for the estimation of metal-ligand stability constants could be summed up as -pickthe closest proxy ligand with the most data. The challenge is to understand what could be meant by 'the closest proxy ligand'. Ideally, the closest proxy ligand would have the same metal coordination sphere as that of the ligand of interest. Such a correlation would have an intercept of zero and the slope would be a function of the inductive effects of the respective ligand sidechains as indicated by the corresponding pKa values. However, ligand sidechains often sterically hinder the metal-ligand interaction or additionally coordinate with the metal ion. Such interactions are likely to produce negative and positive intercepts, respectively. By the same argument, ligands with a negative charge of 1 on an oxygen atom can be expected to behave similarly.

Analysis of the stability constant literature for monovalent oxygen ligands shows that there are abundant experimental stability constants for metal-hydroxide and metal-acetate complexes, which guided our decision to use acetate and hydroxide as the closest proxy ligands to investigate multiple monovalent oxygen ligands together. While metal-acetate LFERs were successful for most carboxylates, metal-hydroxide correlations were more successful for alcohols

and inorganic monovalent oxygen ligands, as described below. Choosing between acetate and hydroxide as the proxy ligand is based on the structure of the ligand and tested with the applicability of the LFER (*i.e.*, considering slope, intercept, and correlation coefficient).

Experimental values of the dissociation constant, pK_a, are available for almost all compounds that produce O⁻ ligands. As a result, we included protonation constants along with the metal stability constants in our correlations, which enhanced individual correlations and considerably expanded our estimation capabilities. We also found that a substantial number of logK_{ML} measurements are available for only a few ligands. Thus, we have divided the ligands into the following categories (1) ligands with many logK_{ML} data, (2) ligands with few logK_{ML} data, (3) ligands with no logK_{ML} data.

3.2 Estimation strategy for entropy of association

Compared to stability constants, many fewer attempts have been made to estimate standard-state entropy changes (ΔS°_{ML}) for metal-ligand reactions (Cobble, 1953a; 1953b; Hinchey & Cobble, 1970; Shock and Koretsky, 1993; 1995, Sverjensky et al., 1997; Prapaipong et al., 1999; Prapaipong and Shock, 2001). This is understandable as there are limited ΔS°_{ML} data in the literature. As the previous attempts included only a few O⁻ ligands, there was considerable scope for making new estimates.

Our entropy estimation strategies are completely analogous to our stability constant estimation strategies mentioned above we have correlated metal-ligand ΔS°_{ML} values against values of metal-acetate and metal hydroxide ΔS°_{ML} . This approach differs from that employed in previous papers from this research group in which metal-ligand ΔS°_{ML} values were correlated with the third-law entropy of the metal ions. Thus, yet another motivation behind our work was

to compare the two strategies. As our correlations possess a lower uncertainty (± 2 cal (mol K)⁻¹ vs. ± 5 cal (mol K)⁻¹ obtained with correlations presented in previous papers, we believe these new correlations will yield more accurate estimates.

4. Results

4.1 Estimating stability constants at 25°C and 1 bar

4.1.1 Ligands with many logKML data

Among the O ligands, the most measurements of logK_{ML} are for hydroxide and acetate with 69 and 52 values, respectively. While both are O ligands, acetate has a slight bidentate character owing to resonance between its two carboxyl oxygens compared to the monodentate character of hydroxide. Thus, hydroxide is a close proxy ligand to estimate metal-acetate stability constants owing to the similarity in overall charge and the abundant supply of logK_{ML}. A correlation between the two datasets was obtained (Fig. 1) which demonstrated that metalacetate stability constants could be estimated from metal-hydroxide stability constants within ± 0.5 log units, on the order of experimental uncertainty. The slope is close to the ratio of the respective pKa values and the slightly positive intercept is in accordance with the slight bidentate nature of acetate. Theoretically, the intercept for LFER with hydroxide for O ligands should be zero and for polydentate O ligands should increase in increments of log₁₀(55.5) or 1.74 (Adamson, 1954; Martell & Hancock, 1996). The log₁₀(55.5) factor can be derived from a dimensionless expression of the equilibrium constant and refers to the molality of 1 kg of pure water. This phenomenon has been investigated thoroughly for analogous amines and is known as the chelate effect (Hancock & Marsicano, 1976). While the intercept here (0.19) is considerably less than 1.74, the repeated appearance of such intercepts for carboxylate vs. hydroxide LFERs

Relationship between the two monovalent O⁻ ligands with most thermodynamic data

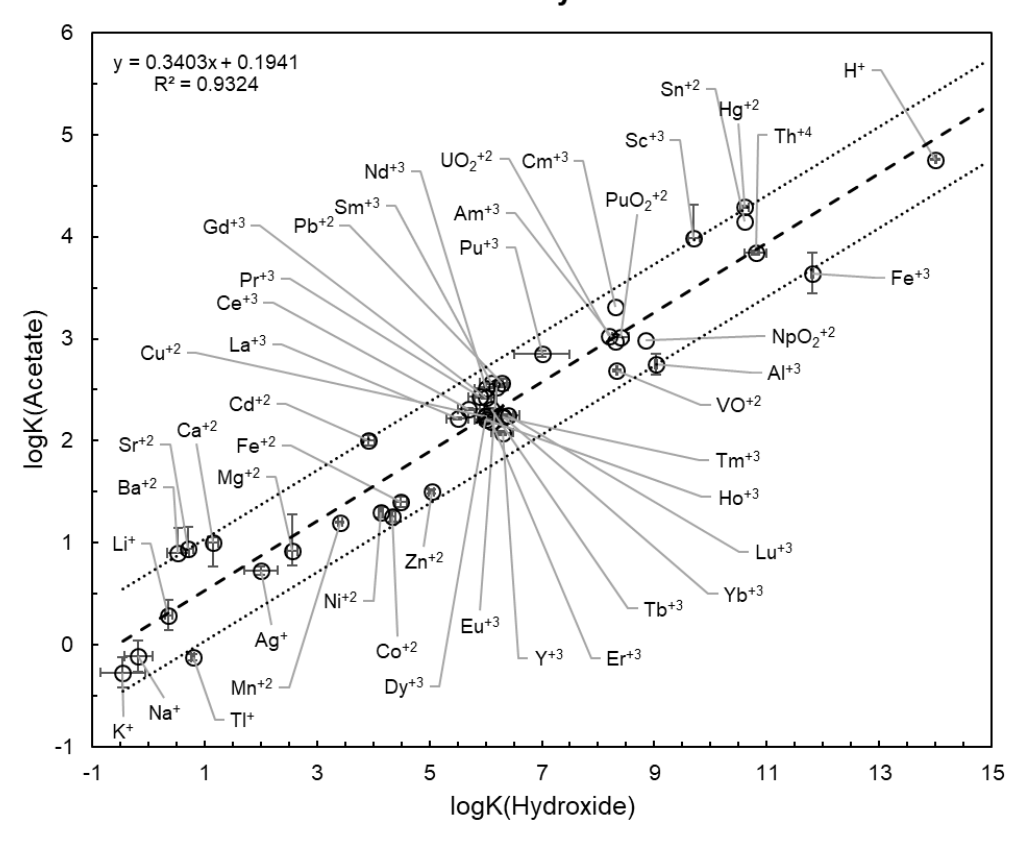


Fig 1. LFER between acetate and hydroxide stability constants with 44 metal ions and proton. Error bars correspond to uncertainties in experimental measurements. Error bars are absent for some metal ions as they weren't reported in the original report. The dashed line is the trendline (equation on top) and the dotted lines represent the estimation uncertainty of \pm 0.5 log units which is of the order of experimental measurements. As can be seen from the figure, all points lie within the estimation uncertainty.

(in detail below) suggests that there is a partial bidentate character to these ligands. The error bars in this figure correspond to the experimental uncertainties reported in the original papers. As can be seen in the figure, the correlation is within \pm 0.5 log units of the stability constants for all the 44 ionic species. Similar uncertainties exist for other correlations. For consistency, we have used the limit of \pm 0.5 log units as the target of estimation in our correlations, which is on the order of experimental uncertainty. It is important to note that a slope of greater than 1 in any acetate or hydroxide correlation (discussed below) can enhance this uncertainty, so we have worked to avoid steep slopes. Note also that the ultimate purpose of these correlations is to create a foundational framework that has wide-ranging applications. These correlations have been created using measurements of hundreds of scientific reports which are bound to have experimental variability. The consistent applicability of these correlations to a variety of ligands supports the utility of this approach.

In aqueous solution a ligand coordinates with a metal ion via its functional groups that have high electron density (Martell & Hancock 1996). Therefore, the interaction of a metal ion with a mono-alkyl carboxylate like propanoate can be expected to be similar to that with acetate. This is the case as shown in Fig. 2 where an LFER between metal-propanoate complexes and metal-acetate complexes has both slope and R² close to 1 and an intercept close to 0. This LFER allows estimates of stability constants of 20 additional metal-propanoate complexes with substantial accuracy (as the number of experimentally constrained metal-acetate stability constants is 52 while that for metal-propanoate complexes is 32, please see the Supplementary Table for more details). Additionally, a slightly weaker relationship was also obtained between stability constants of metal-propanoate vs. metal-hydroxide complexes. While the values of slope and R² displayed on the figure are expected, the intercept differs substantially from 0. One

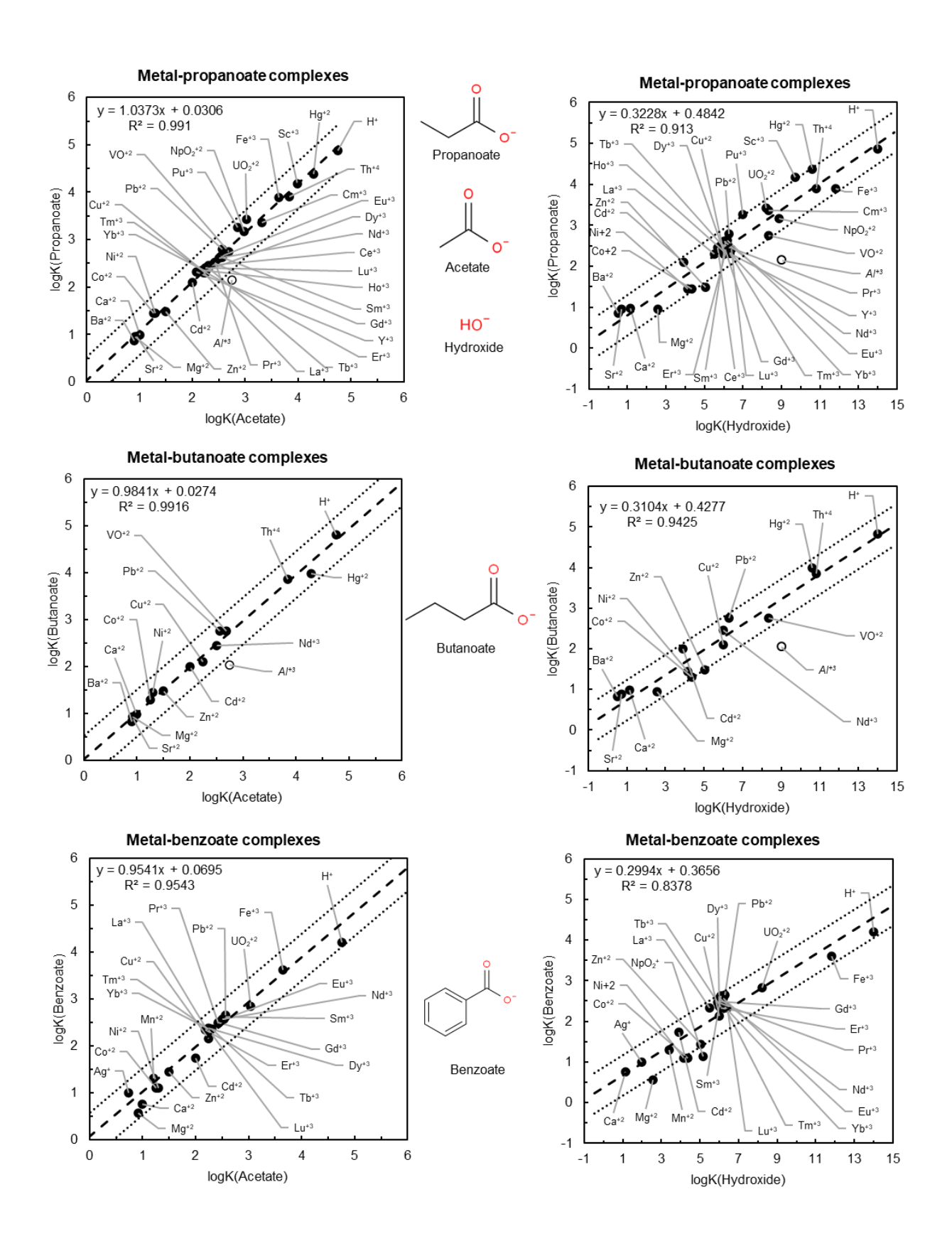


Fig 2. LFERs for carboxylic acids with different side groups (contd.)

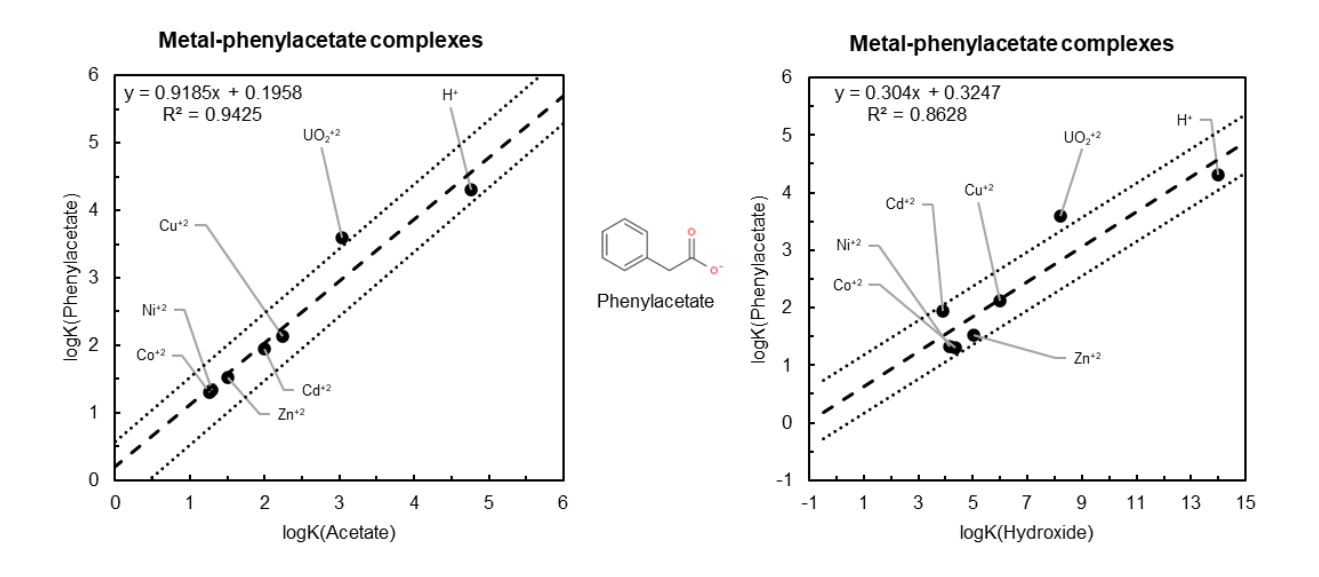


Fig 2. (contd.) LFERs for carboxylic acids with different side groups

possibility for the non-zero intercept arises from resonance, if both the oxygens of the propanoate have a partial negative charge and hence both groups participate in the interaction with a metal ion. As explained above, the theoretical intercept for a bidentate O⁻ ligand with hydroxide should be 1.74. While the intercept here (0.48) is considerably less, the repeated appearance of such intercepts for carboxylate vs. hydroxide LFERs (in detail below) suggest that there is indeed a partial bidentate character to these ligands. Nonetheless, as there are more experimentally determined association constants for hydroxide complexes than for acetate complexes, an additional 17 estimates for metal-propanoate complexes are possible with the LFER shown in Fig. 2 (Supplementary Table), albeit with greater uncertainty compared to the acetate-based estimates.

As in the case of propanoate, the butanoate vs. acetate LFER exhibits both slope and R² close to 1 and an intercept of 0 (Fig. 2), and the corresponding parameters for the hydroxide correlation shown in Fig 2 are almost identical to those for propanoate. To investigate the involvement of aromatic groups in the metal-ligand coordination, we correlated benzoate and phenylacetate complexes in the same manner and found LFER results, shown in Figs 2, to be similar to those for propanoate and butanoate. This suggests that it is predominantly the carboxylate group in benzoate that interacts with metal ions in aqueous solution.

Analogous plots for nitroacetate, chloroacetate, bromoacetate and iodoacetate in Fig 3 reveal the consequences of inductive effects on LFER correlations built on acetate and hydroxide. Nitro-, chloro-, bromo- and iodo- are electron-withdrawing groups that can reduce the charge density at the carboxylate oxygens, and weaken interactions with metal ions or proton resulting in slopes less than unity. This effect appears to be larger for nitroacetate and less for the halogenated carboxylates. Note that the slopes are similar for the three correlations between

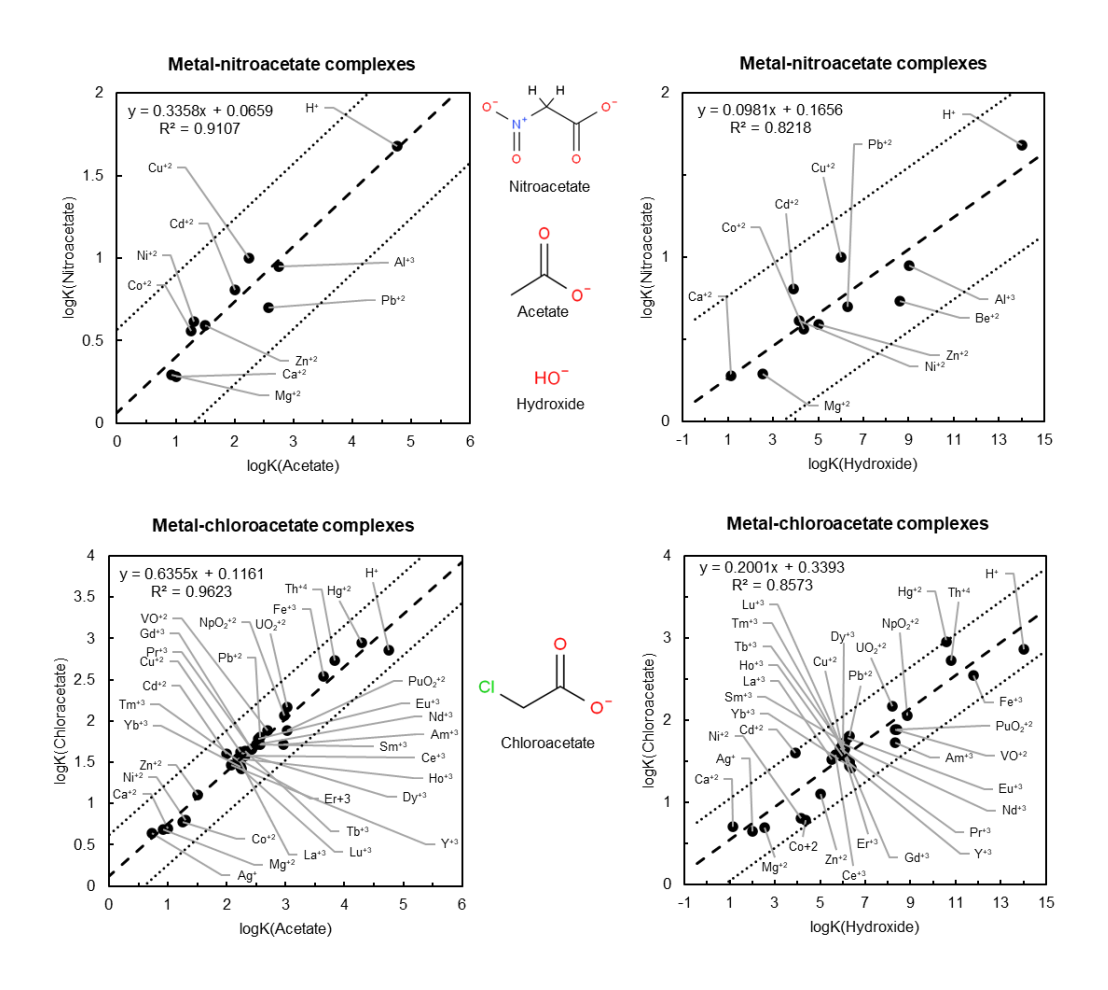


Fig 3. LFERs for carboxylic acids exerting significant inductive effects (contd.)

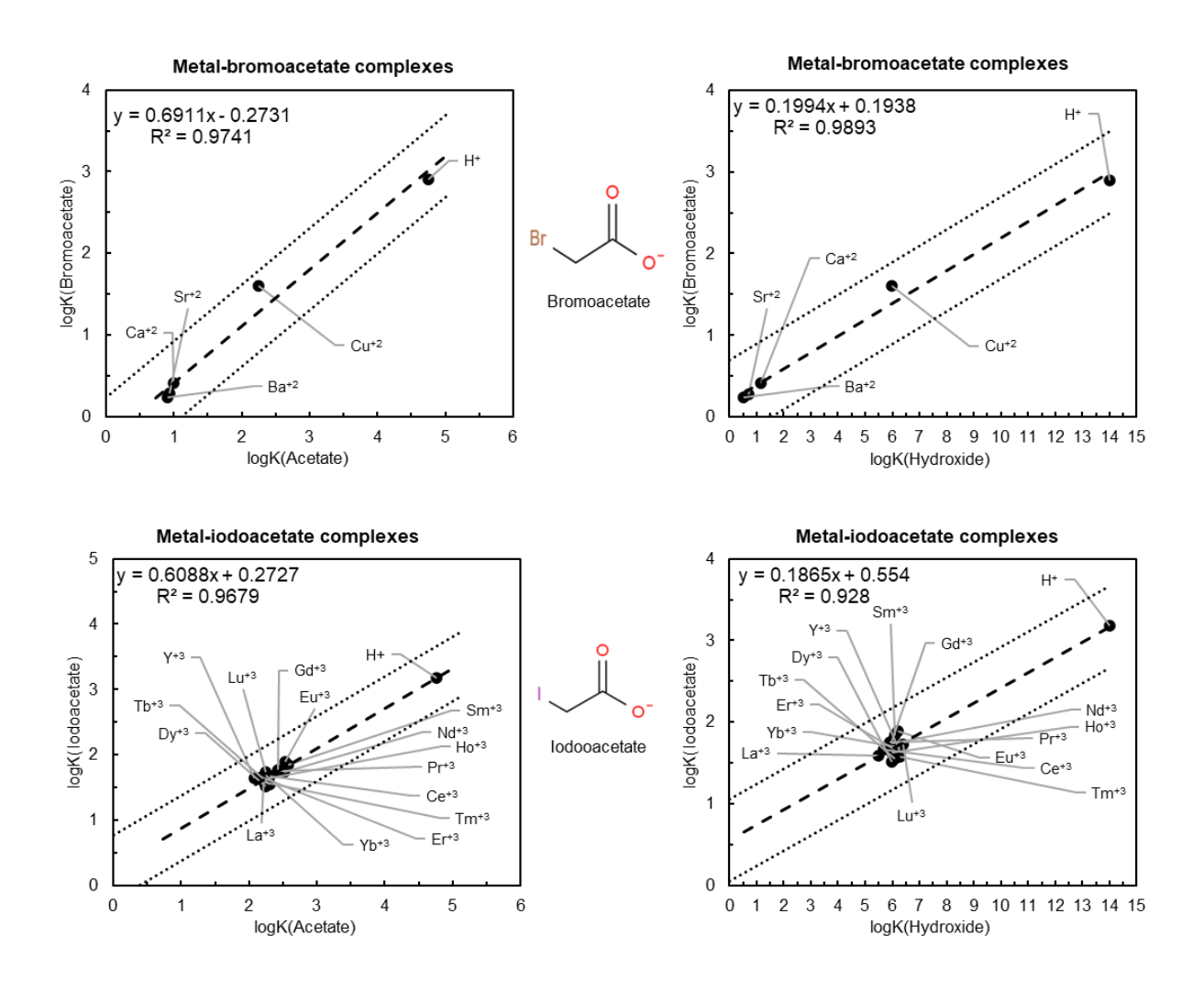


Fig 3. (contd.) LFERs for carboxylic acids exerting significant inductive effects

halogen-substituted ligands and acetate. While intercepts differ among the halogen-substituted ligands, we suspect that the variability in intercepts can be explained by the relative lack of data for bromoacetate and iodoacetate.

As shown in Fig 4, correlations for pivalate and isobutanoate exhibit significantly lower intercepts compared with the ligands discussed above. While logK_{ML} data for these ligands are considerably lower than those for acetate, the pK_a values are almost identical. This indicates the influence of steric effects at play. Perhaps the existence of multiple methyl groups at the alpha carbon of the respective ligands sterically hinders the metal-ligand bond thereby reducing its strength. The reason this is not seen in the case of the proton-ligand interaction may be due to the smaller ionic radius of the proton making the proton-ligand interaction equivalent to that for acetate.

Taken together, Figs. 2, 3 and 4 illustrate deviations from ideality in LFERs. While additional coordinating groups increase the intercept (as seen in the hydroxide correlations of Fig. 2), inductive effects can increase or decrease the slope of the correlation using the ligand pK_a as a guide (as seen in Fig. 3), and steric effects decrease the intercept of the correlation due to the presence of non-coordinating groups close to the metal-ligand coordination sphere (as seen in Fig. 4). Given the complexity and diversity of organic moieties, all these factors can be at play together in varying degrees for some ligands. We found this to be the case in some of the more structurally complicated monovalent oxygen ligands discussed next.

As can been seen in the correlations for ascorbate, aceturate, acetoxyacetate, cyanoacetate, lactate and pyruvate (Fig. 5), the intercepts fall between 0 and 1.74 – the theoretical intercepts for monodentate and bidentate ligands, respectively. Rather than a binary distribution between these intercept values, we found a gradation that increases from ~ 0 (-0.06)

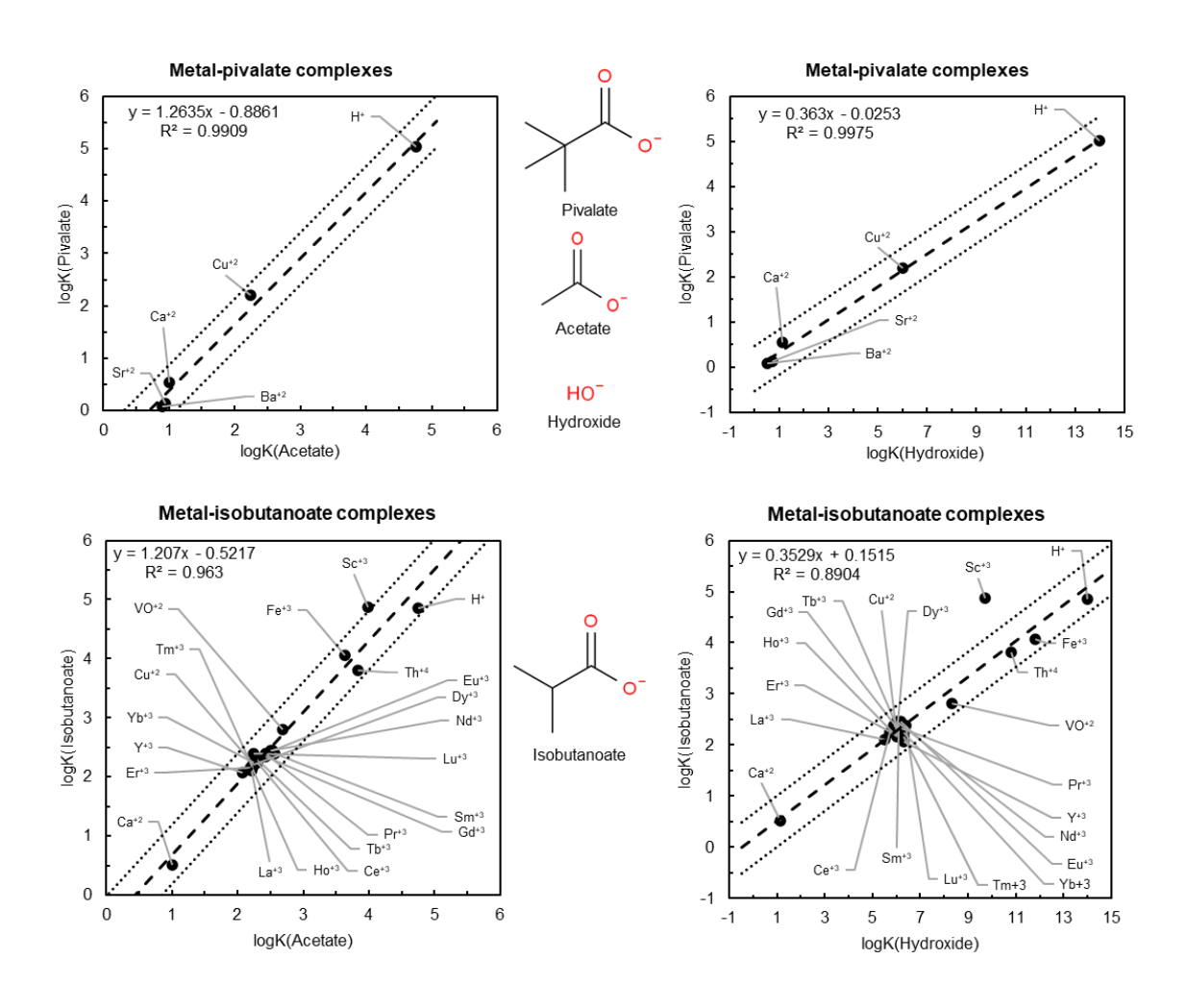


Fig 4. LFERs for carboxylic acids exerting significant steric effects

for ascorbate to 1.06 for pyruvate in the acetate correlations. As an LFER correlation for homodentate ligands like acetate and propanoate has an intercept close to zero, as shown in Fig 2, these departures suggest that the associated side-chains of the ligands in Fig. 5 interact variably with the metal ions.

Even though ascorbate does not have a carboxylate group, its log K_{ML} data correlate closely with those for acetate while with hydroxide the correlation yields a slope and intercept akin to other carboxylates. The intercepts for aceturate are slightly higher than those for ascorbate, perhaps due to the presence of an oxygen at the gamma (γ) position, but lower than those for acetoxyacetate, which has an additional oxygen at the beta (β) position. The influence of the position and nature of these additional functional groups can be seen in the correlations of cyanoacetate, lactate and pyruvate. While cyanoacetate has a cyano-group at the beta position, lactate has a hydroxyl group at the alpha (α) position and pyruvate has a carbonyl oxygen at the alpha position. If the close proximity of other functional groups to the carboxylate group generates a fluidity in increase in log K_{ML} due to dentition, it could explain why lactate and pyruvate have higher intercepts. In addition, the lactate vs hydroxide LFER reveals an influence of metal ionic radius as the small metal ions Be⁺² and Li⁺, together with H⁺ (all Lewis acids), fall below the trend owing perhaps to their inability to coordinate with the alpha-hydroxyl group.

Formate and bicarbonate are two monovalent oxygen ligands with the carboxylate group but without the C-C bond. As the alkyl group is an electron-donating group, the lack of the C-C bond is perhaps the reason why the formate vs. acetate LFER (Fig. 6) has a lower slope. As the coefficient of determination (R^2) for the hydroxide correlation was higher than the acetate correlation, we used metal-hydroxide stability constants to estimate metal-formate logK_{ML} (see Supplementary Table for details). Ba⁺² and Sr⁺² were avoided in the correlation as the original

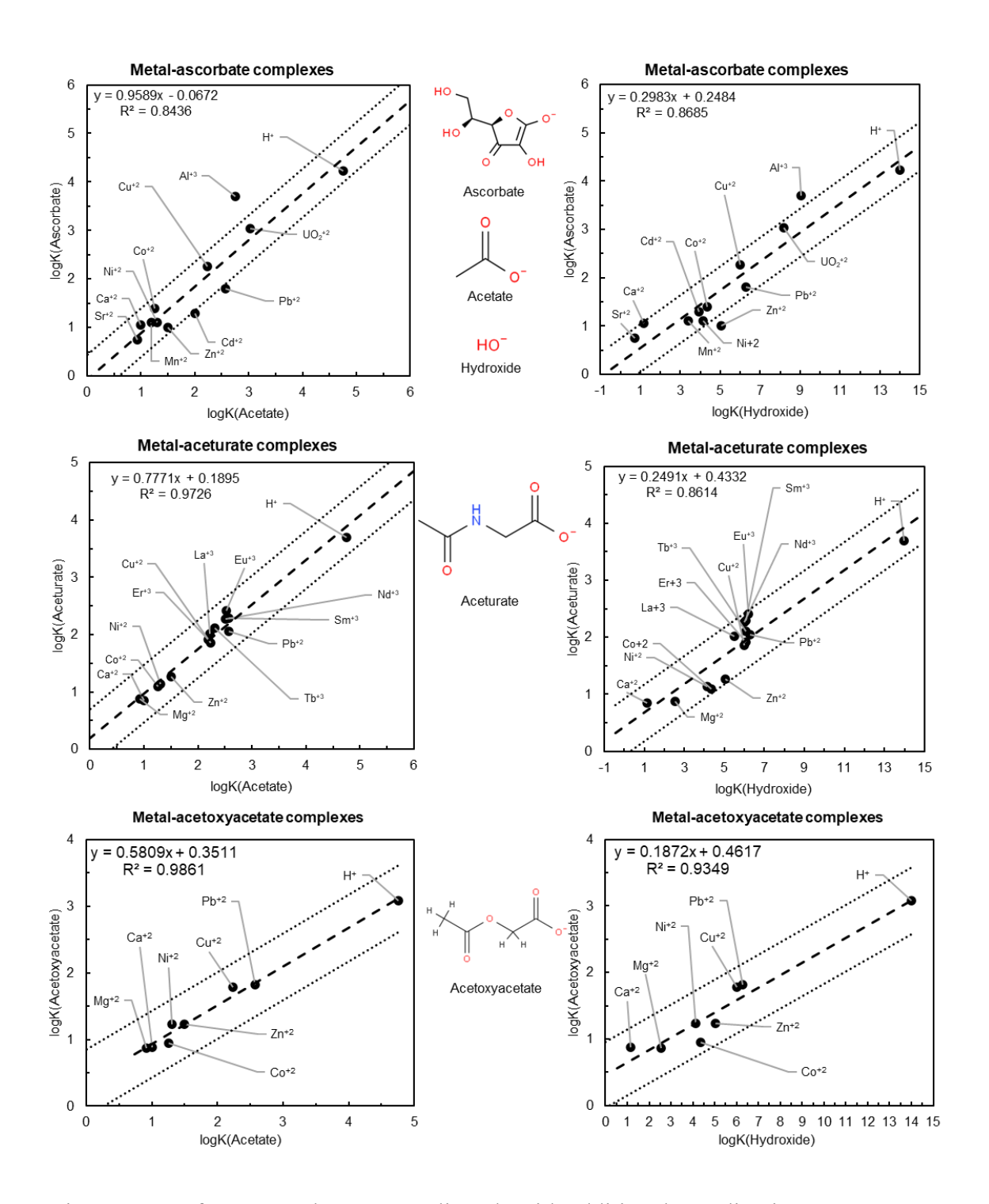


Fig 5. LFERs for monovalent oxygen ligands with additional coordinating functional groups with increasing additional denticity (contd.)

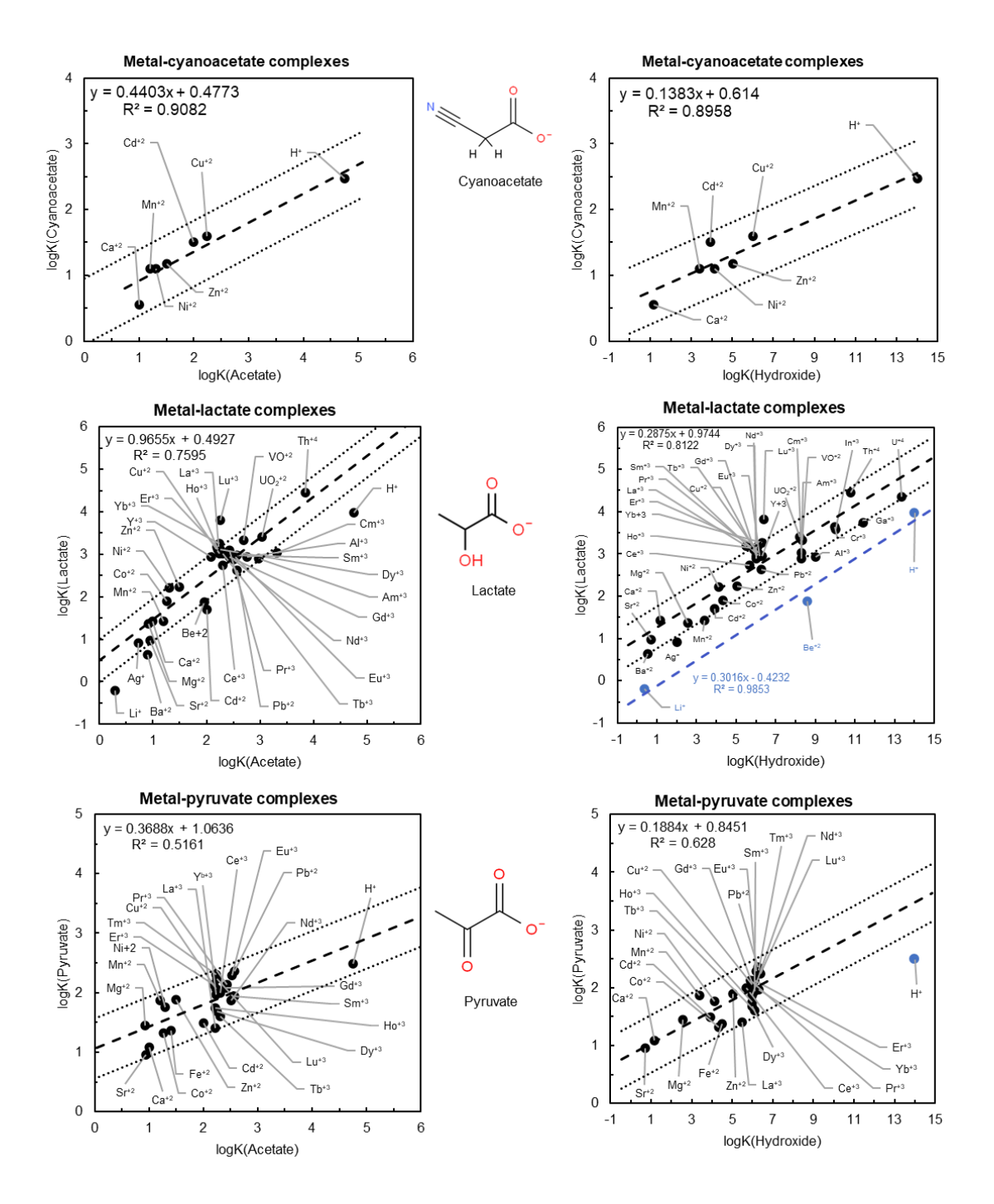


Fig 5. (contd.) LFERs for monovalent oxygen ligands with additional coordinating functional groups with increasing additional denticity. Blue circles and dashed line in lactate and pyruvate denote monodentate coordination

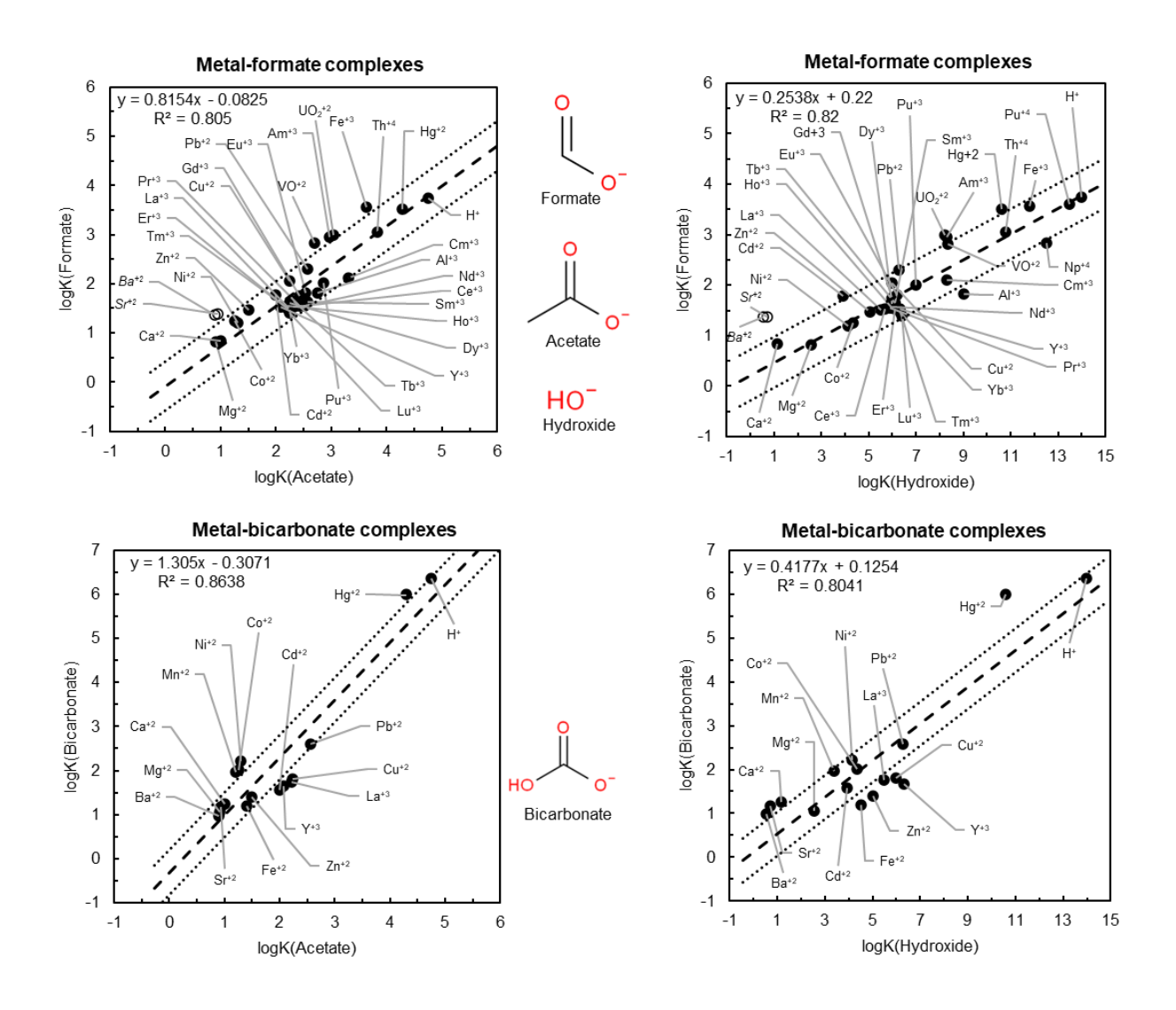


Fig 6. Both acetate and hydroxide LFERs seem equally applicable for two monovalent oxygen ligands with the carboxylate group but without C-C bond. The hollow circles are experimental measurements that were rejected upon critical evaluation from the literature.

report had excessively high stability constants for multiple ligands (Nancollas, 1956). It is worth noting that these metals plot on the correlation if the acetate stability constants from the same paper are used, suggesting a systematic bias. The intercepts of bicarbonate LFERs are lower than expected despite the presence of an additional metal-coordinating group (the hydroxyl group). Perhaps the very close proximity of these metal-coordinating groups is to explain for these observations.

Analogous correlations for monovalent oxygen ligands without the carboxylate group like phenol, borate and silicate show that hydroxide is a closer proxy ligand than acetate (Fig. 7). While this makes structural sense, hydroxide correlations also exhibit much lower slopes than the acetate correlations, consistent with the high pK_a values of these ligands, which is a positive contribution to the accuracy of these estimates. While the negative intercept for the phenol correlation may stem from the higher steric hindrance of the phenyl group, the positive intercepts of borate and silicate may result from the presence of additional hydroxyl groups on the ligand. Additionally, high cation size and the consequent lack of dentition for Ca+2 and Mg+2 may explain the low metal-silicate logK_{ML} values for these cations.

While a similar observations were made for nitrite (Fig. 7.a), these LFERs for dihydrogenphosphate (H₂PO₄⁻) and iodate (Fig. 8) reveal a different phenomenon. The measured pK_a values for these ligands were considerably smaller than expected from the trendline and we suggest that this may be due to the presence of additional metal-coordinating oxygens that increase the strength of the metal-ligand bond but can't do the same for the proton due its smaller size (similar to the phenon observed with lactate and pyruvate).

4.1.2 Ligands with limited $log K_{ML}$ data

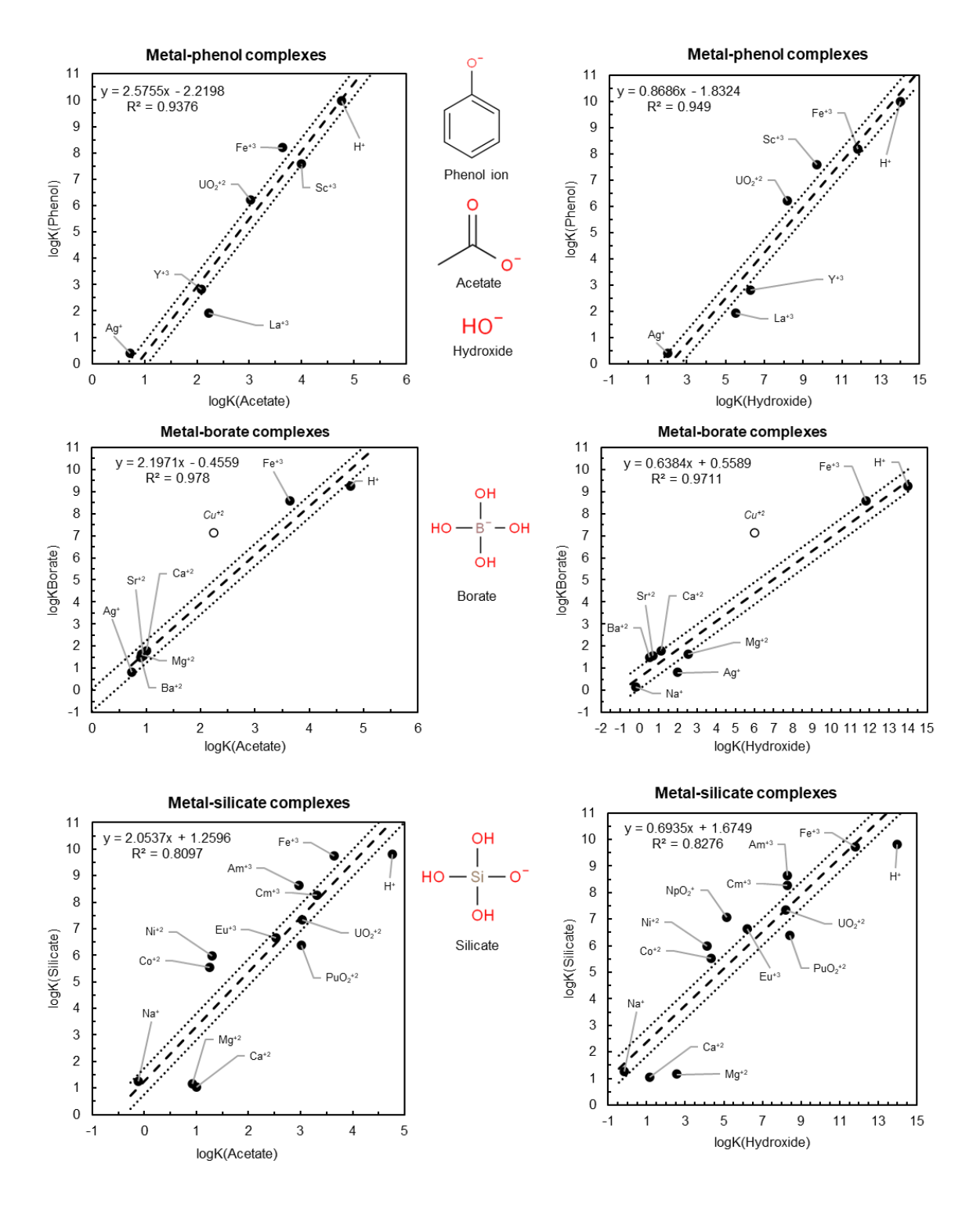


Fig 7. Hydroxide LFERs better than acetate LFERs for these monovalent oxygen ligands with high pK_a and no carboxylate group. The hollow circles are experimental measurements that were rejected upon critical evaluation from the literature.

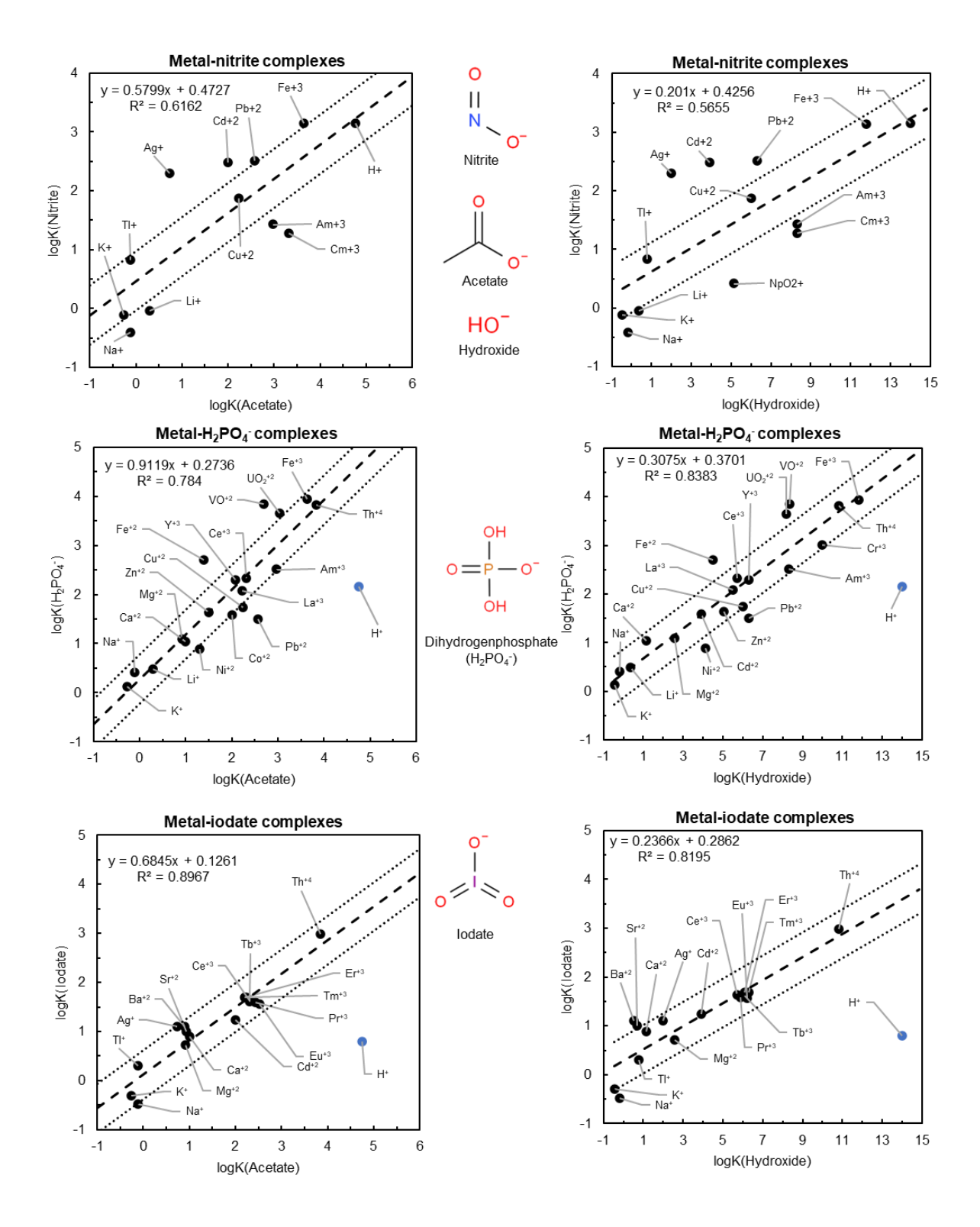


Fig 8. LFERs for some diverse inorganic monovalent ligands. The higher $logK_{ML}$ (black) for dihydrogenphosphate and iodate is perhaps due to higher denticity. pK_a values (blue) have been correspondingly plotted separately.

The number of ligands with limited logK_{ML} data far exceeds that for which abundant $log K_{ML}$ data exist (see Supplementary Table for details). In many cases regressing the scant LFER data generates slope and intercept values that are unlike those obtained from more complete datasets. Using such regression results would likely induce large uncertainties in estimated values. To circumvent this problem, we regressed the LFER data by setting the intercept to zero and obtaining slopes from 1-prameter fits that largely governed by the ligand pK_a. As a test of the usefulness of these correlations, we compared estimates from 1-parameter fits with those from 2-parameter fits for two ligands for which a moderate amount of logK_{ML} data were available: 3-chloropropanoate and phenoxyacetate as shown in Fig. 9. The acetate correlations can be compared in Fig. 9(a) while the hydroxide correlations can be compared in Fig. 9(b). As seen in both cases, the 1-parameter correlations can be fit to all available stability constant data within ± 0.5 log units. These correlations gave us confidence to set up similar correlations for a host of ligands with four or less logK_{ML} values, some of which are shown in Fig. 10, in which Fig. 10(a) shows acetate correlations and Fig. 10(b) depicts hydroxide correlations. The resulting 1-parameter slopes were used to estimate stability constants for 2625 additional metal-ligand complexes comprising of 75 metal ions and 35 monovalent oxygenbearing ligands. While the acetate correlations were given preference for carboxylates, the hydroxide correlations were used to estimate metal-phenol stability constants.

4.1.3 Ligands for which there are no logK_{ML} data

While there are no $logK_{ML}$ measurements for most of the ligands in our compilation (157), we found pK_a values for all of them. Ligand pK_a values were used to estimate slopes by setting the intercepts to zero, and the resulting slope values are depicted in Figs. 11 & 12. Since

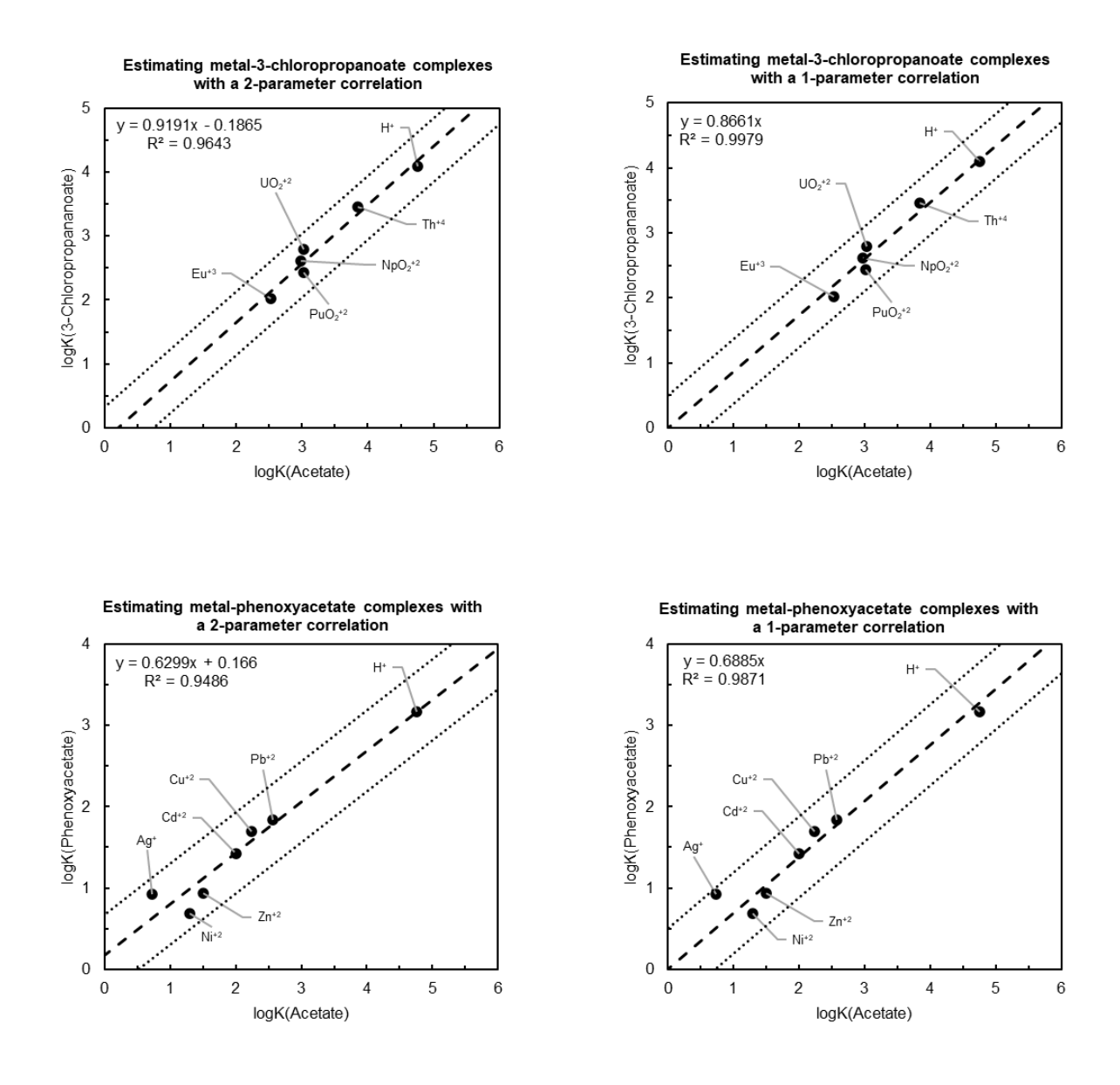


Fig 9(a). Comparison between 2-parameter and 1-parameter acetate LFERs for some monovalent oxygen ligands.

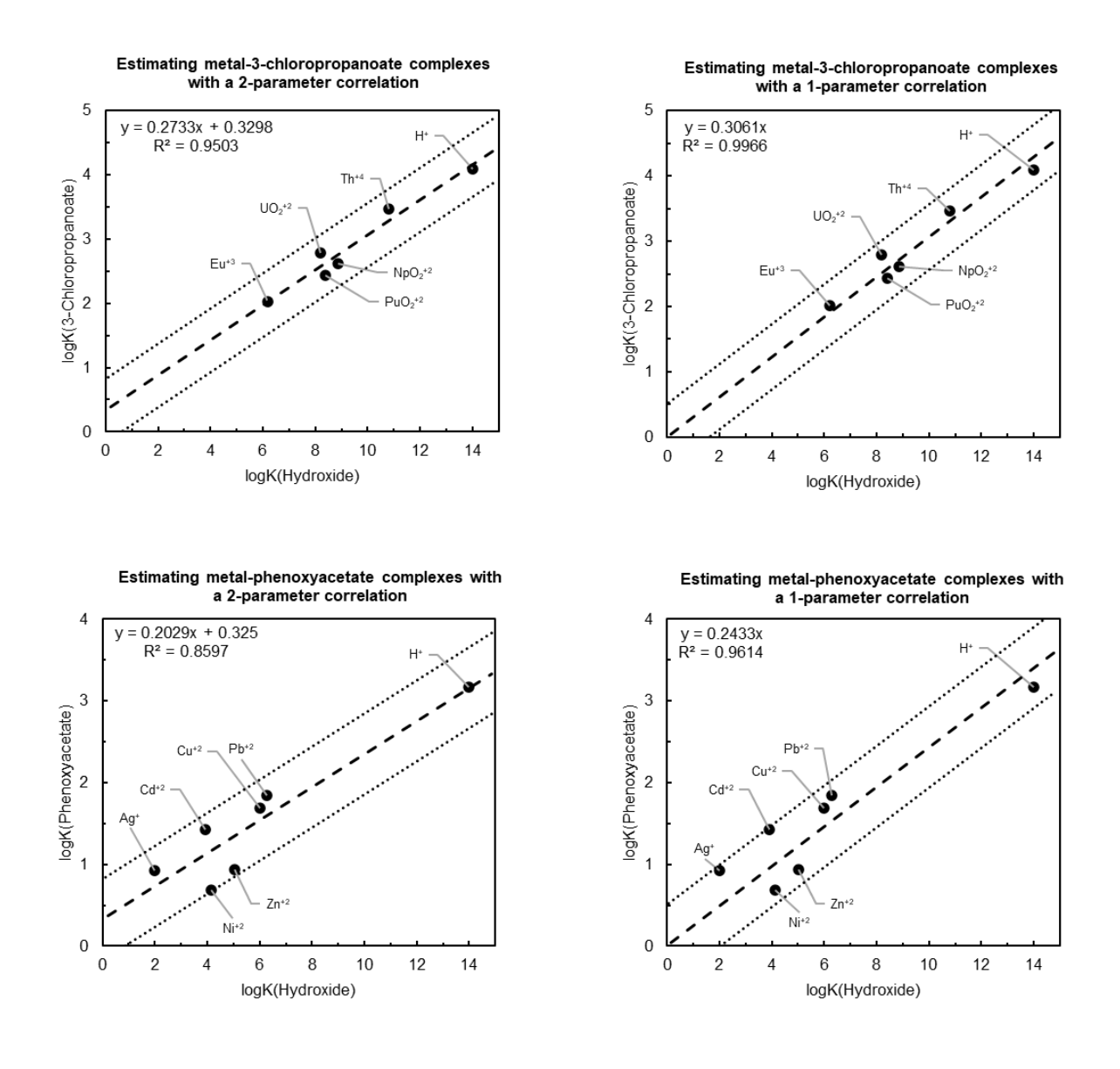


Fig 9(b). Comparison between 2-parameter and 1-parameter hydroxide LFERs for some monovalent oxygen ligands.

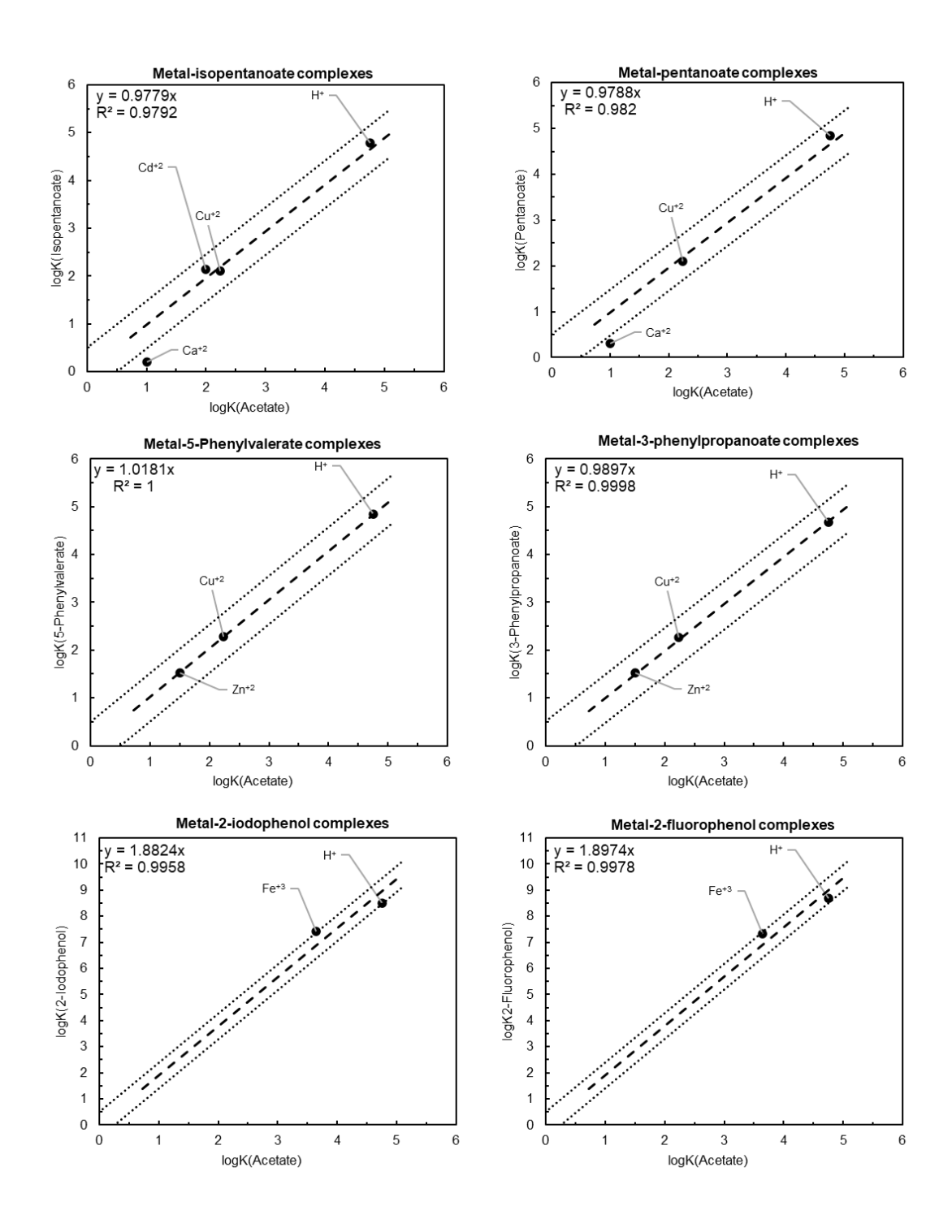


Fig 10(a). 1-parameter acetate LFERs for some monovalent oxygen ligands.

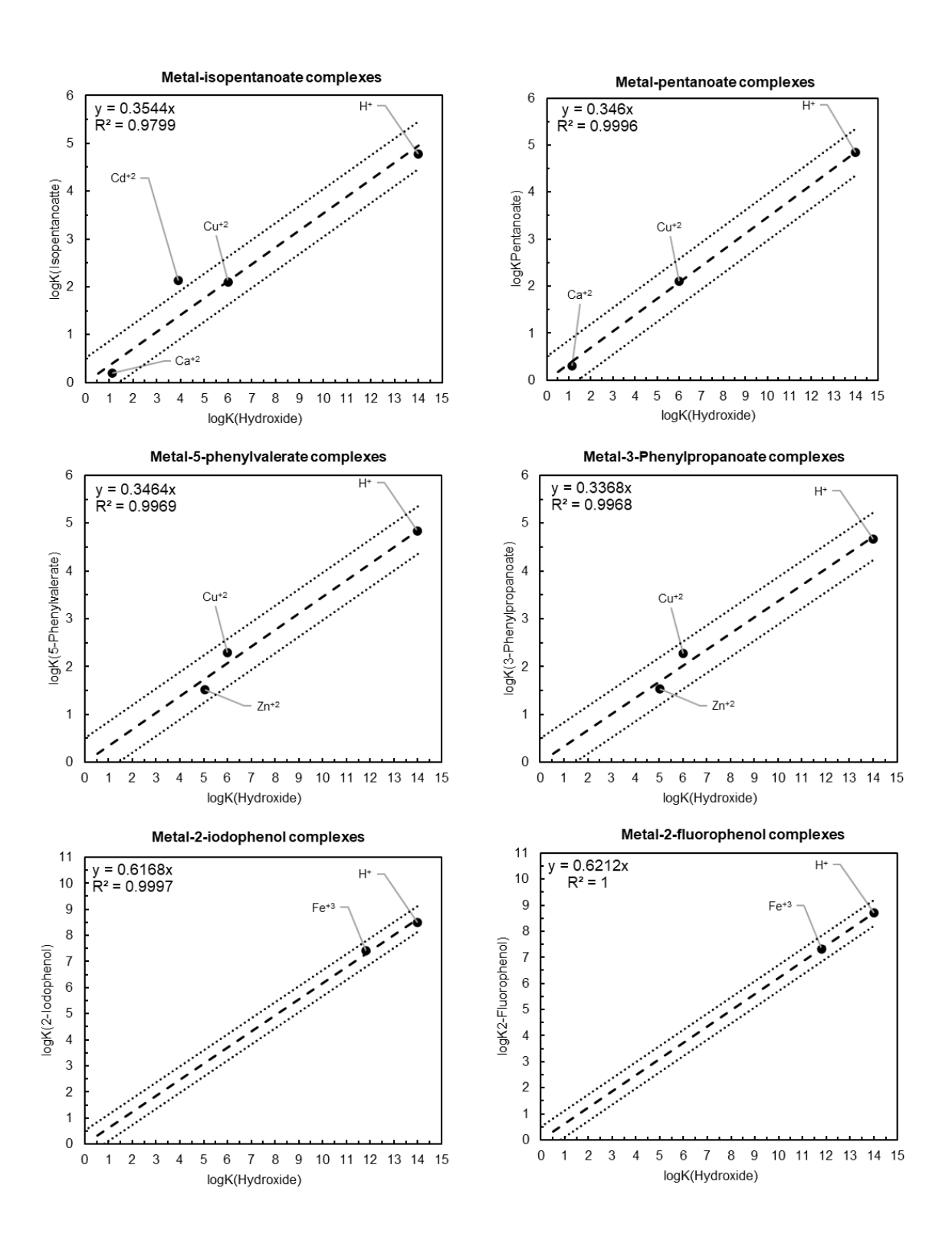


Fig 10(b). 1-parameter hydroxide LFERs for the monovalent oxygen ligands of Fig. 8.

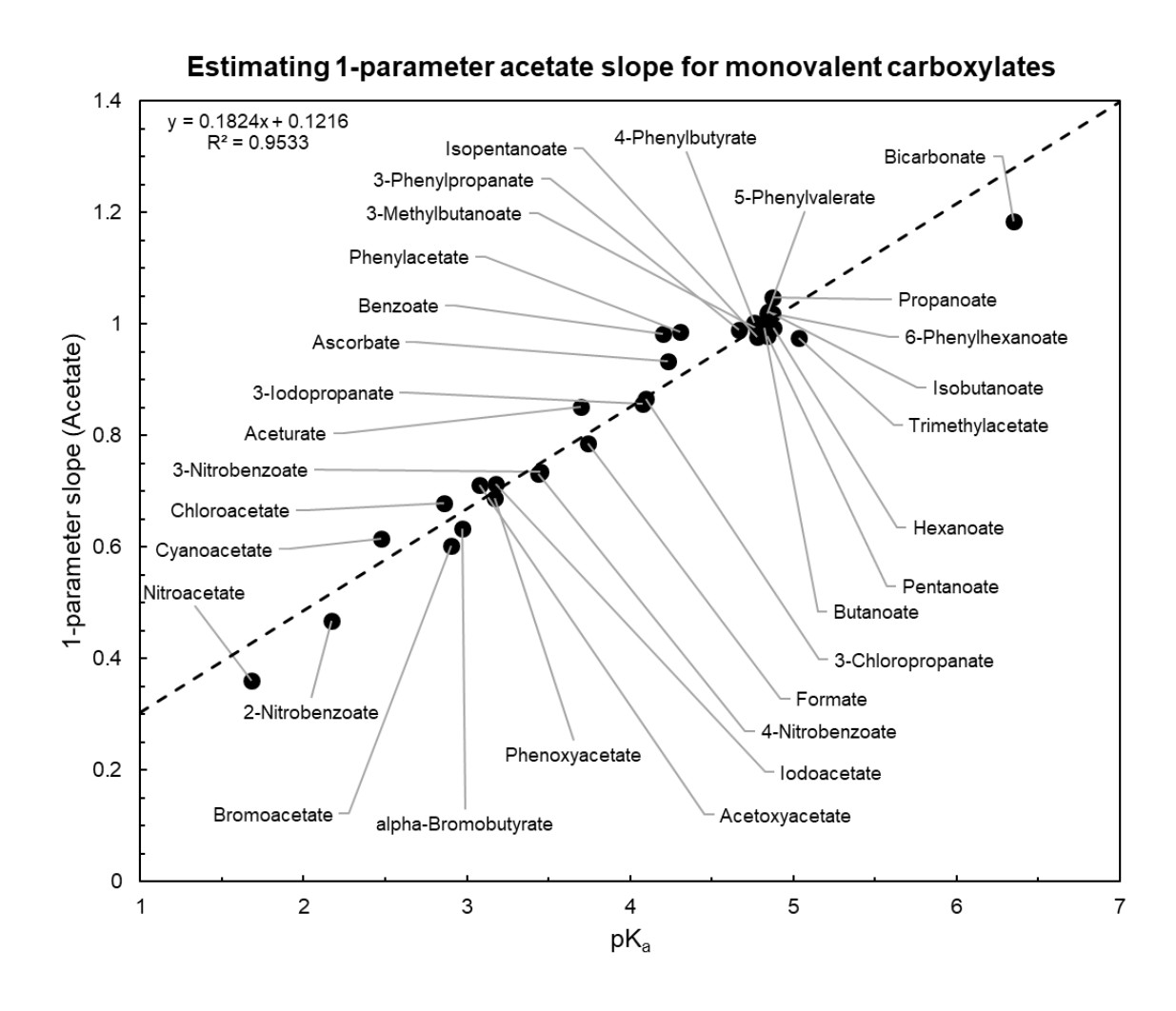


Fig 11. Estimating any metal-carboxylate from its pK_a.

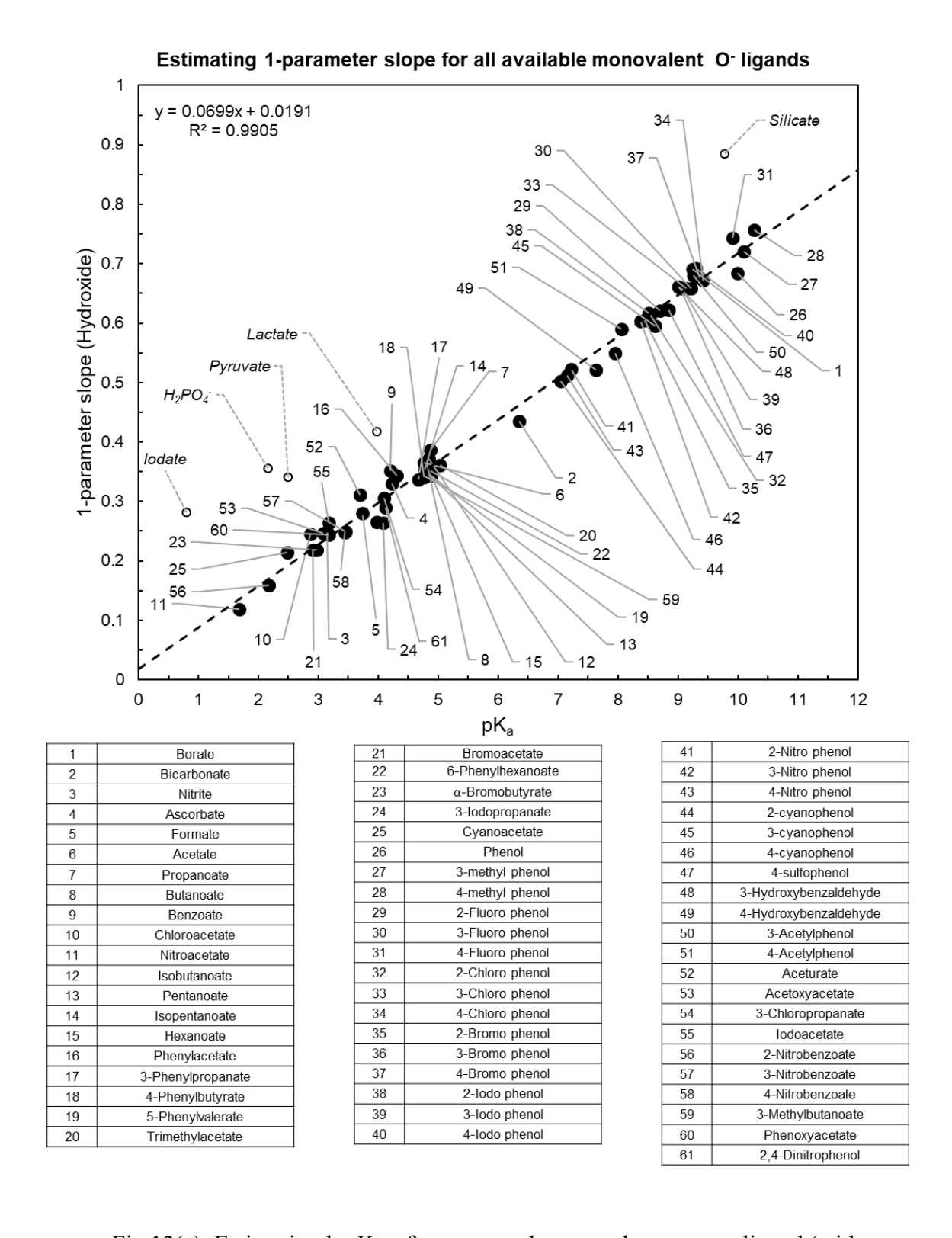


Fig 12(a). Estimating $logK_{ML}$ for any metal-monovalent oxygen ligand (with exceptions) from its pK_a using hydroxide correlations.

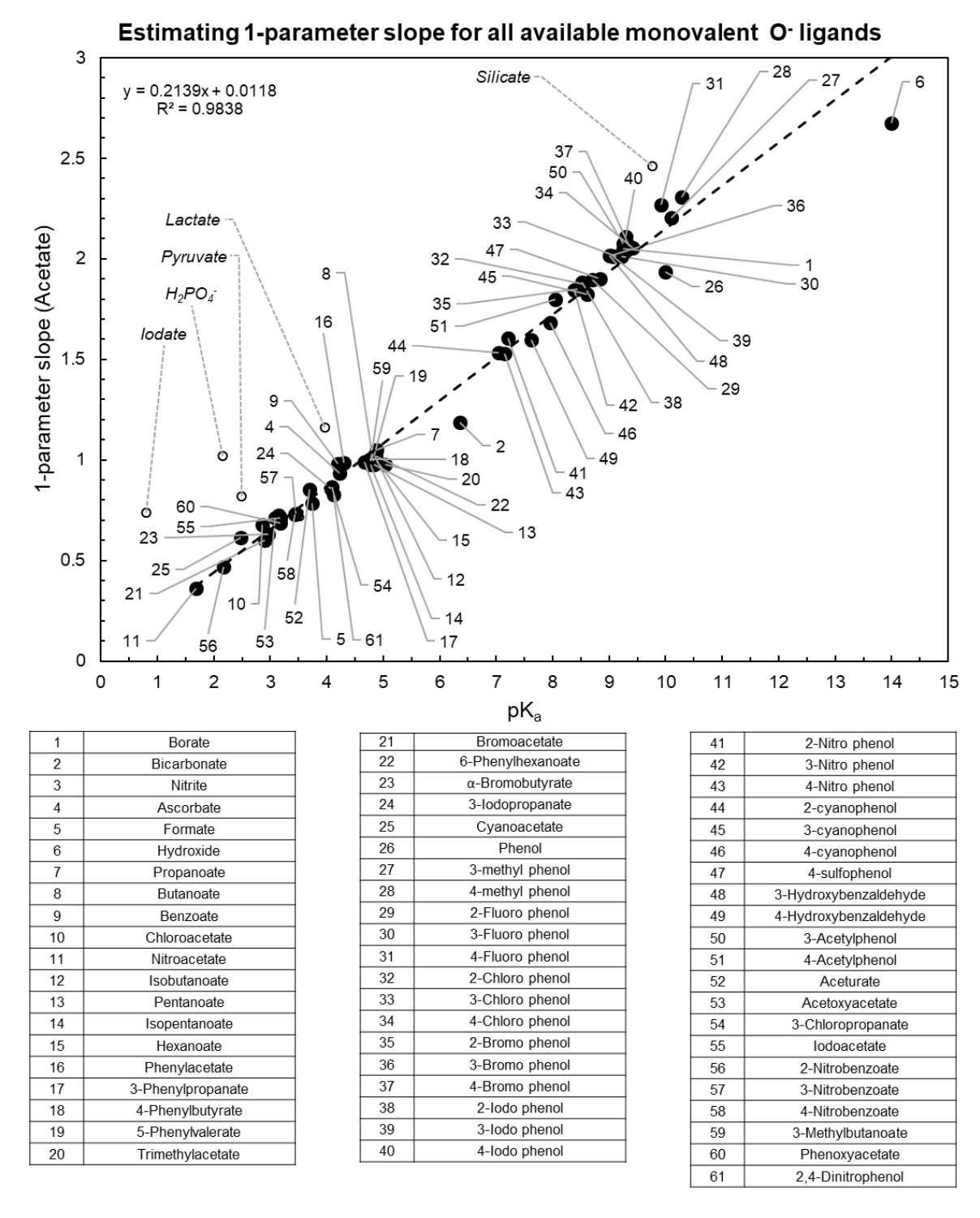


Fig 12(b). Estimating $logK_{ML}$ for any metal-monovalent oxygen ligand (with exceptions) from its pK_a using acetate correlations.

acetate correlations offered higher accuracy over the hydroxide correlations, a separate acetate correlation was made using only the data available from carboxylates (Fig. 11). Correlation between ligand pKa and 1-parameter hydroxide correlations are shown in Fig. 12(a) while those for 1-parameter acetate correlations are shown in Fig. 12(b). Ligands with additional functional groups like lactate and pyruvate were excluded from this correlation for reasons mentioned in the previous sections and such ligands were excluded from the estimation inventory. While Fig. 11 was adopted for carboxylates, Fig. 12(a) was used for the metal ions for which logK_{M-acetate} measurements are unavailable. Conversely, Fig. 12(a) was employed for phenols and aldehydes while Fig. 12(b) was used to for the metal ions without logK_{M-hydroxide} measurements. These correlations were used to make an additional 11,775 logK_{ML} estimates.

4.2 Estimating entropy of association at 25°C & 1 bar

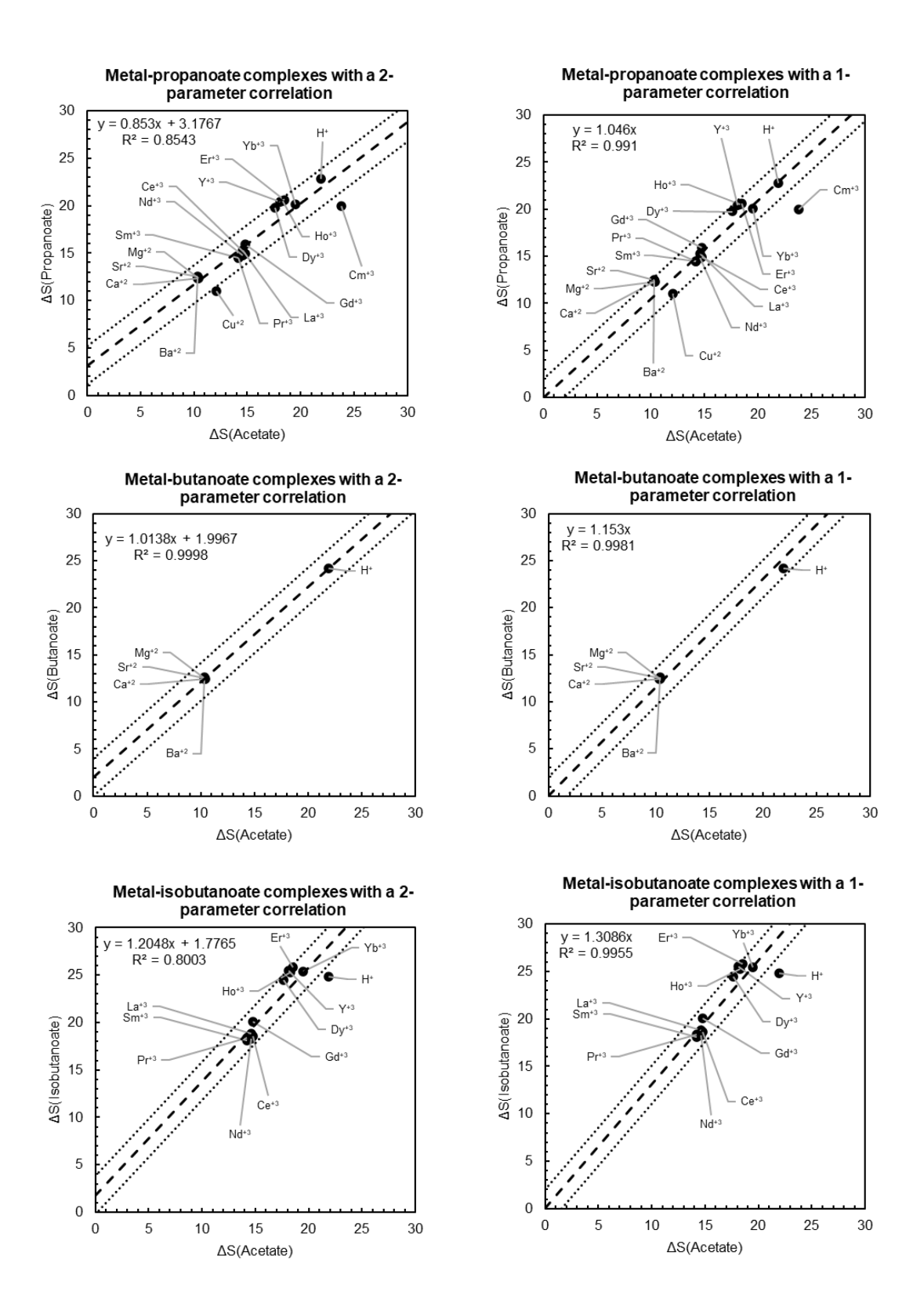
The strategy we developed to estimate metal-ligand complexation entropy is analogous to that for metal-ligand stability constants: *use the closest proxy ligand with the most data*. As with stability constants, entropy of association correlations for monovalent oxygen ligands can be broadly divided into carboxylates, phenols, and inorganic ligands. As the presence of additional coordinating groups can increase the metal-ligand reaction entropy via the 'chelate effect' (Martell & Hancock 1996), we considered ligands comprised of a single coordinating group. Since the standard state enthalpy (ΔH°), entropy (ΔS°) and Gibbs energy (ΔG°) of a reaction are related ($\Delta G^{\circ} = \Delta H^{\circ} - T \Delta S^{\circ}$), and the stability constant and Gibbs energy of reaction are related ($\Delta G^{\circ} = -2.303RTlogK$), knowing both the logK_{ML} and entropy of association yields the enthalpy of the complexation reaction. These three properties can be used to obtain the temperature dependence of log K using the van't Hoff equation in the form

$$logK(T) = \frac{-\Delta_r H^{\circ}_{Tr}}{2.303RT} + \frac{-\Delta_r S^{\circ}_{Tr}}{2.303R}$$
 (Eqn. 2)

to estimate the temperature dependence of stability constants from 0° to 125° C using the standard enthalpy and entropy of association at the reference temperature (Tr = 298.15K) and pressure (Pr = 1 bar). Holding the standard enthalpy and entropy of association constant implies that the heat capacity of association can be approximated by zero. While generally not suitable at temperatures higher than ~125°C, this relationship allows estimates at lower temperatures where changes in heat capacity of association are minimal (Shock and Koretsky, 1995; Prapaipong et al., 1999; Praipong & Shock, 2001). Resulting estimates of the temperature dependence of log K_{ML} cover the known temperature range of microbial life, an allow predictions of metal speciation throughout the temperature range of the known biosphere.

4.2.1 Estimating entropy of association for carboxylate complexes using experimental ΔS°_{ML} data

Investigation of the literature revealed only ten monovalent O-bearing ligands with entropy of association measurements for two or more metal ions: hydroxide, acetate, propanoate, butanoate, isobutanoate, chloroacetate, 3-chloropropanoate, formate, benzoate and phenylacetate. Analogous to the case of stability constants, hydroxide and acetate were the ligands with the most ΔS°_{ML} measurements (26 and 31 respectively) and hence, correlations were made using the respective sets of data. A lack of correlation between metal-hydroxide and metal-carboxylate entropy (not shown) suggested that hydroxide is a poor proxy ligand for carboxylate ligands. Instead, all carboxylates were observed to correlate closely with acetate even if a one-parameter relationship was used. These relations are illustrated in Fig. 13, which includes two-parameter and one-parameters fits side-by side for the eight organic-ligand entropy of association plotted



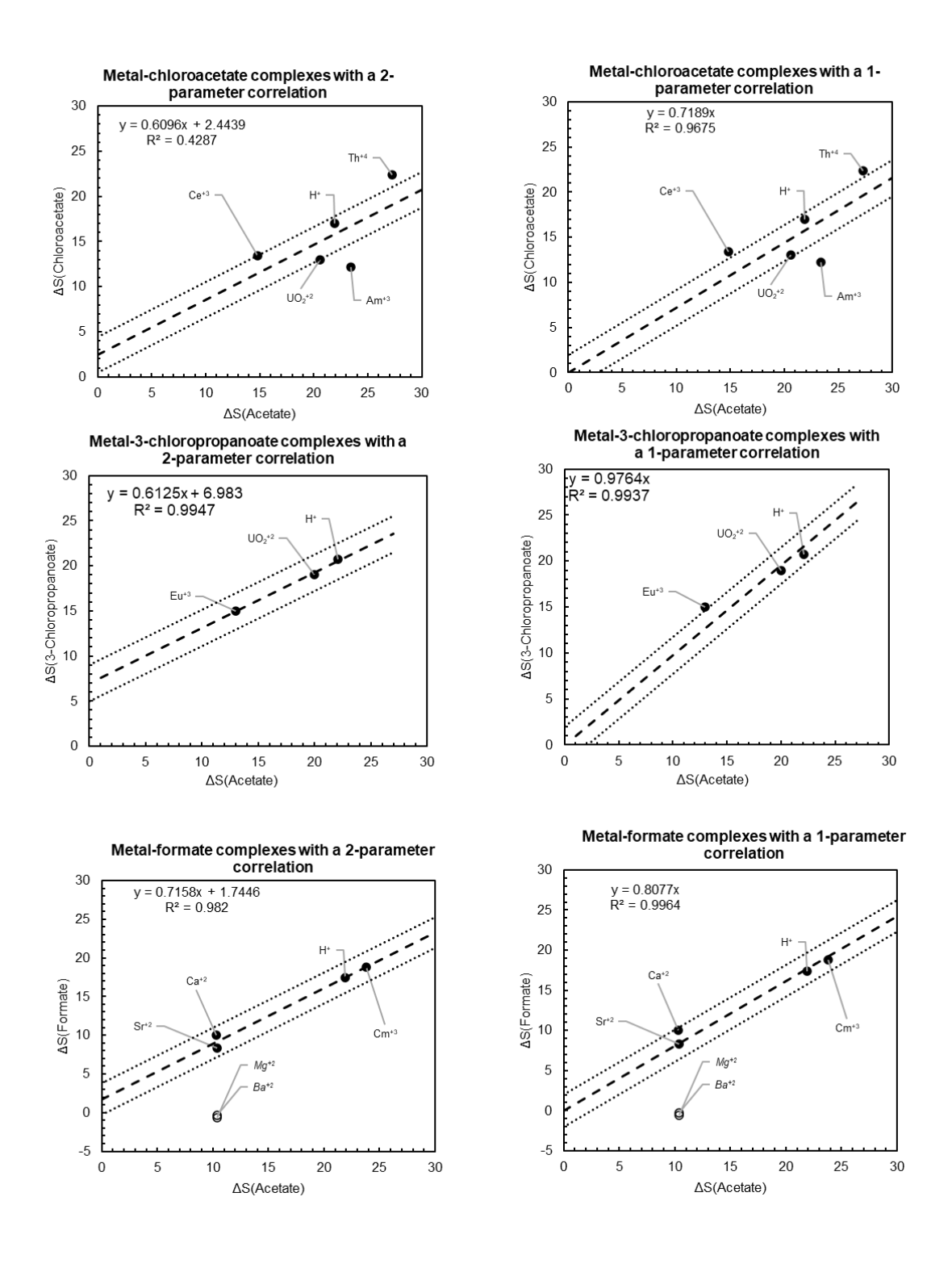


Fig 13. (contd.) Entropy estimates for metal-carboxylates with available data.

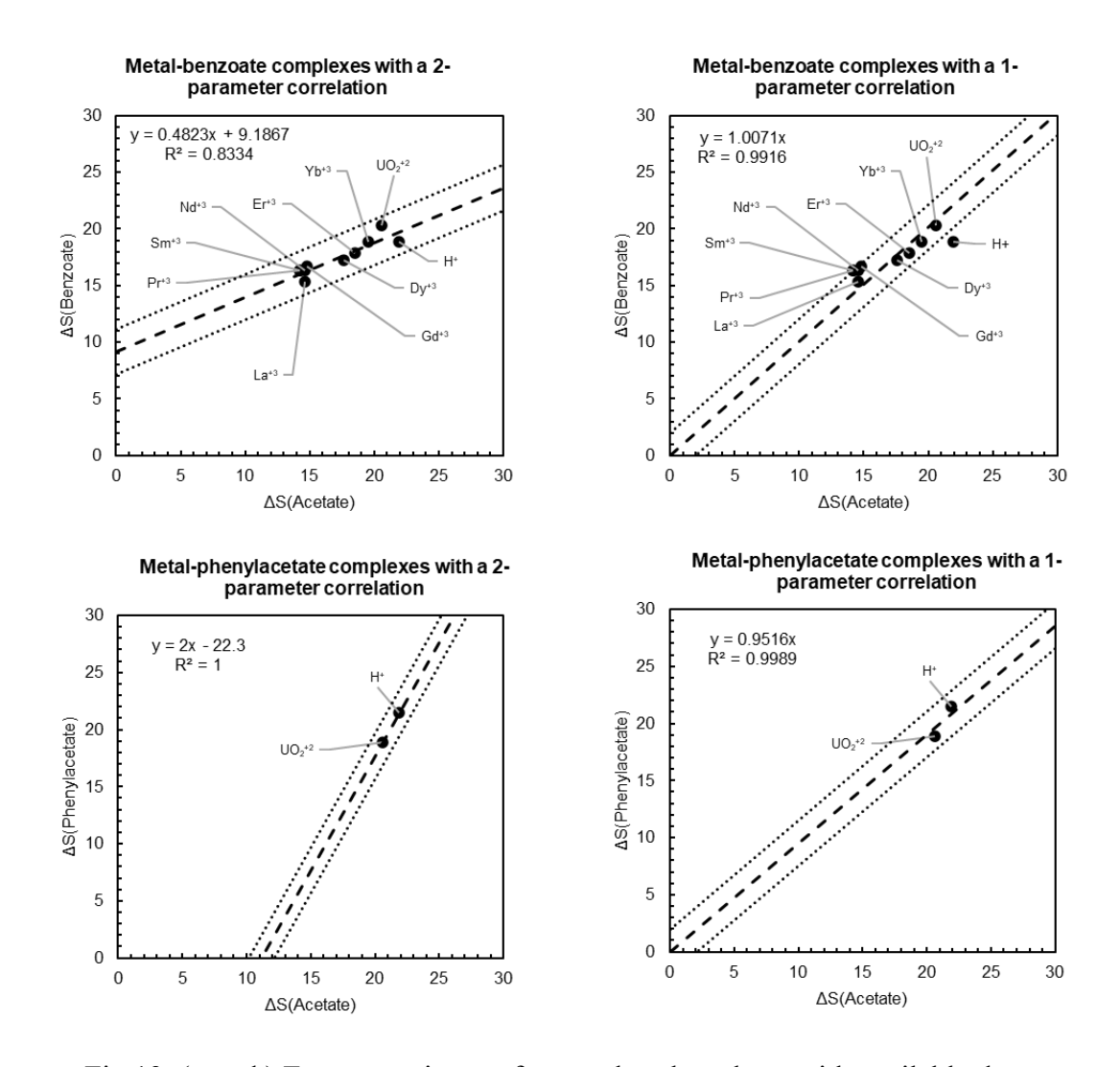


Fig 13. (contd.) Entropy estimates for metal-carboxylates with available data.

against those for acetate. Due to the limited availability of experimental values, using the 1-parameter correlations allows greater variety and number of estimates and precludes skewness of data. Despite the slight loss of accuracy, the one-parameter fit accommodates an induced uncertainty envelop of \pm 2 cal mol⁻¹ K⁻¹, which minimizes the resulting uncertainty in the calculated temperature dependence of log K.

4.2.2 Estimating entropy of association for carboxylate complexes using $\Delta S^{\circ}{}_a$ and pK_a data

As the experimental data for metal-ligand entropy of association is very limited, we explored correlations with ligand protonation entropy that was more prevalent. We found that the one-parameter slopes obtained from Fig. 13 exhibit a strong correlation with the ligand protonation entropy as shown in Fig. 14. The resulting correlation permits estimates of hypothetical slopes for one-parameter fits of ΔS°_{ML} against the corresponding property of acetate complexes for 43 ligands (listed in Fig. 15) for which only the protonation entropy (ΔS_a) is known, and can be used to estimate the ΔS°_{ML} values for any similar carboxylate ligand for which ΔS_a value may be available.

In addition to a relationship between ΔS_a and the 1-parameter entropy slopes, we also found a correlation between ΔS_a and pK_a for carboxylate ligands as shown in Fig. 15. While the correlation includes a variety of ligands, we excluded substituted benzoates as they deviated considerably from the correlation. We suspect that the presence of additional resonance structures may contribute to this observation. However, it should be noted that many of these ΔS_a values are based on single studies, which could benefit from additional experimental verification. Nonetheless, this correlation provides protonation entropy and 1-parameter slopes (from Fig. 14)

Metal-carboxylate entropy 1.5 y = 0.0571x - 0.1945 R² = 0.8416 1.4 Isobutanoate 1.3 Butanoate 3-Chloropropanate Propanoate Benzoate Formate Phenylacetate 0.7 Chloroacetate 0.6 0.5

Fig 14. Estimating 1-parameter slopes (acetate) from protonation entropy of the ligand. This correlation provides reasonable estimates of metal-carboxylate entropy when only protonation entropy is known.

ΔS_a (cal/mol/K)

22

23

24

25

26

27

28

29

30

15

16

17

18

19

20

21

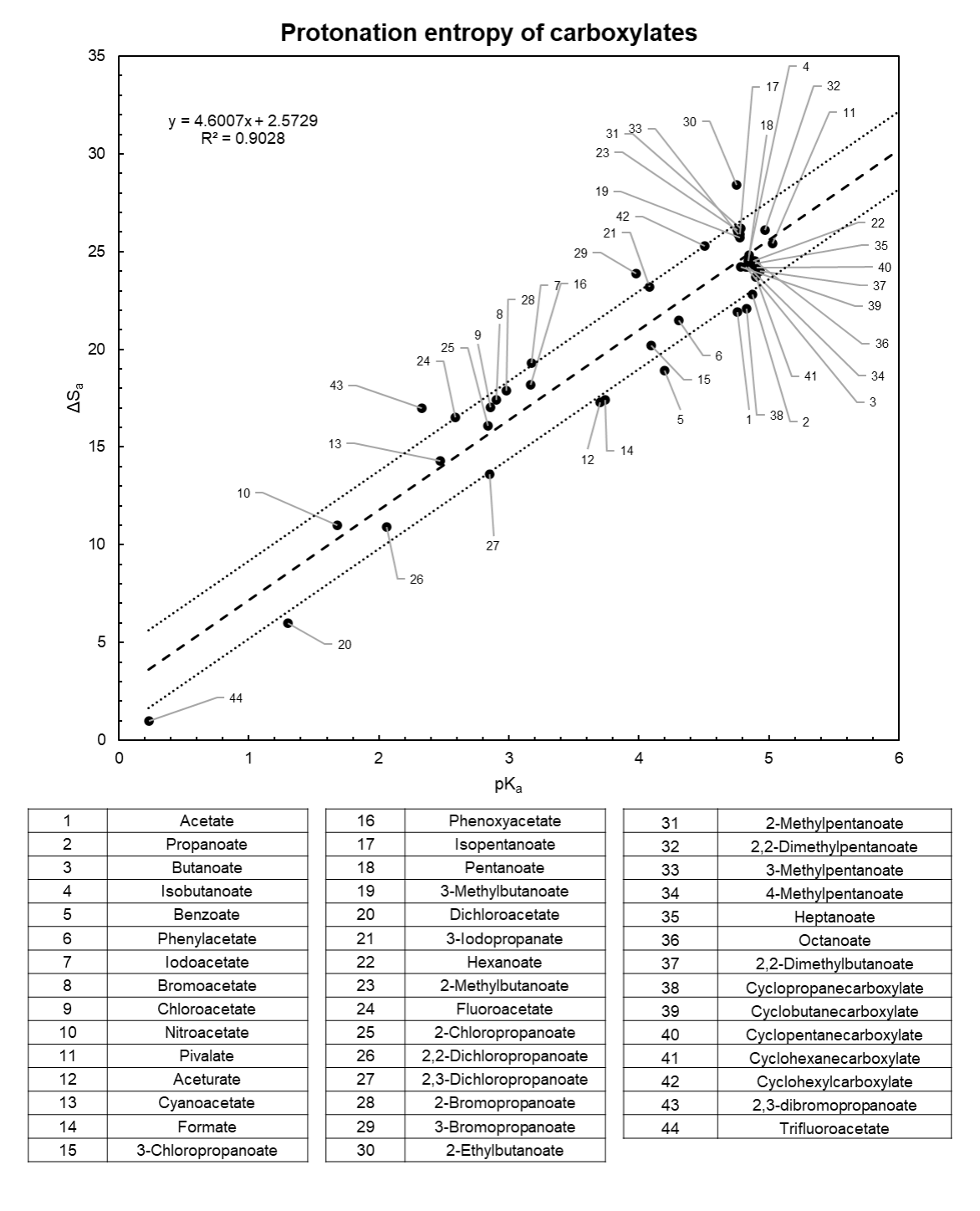


Fig 15. Correlation between protonation entropy and protonation stability constant for carboxylates.

for 67 additional carboxylate ligands for which only pK_a is known (see Supplementary Table for more details). These correlations help us estimate an additional 2077 ΔS°_{ML} values.

4.2.3 Estimating entropy of association for phenol complexes using experimental ΔS°_{ML} data

While ΔS°_{ML} measurements are rare for carboxylates, this information was even sparser for metal-phenol complexes. However, the correlations between experimental metal-ligand complexation entropy, ligand protonation entropy and metal-hydroxide complexation entropy suggests that metal-phenol ΔS°_{ML} values can be estimated in a manner analogous to metal-carboxylate complexation entropy albeit with a slight loss of accuracy.

The available experimental metal-phenol complexation entropy data only consisted of a 11 ferric-phenol complexes. As hydroxide was the proxy ligand of choice for phenol stability constant estimation, we chose hydroxide as the proxy ligand for ΔS°_{ML} estimation as well. We correlated these values along with the ligand protonation entropy with metal-hydroxide complexation entropy using 1-parameter correlations in Fig. 16 similar to carboxylate correlations in Fig. 13. As may be seen from the figure, only a few correlations are able to predict ΔS°_{ML} within the acceptance threshold of ± 5 cal mol⁻¹ K⁻¹. While we realize that these correlations individually do not suggest a strong relationship, the collective trend over these 11 correlations along with the overall estimation strategy in this work gives us confidence that these correlations may be used to obtain approximate values of metal-ligand complexation entropy. We highly encourage experimental investigations in this regard that can help us evaluate these correlations. The 1-paramater slope values from these correlations were used to estimate ΔS°_{ML} of 297 additional complexes (see Supplementary Table for details).

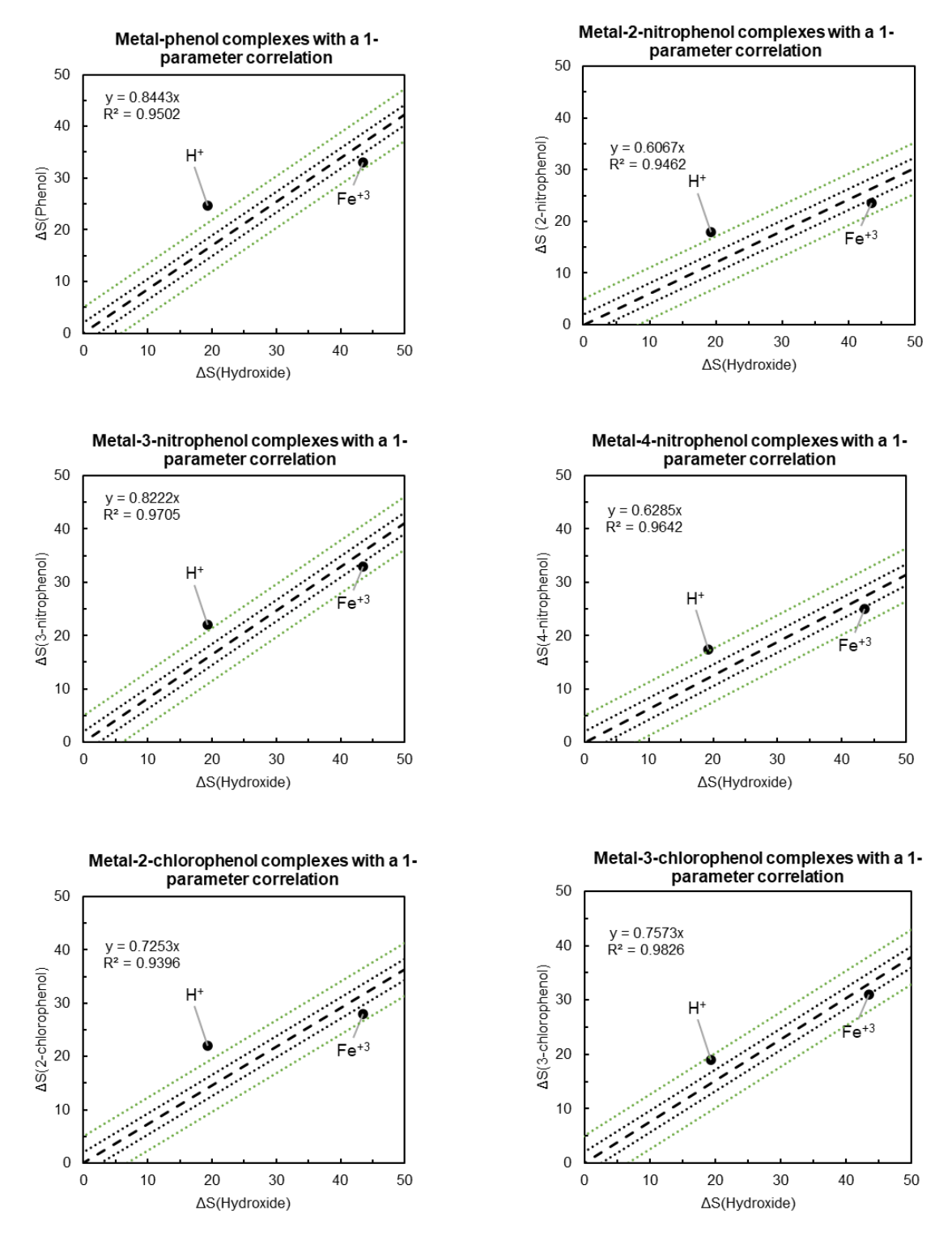


Fig 16. 1-parameter estimation for metal-phenol complexation entropy with available data. Dashed line represents the best fit line. Black dotted line represents uncertainty envelope of ±2 cal.mol⁻¹.K⁻¹. Green dotted line represents uncertainty envelope of ±5 cal.mol⁻¹.K⁻¹. (contd.)

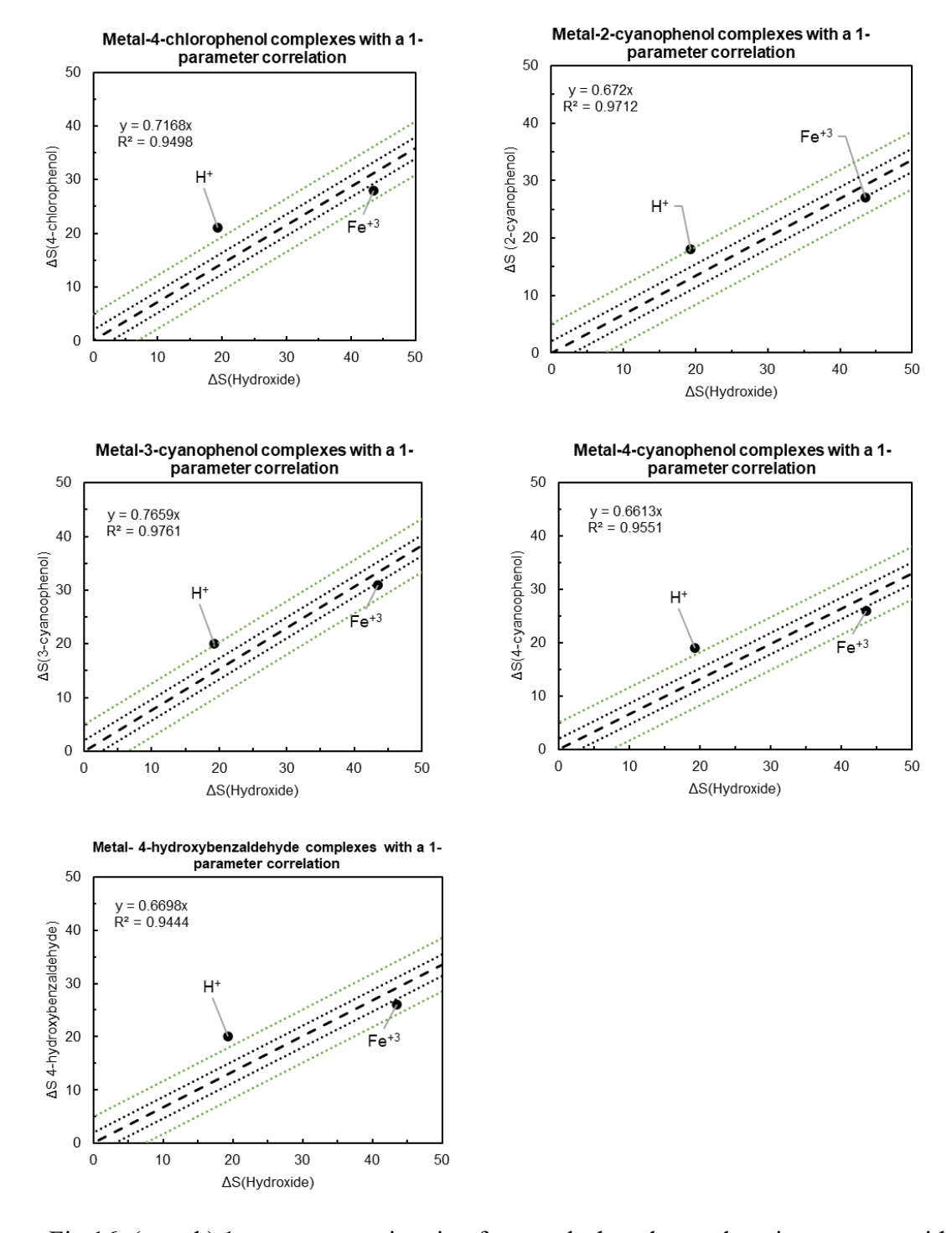


Fig 16. (contd.) 1-parameter estimation for metal-phenol complexation entropy with available data. Dashed line represents the best fit line. Black dotted line represents uncertainty envelope of ± 2 cal.mol $^{-1}$.K $^{-1}$. Green dotted line represents uncertainty envelope of ± 5 cal.mol $^{-1}$.K $^{-1}$.

4.2.4 Estimating entropy of association for phenol complexes using experimental ΔS°_a and pK_a data

Analogous to carboxylates, we explored methodologies to estimate metal-phenol complexation entropy using ΔS_a and pK_a as experimental data for these values was more prevalent in the literature. In Fig. 17, we obtained a strong relationship between ferric-phenol complexation entropy with phenol protonation entropy that enabled use to estimate ΔS°_{ML} values for 22 ferric complexes. Analogous to the methodology of Section 4.2.3, we then used metal-hydroxide complexation entropy and ferric-hydroxide complexation entropy to estimate 594 additional ΔS°_{ML} values.

Additionally, we found a close relationship between ΔS_a and pK_a values for phenols as shown in Fig. 18 analogous to that for carboxylates albeit with different slope and intercept, as demonstrated in Fig. 19. This relationship helped us estimate ΔS_a values for 34 additional phenols for which only pK_a values were available. We then used the relationship between $\Delta S_{Fe-Ligand}$ and ΔS_a from Fig. 17 and the methodology described above to estimate ΔS^o_{ML} values of 952 metal-phenol complexes.

4.2.5 Estimating entropy of association for inorganic O-complexes

As hydroxide was the closer proxy ligand for silicate in $logK_{ML}$ estimation, we used metal-hydroxide complexation entropy to estimate corresponding metal-silicate ΔS°_{ML} values. Support for this approach is offered by the correlation for metal-silicate complexes shown in Fig. 20. While this correlation does not yield estimates of ΔS°_{ML} within ± 2 cal mol⁻¹ K⁻¹, it does yield estimates within ± 5 cal mol⁻¹ K⁻¹. Metal-hydroxide complexation entropy were also used to

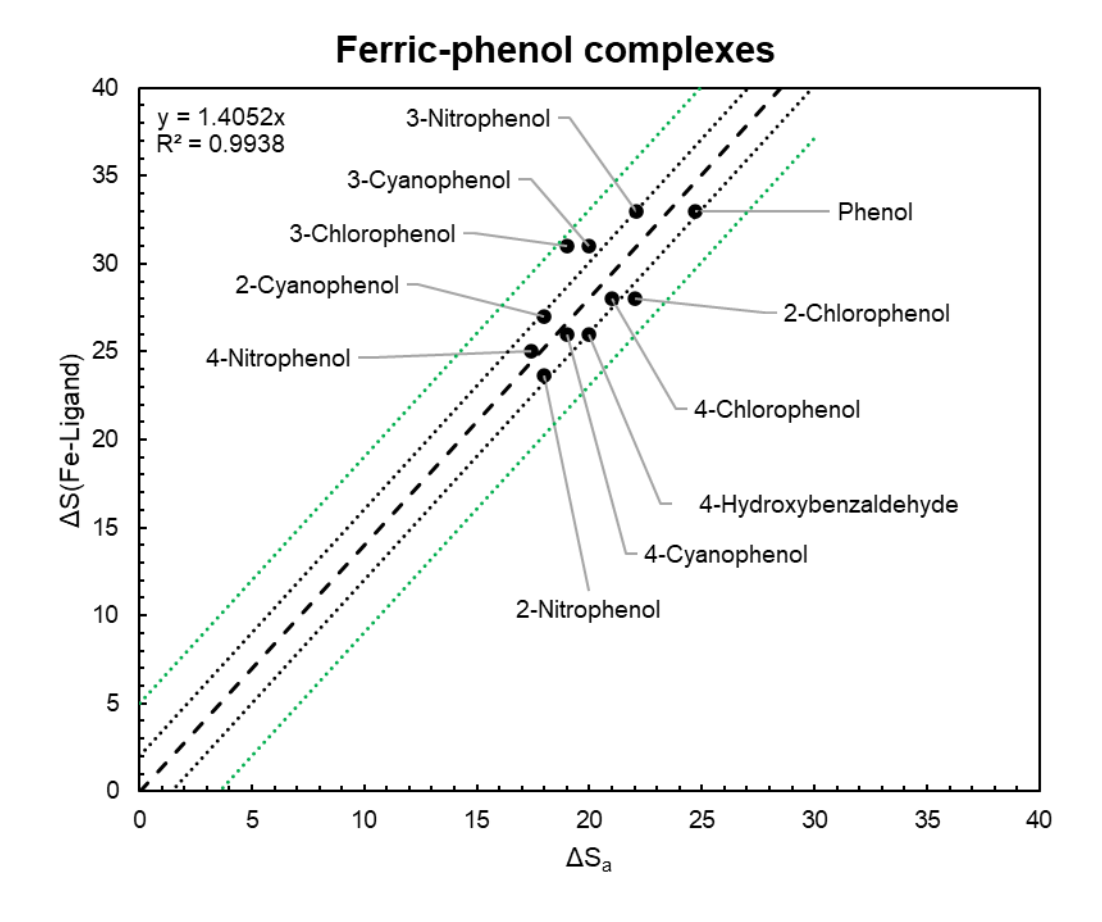


Fig 17. 1-parameter correlation between ferric-phenolate complexation entropy with phenol protonation entropy. Dashed line represents the best fit line. Black dotted line represents uncertainty envelope of ± 2 cal.mol $^{-1}$.K $^{-1}$. Green dotted line represents uncertainty envelope of ± 5 cal.mol $^{-1}$.K $^{-1}$.

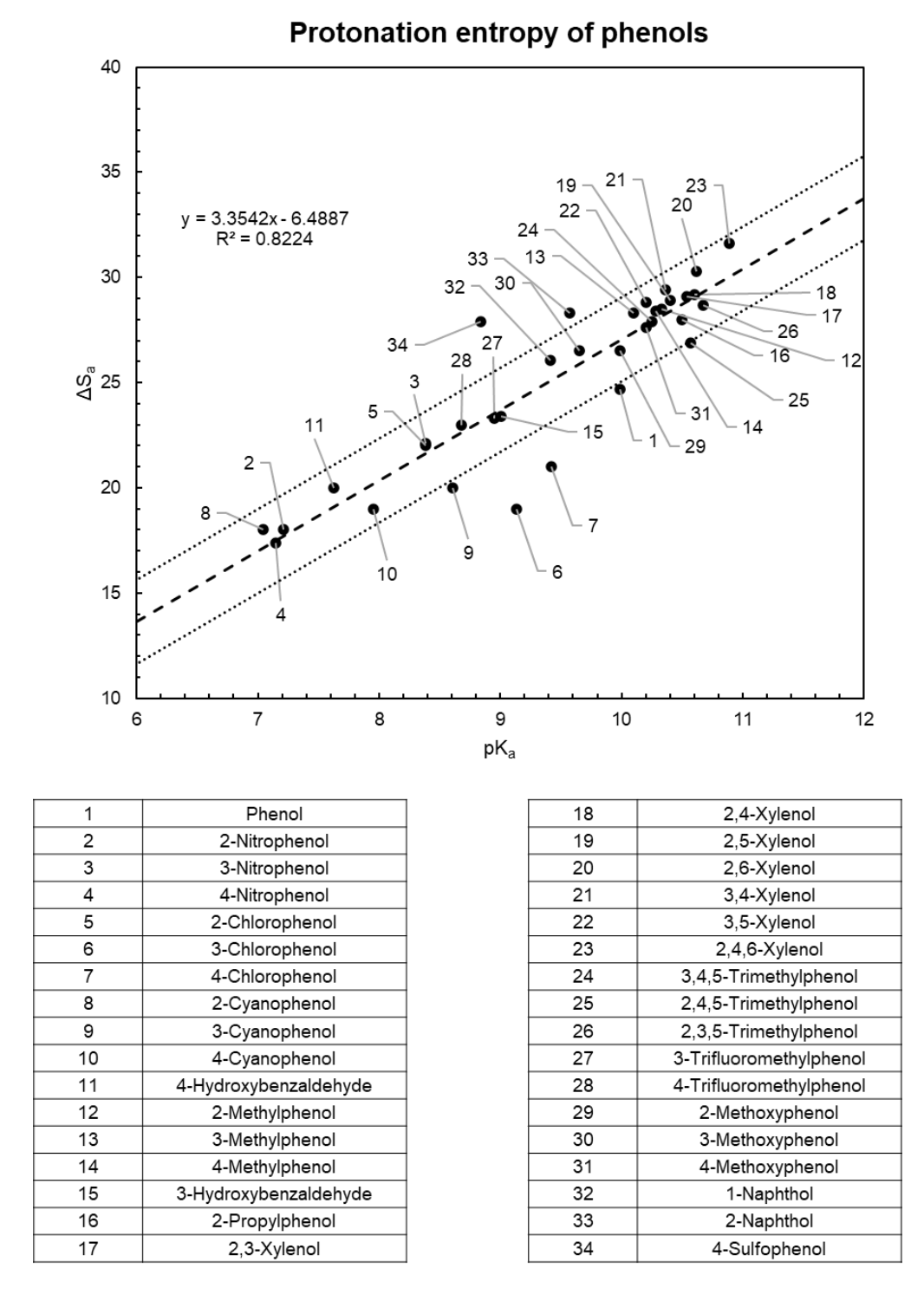


Fig 18. Correlation between protonation entropy and protonation stability constant for phenols.

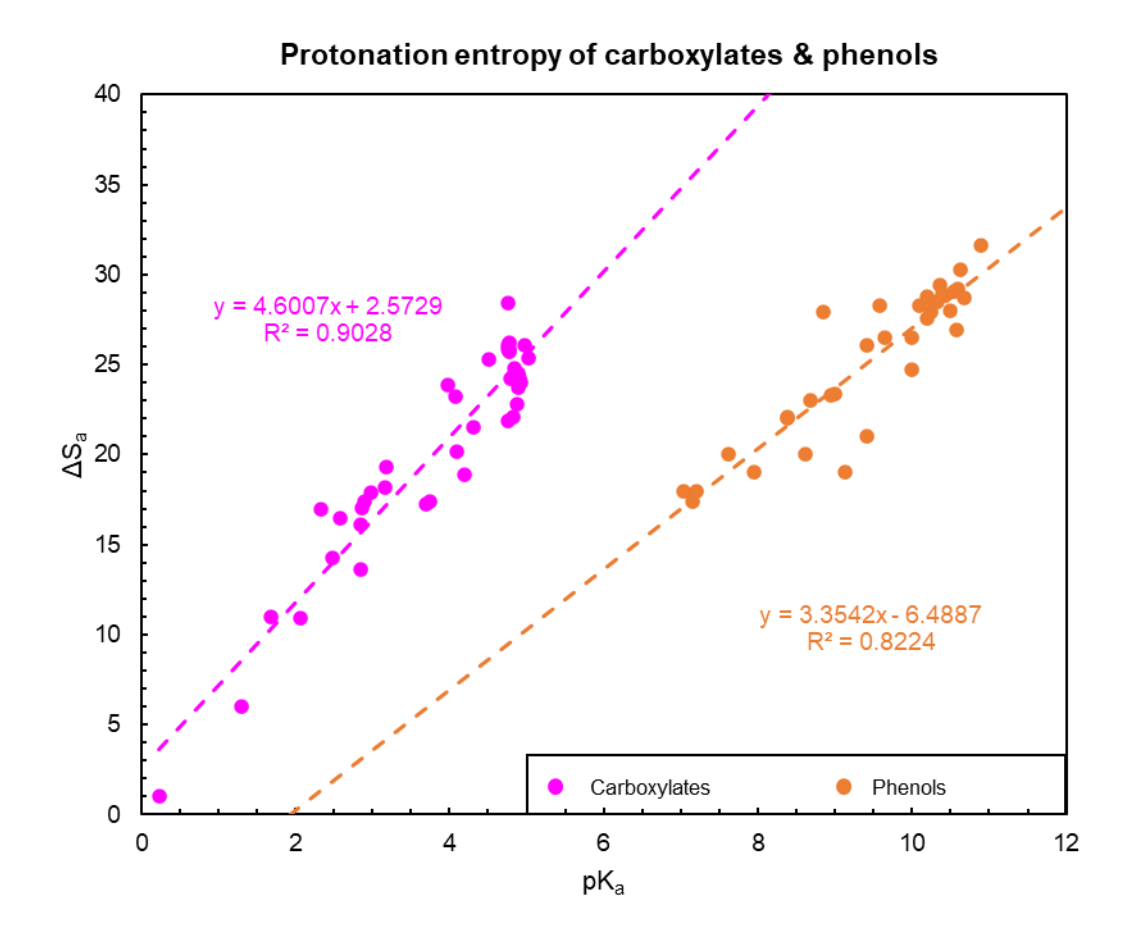
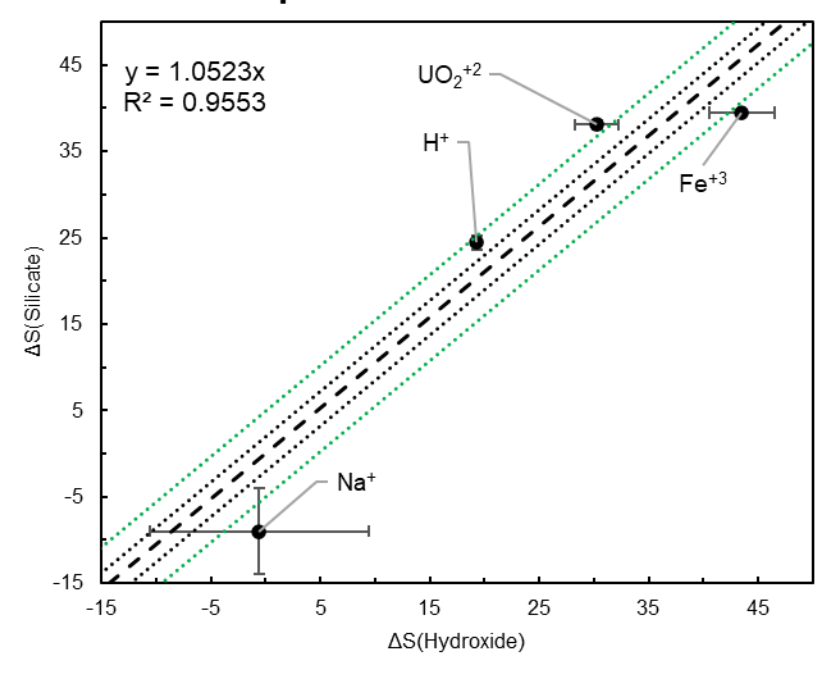


Fig 19. Correlation between protonation entropy and protonation stability constant for carboxylates and phenols. As can be seen from the slopes and intercepts, the relationship is different for the two categories of monovalent O ligands.

Metal-silicate complexes with a 1parameter correlation



Metal-nitrite complexes with a 1parameter correlation

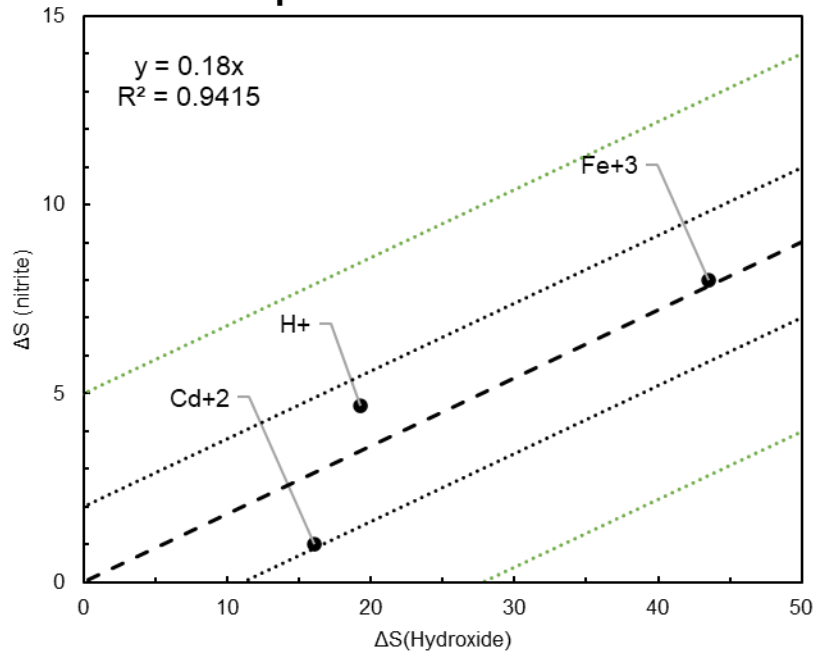


Fig 20. 1-parameter estimation for entropy of metal-inorganic complexes with available data. Error bars refer to experimental uncertainty reported in original papers. Dashed line represents the best fit line. Black dotted line represents uncertainty envelope of ± 2 cal.mol⁻¹.K⁻¹. Green dotted line represents uncertainty envelope of ± 5 cal.mol⁻¹.K⁻¹.

estimate metal-nitrite ΔS°_{ML} values as the correlation was based on three experimental values in comparison to the two values for acetate complexes and is therefore expected to be more robust.

5. Discussion

To evaluate the implications of our estimates of stability constants and standard entropy changes at 25°C and 1 bar, we have obtained the temperature dependence of stability constants and simulated metal speciation in three geochemically relevant systems where our estimations can be directly applied. The first sub-section (Section 5.1) includes logK extrapolations up to 125 °C that were obtained using the van't Hoff equation for a wide category of metal-ligands complexes - complexes for which both experimental log K_{ML} and ΔS°_{ML} were available, complexes for which only experimental log K_{ML} and ΔS_{a} were available, complexes for which only pK_a and ΔS_{a} are available, and metal-ligand complexes for which only pK_a values are available. In the next subsection (Section 5.2), we have obtained metal speciation calculations for one experimental system that serves as a model for hydrothermal redox reactions and two mixing fluids of seafloor hydrothermal systems that have the capacity for abiotic generation of O⁻ ligands. The examples discussed here are but few of the multifarious applications where these estimates may be used and we highlight some of these in Section 5.3.

5.1 Temperature dependence of stability constants

5.1.1 Metal-carboxylate complexes

 ΔS°_{ML} values for eight geobiologically relevant metal ions (Al⁺³, Na⁺, Fe⁺³, Fe⁺², Zn⁺², Ba⁺², La⁺³ and Th⁺⁴), either obtained from the literature or estimated from Fig. 13 from experimental $\Delta S^{\circ}_{M-Acetate}$ values, together with experimental or estimated logK_{ML} values, were

used to obtain the van't Hoff plots as per Eqn. 2 as shown in Fig. 21 (details in Supplementary Tables). Since no experimental measurement for the ferric-acetate complexation entropy was found, a value of 29.42 cal mol⁻¹ K⁻¹ was estimated using the benzoate correlation in Fig. 13 and the experimental $\Delta S^{\circ}_{M\text{-Benzoate}}$ of 29.63 cal mol⁻¹ K⁻¹ reported by Basaran et al. (1994). We have not included such second-order estimates in the Supplementary Tables as they might have higher uncertainty, but provisional values can be obtained when no experimental data exists. For most metal ions, stability constants increase with temperature while for very few metals like Fe⁺², $log K_{ML}$ decreases with temperature. This arises from the low ΔS°_{ML} value for ferrous-acetate, which results in a negative enthalpy of association in comparison to the endothermic values for other complexes. Using this same argument we predict that the K⁺-carboxylate complexes will have a trend similar to that of the ferrous complexes. It is perhaps worth noting that ligands with disparate 1-parameter slopes like isobutanoate and chloroacetate (see Fig. 14) exhibit contrasting temperature dependences, whereas those with similar 1-parameter slopes such as propanoate and phenylacetate have similar predicted log K_{ML} trends. It is perhaps also worth noting here that these van't Hoff plots include metal-ligand complexes for which both logK and ΔS°_{ML} values were experimentally obtained (for example Ba⁺² & La⁺³-propanoates) and those for which both values were estimated (for example Ba⁺² & La⁺³-phenylacetates).

Consequences of estimating the temperature dependence of log K_{ML} for diverse carboxylates are illustrated in Fig. 22, which shows predictions for zinc and ferrous complexes of three carboxylates for which only the protonation entropy are known. These ligands were selected because they offer a wide range of ΔS°_{a} values that correspondingly yield disparate 1-parameter slopes based on the relationship in Fig. 14. Zinc and ferrous ions were selected for this comparison as they have similar log K_{ML} values at 25°C and 1 bar. As can be seen in Fig 22, the

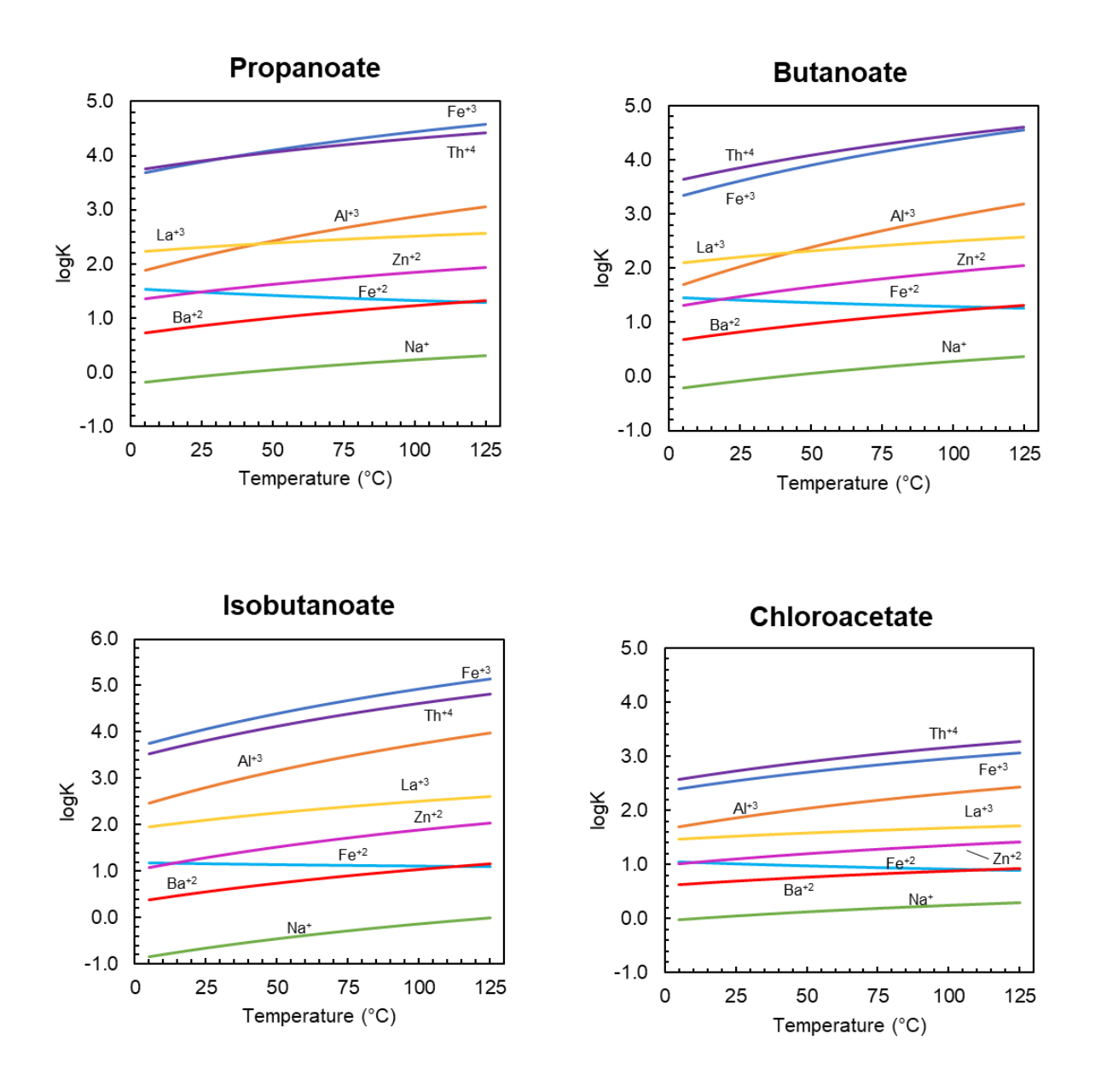


Fig 21. Van't Hoff plots displaying temperature dependence of metal-carboxylate stability constants using 1-parameter entropy estimates from Fig. 13 (contd.)

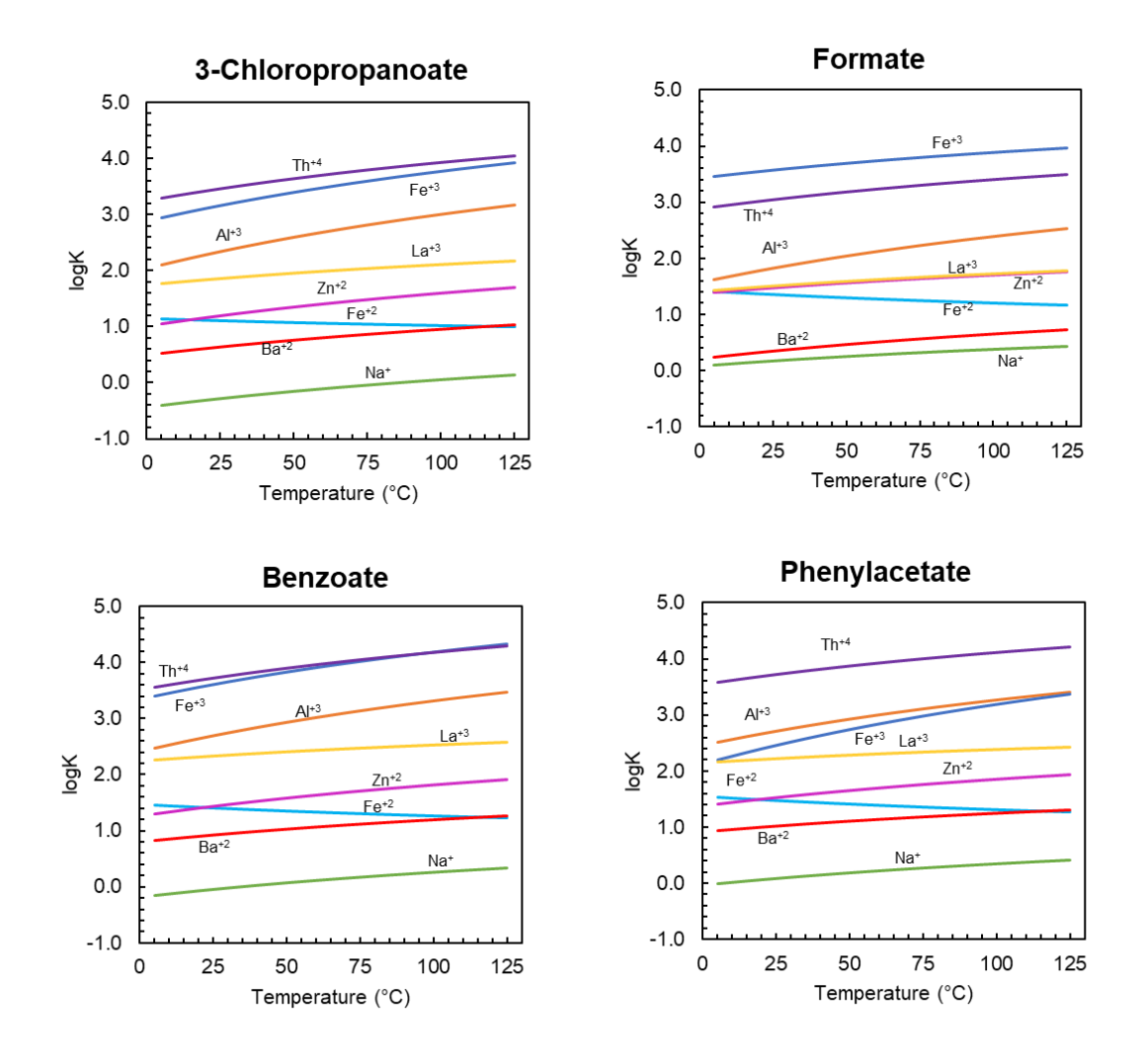


Fig 21. (contd.) Van't Hoff plots displaying temperature dependence of metal-carboxylate stability constants using 1-parameter entropy estimates from Fig. 13.

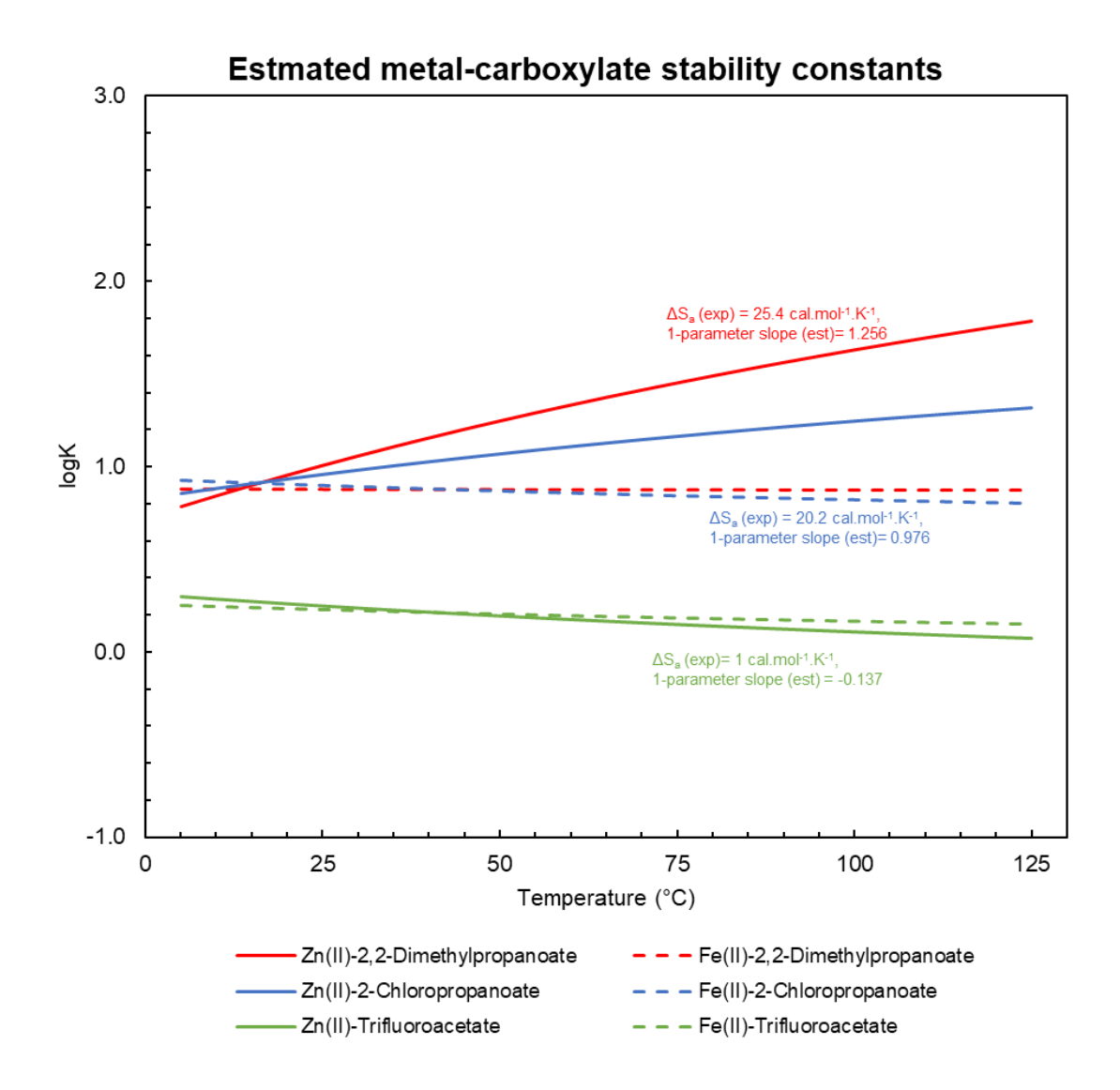
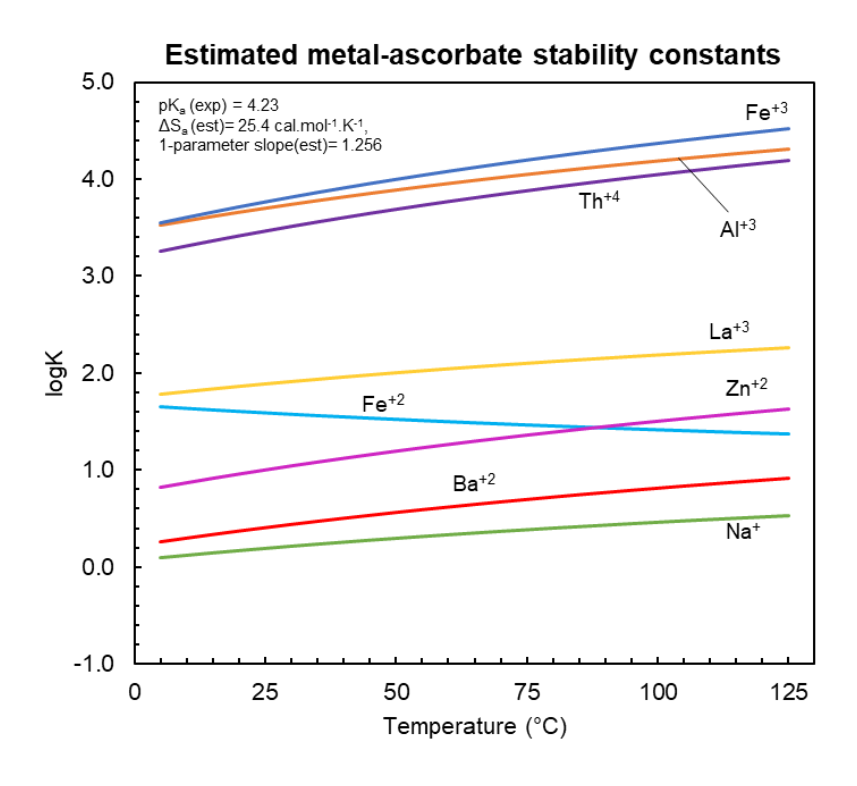


Fig 22. Van't Hoff plots for select metal-carboxylate complexes created using only the ligand protonation entropy from relationship obtained in Fig. 14.

predicted temperature dependences of the association constants for the zinc complexes (solid curves) differ starkly for the three ligands: logK_{ML} increases with temperature for zinc-2,2-dimethylpropanoate and chloroacetate complexes, but decreases for zinc-trifluoroacetate complexes. This range of differences is a direct consequence of the greater protonation entropy of 2,2-dimethylpropanoate compared to the lesser protonation entropy of trifluoroacetate. Note that this disparate temperature dependence is not exhibited by predictions for the ferrous complexes, which is a direct consequence of the low entropy of the ferrous-acetate complex.

There are many monovalent O-bearing ligands for which minimal experimental data exist yet their capacity to form complexes with metals may influence geochemical or biological processes. As examples, we focus here on two biologically relevant carboxylates for which no experimental entropy of association data exist: ascorbate, better known as vitamin C, which is an essential biological nutrient, and valproate, which is a prominent epilepsy drug. Predicted association constants for these ligands and the metals used in Fig 21 are shown in Fig 23. Stability constants for ascorbate were estimated using the LFER shown in Fig. 5 while those for valproate were estimated using the 1-parameter slope predictor from Fig. 11. The corresponding ΔS°_{ML} values were estimated from experimental pKa values using correlations developed in Figs. 15 and 14. As can be seen in Fig 23, $\log K_{ML}$ increases with increasing temperature for almost all metal ions except the ferrous ion similar to most carboxylates shown in Fig. 21. This is a consequence of the fact that the pKa values for these ligands are similar to the ligands considered in the construction of Fig. 21. In addition to the two ligands considered here, such plots can be obtained for 68 additional ligands.

5.1.2 Metal-phenol complexes



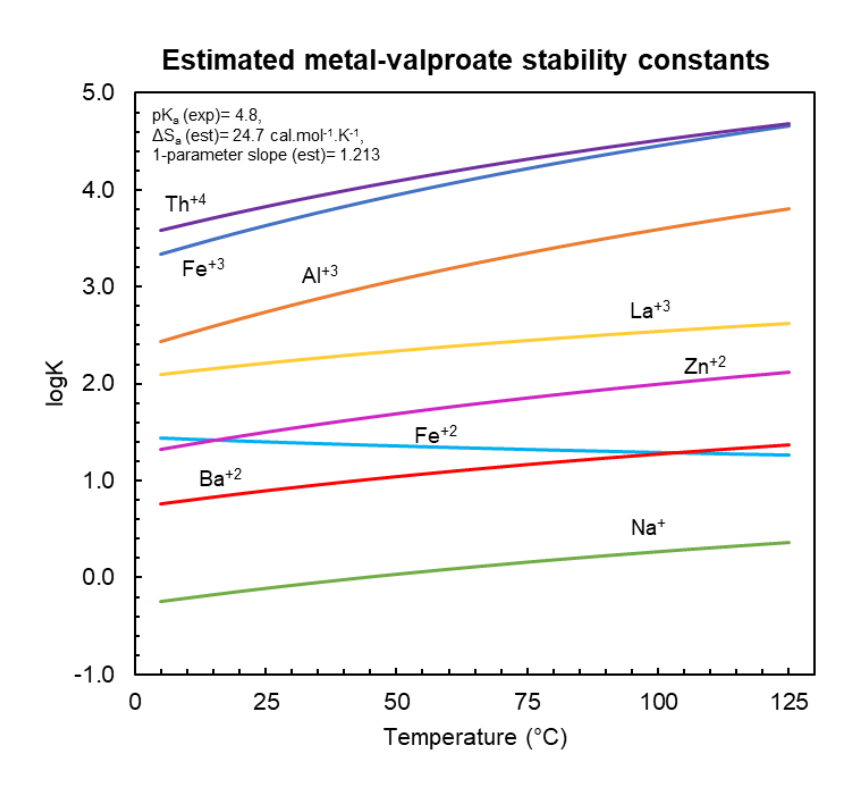


Fig 23. Van't Hoff plots created using only the carboxylate ligand protonation constant from relationship obtained in Fig.15 & Fig.14.

Similar plots can be generated for metal-phenol complexes. Those for ferric-phenol complexes shown in Fig. 24 were generated using the experimentally obtained logK and ΔS°_{ML} values available in the literature. Note that even though the ΔS°_{ML} values for ferric-phenols are similar to those of the carboxylates, the temperature dependence of the stability constants gently decreases rather than increasing, which is due to a difference in the sign in the corresponding enthalpies of association. Analogous curves were generated for ferric complexes of six other phenols for which only pKa and ΔS°_{a} are known, as shown in Fig. 25. In these cases we estimated logKFe(III)-L using the correlation shown in Fig. 12(a) and $\Delta S^{\circ}_{Fe(III)-L}$ with the correlations in Fig. 16. As in the case of the curves shown in Fig. 24, stability constants for most ferric-phenol complexes in this figure decrease somewhat with increasing temperature. The rather constant nature of stability constants in the case of 2,4,6-trimethylphenol is consistent with it having the least negative enthalpy of association of this set of predicted values.

As mentioned above, experimentally determined entropy of association for metal-phenol complexes are scarce. Nevertheless, it is possible to make estimates using methods outlined above even in cases where only pK_a values are known. Examples are shown in Fig. 26 for association of the metal ions 2,4,6-trinitrophenol and 2-methoxy-4-methylphenol, which were selected as they have the lowest and the highest pK_a values, respectively, for this category of ligands. Additionally, 2,4,6-trinitrophenol can enter the environment through human activities owing to its use as an explosive and antiseptic agent. As in the case of the estimates shown in Fig. 24, these stability constant predictions were obtained using the correlation shown in Fig. 12(a), and a combination of the correlations shown in Figs. 17 and 18 to obtain the corresponding $\Delta S^{\circ}_{Fe(III)-L}$ values. The remaining ΔS°_{ML} values were obtained by multiplying metal-hydroxide entropy of association with corresponding $\Delta S^{\circ}_{Fe(III)-Hydroxide}$ values.

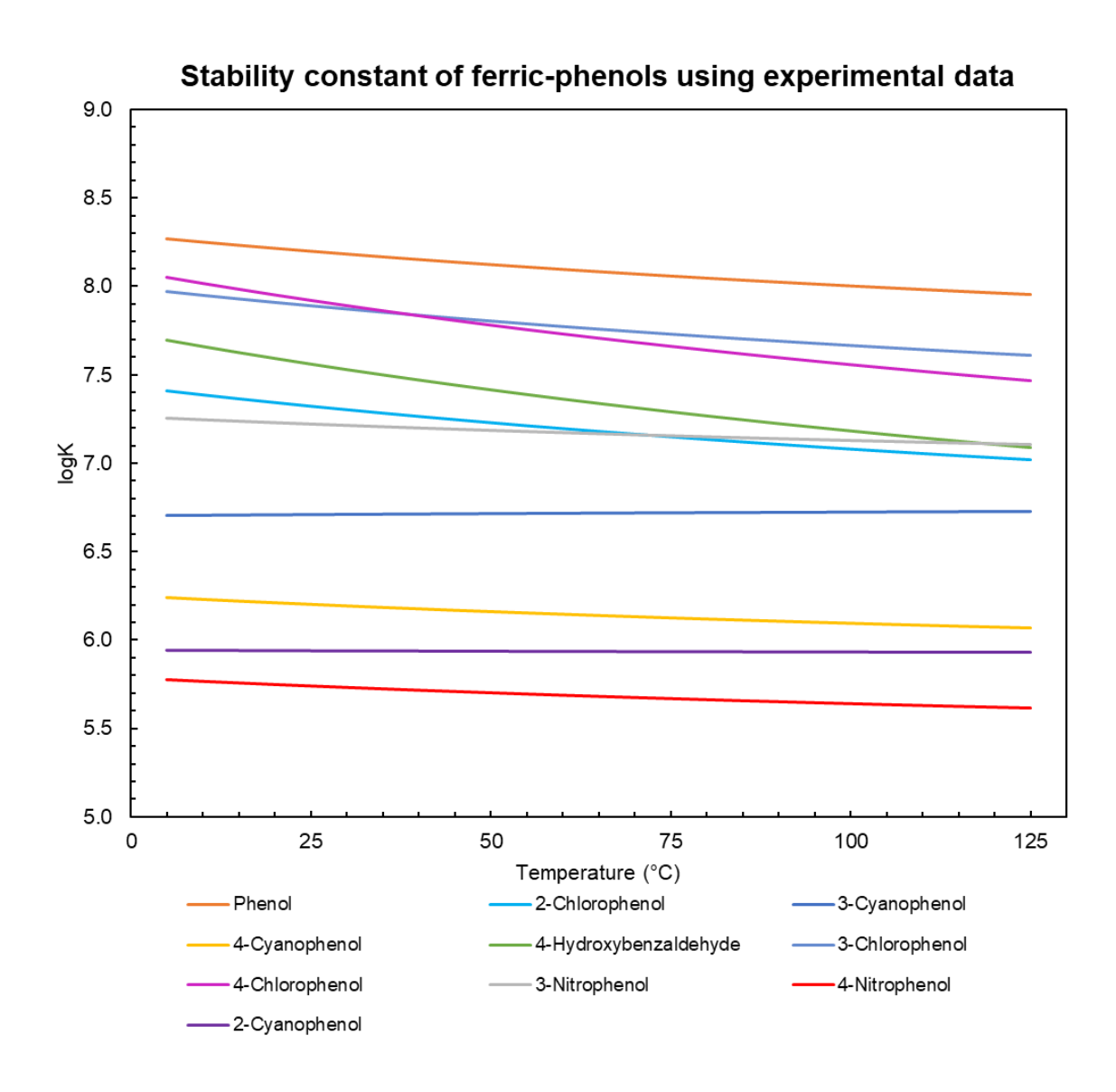


Fig 24. Van't Hoff plots displaying temperature dependence of ferric-phenol stability constants using 1-parameter entropy estimates from Fig.16 and $\Delta S_{M-Hydroxide}$ from Supplementary Table.

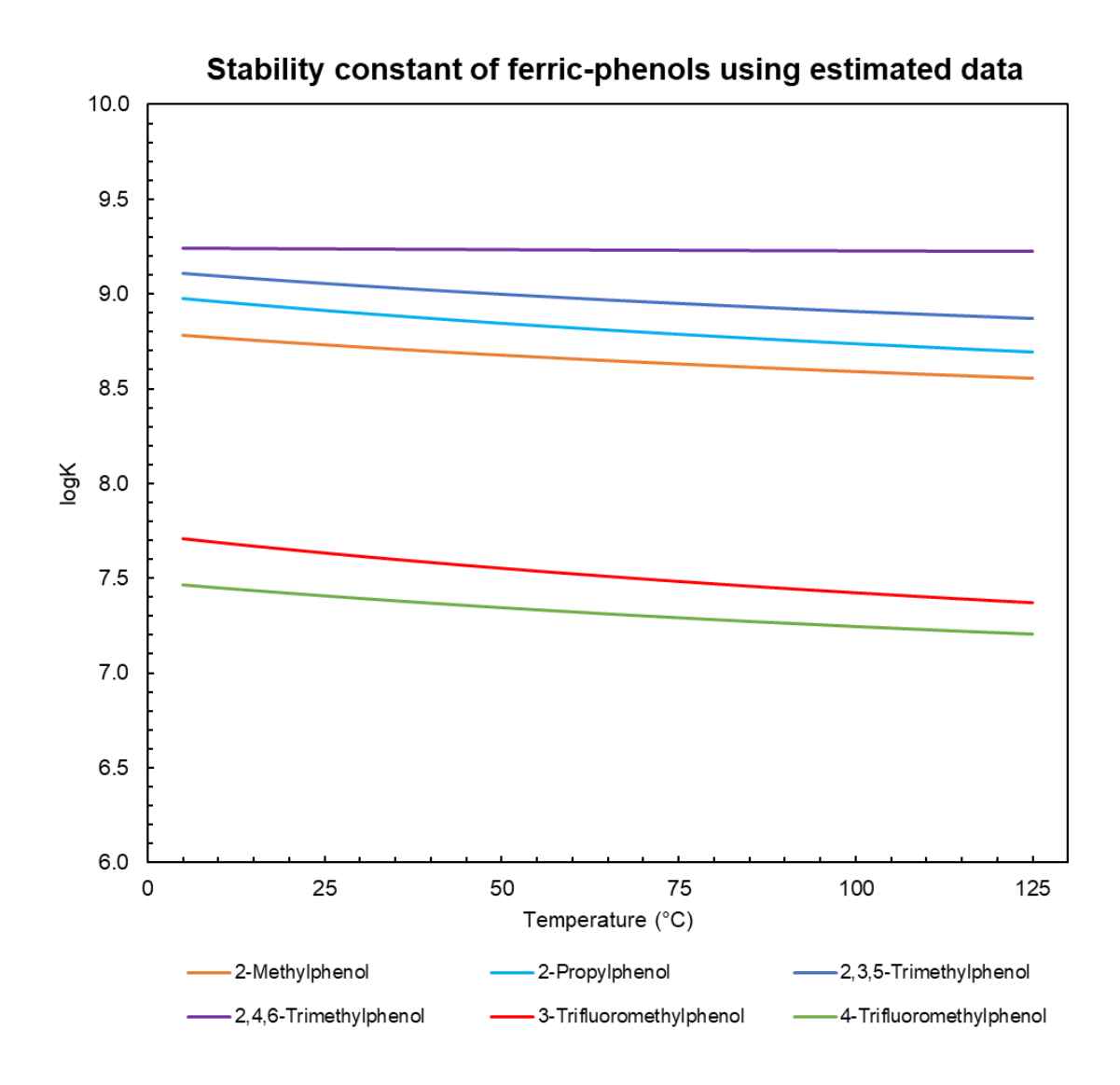


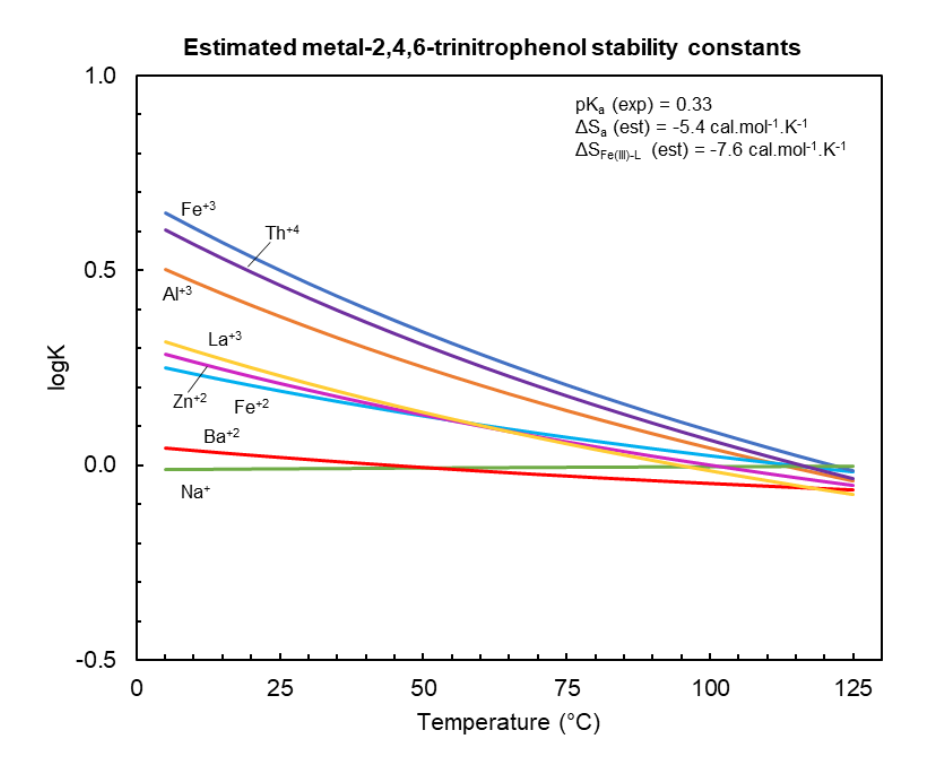
Fig 25. Van't Hoff plots created using only protonation thermodynamics of phenols. Stability constants were estimated from Fig.12(a) and entropy was estimated using correlation in Fig.17 and $\Delta S_{M-Hydroxide}$ from Supplementary Table

As can be seen from Fig. 26, we predict a drastic change in the temperature dependence of 2,4,6-trinitrophenol and 2-methoxy-4-methylphenol complexes owing to the \sim 10 orders in magnitude of difference in the protonation constants.

5.1.3 Metal-inorganic O-complexes

Analogous plots of predicted association constants for silicate and nitrite complexes obtained in a similar manner are shown in Fig. 27. In the case of silicate, the $logK_{ML}$ values at the reference conditions are from the literature or estimated using the hydroxide correlation in Fig. 7 and ΔS°_{ML} values were obtained using the correlation shown in Fig. 20 if experimental values were unavailable. Note that the van't Hoff plots for metal-silicate complexes mirror those of the metal-phenol complexes when experimental $logK_{ML}$ and ΔS°_{ML} values exist (as with Fe⁺³ and Na⁺), which lends support to our estimates. Similarly, $logK_{ML}$ values for all metal ions except Fe⁺³ were estimated using the correlation shown in Fig. 8 while ΔS°_{ML} values were obtained using the hydroxide correlation from Fig. 20. The decrease in stability constants with temperature is due to the negative enthalpies of association values for these reactions that arise from the low values of $logK_{ML}$ and ΔS°_{ML} .

Additional predictions shown in Fig 28 were made for two inorganic ligands- $H_2PO_4^-$ and iodate, for which only ΔS°_a values are available. While logK_{ML} values were obtained from the correlations shown in Fig. 8, ΔS°_{ML} values were obtained by multiplying metal-hydroxide entropy of association with corresponding $\Delta S^\circ_{a,L}/\Delta S^\circ_{a,Hydroxide}$ values. The positive temperature dependence of the predicted association constants stems from the large positive values of ΔS°_{ML} predicted from the ΔS°_a values for these ligands.



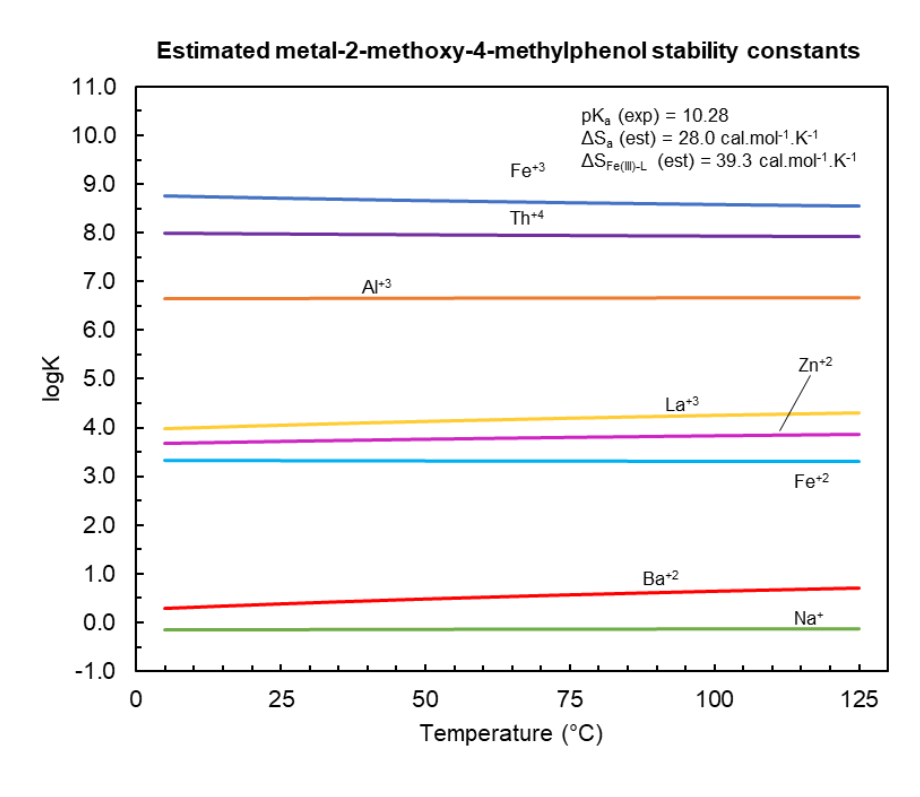
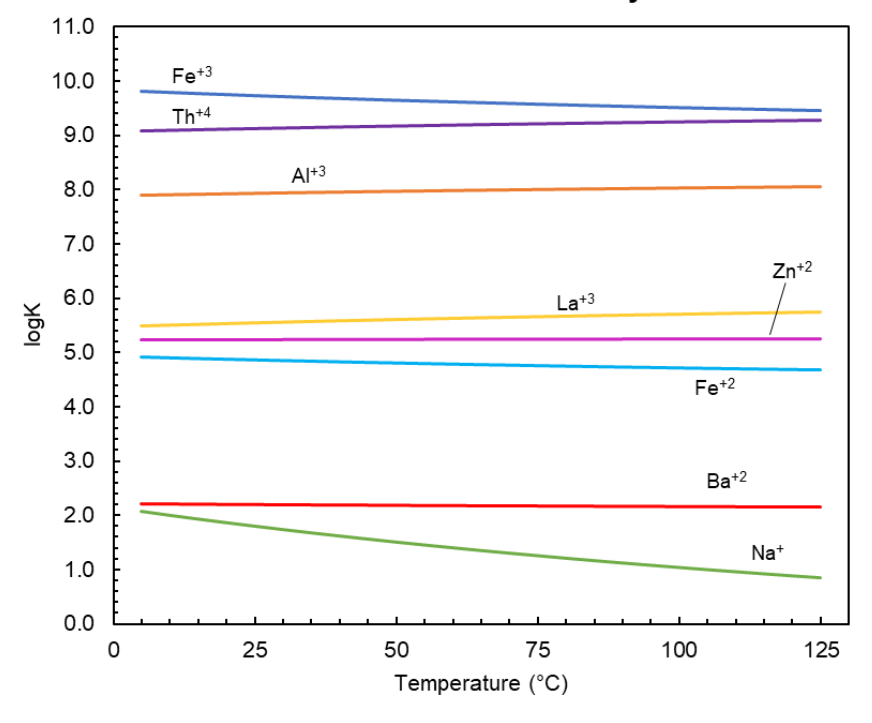


Fig 26. Van't Hoff plots created using only the ligand protonation constant from relationship obtained in Fig.17, Fig.18 and $\Delta S_{\text{M-Hydroxide}}$ from Supplementary Table. Stability constants were estimated from Fig. 12(a).

Estimated metal-silicate stability constants



Estimated metal-nitrite stability constants

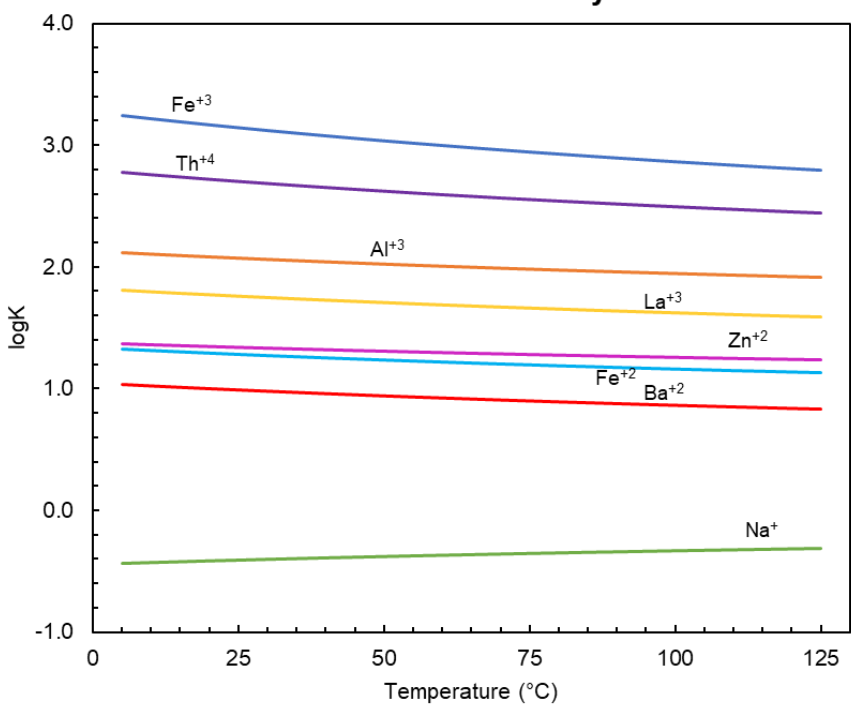


Fig 27. Van't Hoff plots for inorganic ligands from hydroxide entropy data. Stability constants were estimated using Fig. 7 & 8 while complexation entropy was estimated using Fig. 19 & 20.

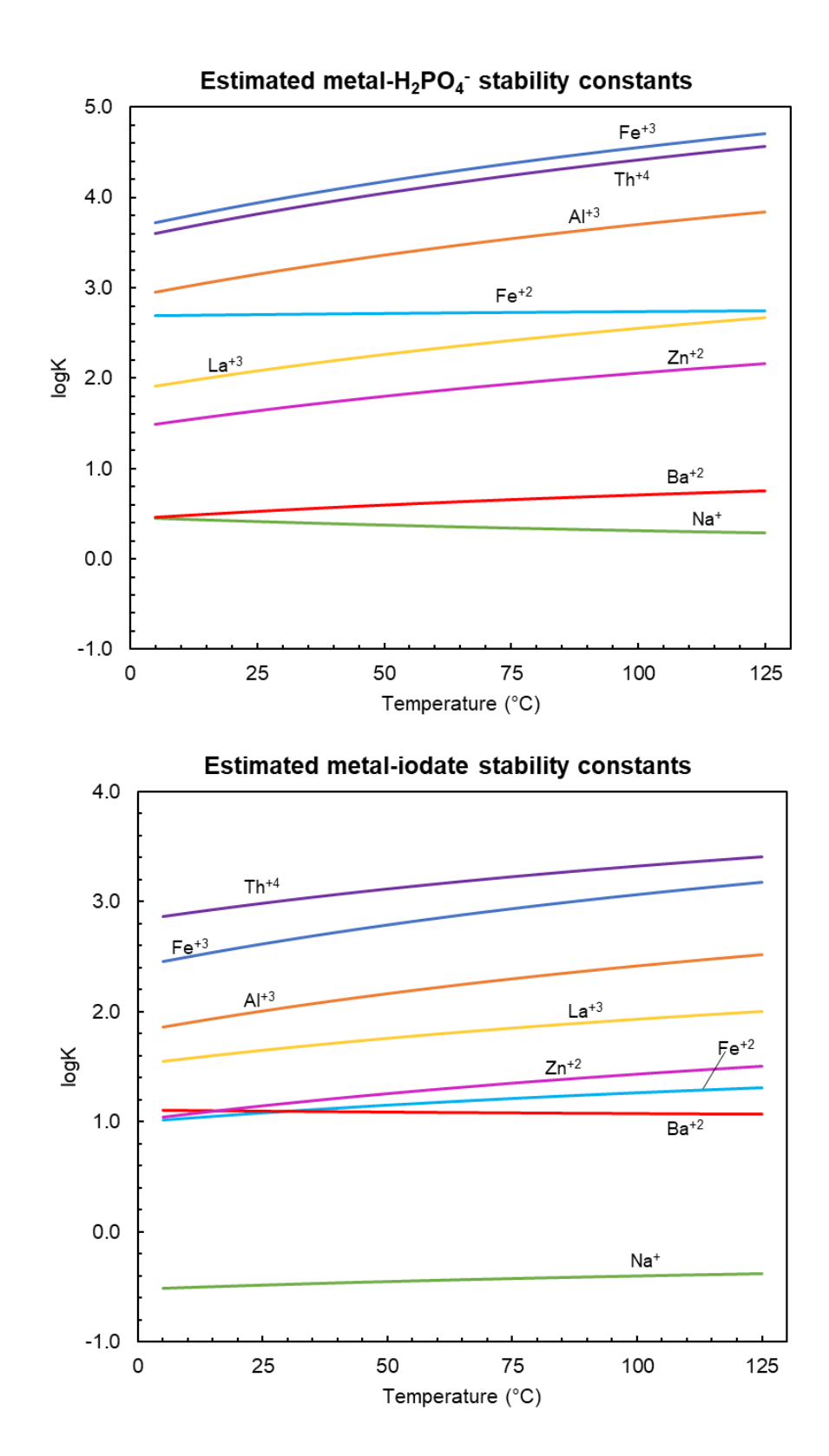


Fig 28. Van't Hoff plots created for inorganic ligands with for which no metal-ligand entropy values were available.

5.2 Applications to hydrothermal systems – Metal speciation in the presence of hexanoic acid

Owing to the elevated presence of metals (Fouquet et al. 1991, Tivey et al. 1995, Edmond et al. 1995, Douville et al. 2002), abundance of life (Lonsdale et al. 1977, Baross & Hoffman 1985, Hoffman et al. 1985), and abiotic organics (Proskurowski et al. 2008, McDermott et al. 2015, McDermott et al. 2020) in or near hydrothermal vents, metal-ligand complexation in hydrothermal systems has been an area of interest for a diverse array of scientific inquiries such as metal transport (Drummond and Palmer 1986, Hennet et al. 1988, Sander and Koschinsky 2007, Sander and Koschinsky 2011, Fitzsimmons et al. 2014, Resing et al. 2015), mineral solubility (Tan 1981, Surdam & Crossey 1985, Lundegard & Kharaka 1990), planetary geochemical evolution (Robbins et al. 2016), elemental cycling (Shaked & Lis 2012, Gledhill & Buck 2012, Wei et al. 2020), marine microbiology (Dick et al. 2013, Ishii et al. 2015, Boyd et al. 2023), and origin of life on Earth and extraterrestrial celestial objects (Hao et al. 2018, Li et al. 2018, Nie et al. 2023, Cable et al. 2021). Here, we focus on the biological implications of metal-organic complexes through speciation analysis of two hypothetical deep-sea hydrothermal mixing fluids at the biologically relevant temperature range of 100-125 °C.

While little is known about how microorganisms from submarine hydrothermal environments interact with metals *in situ*, their interactions can be described in three ways: the metals are used as an energy source in dissimilatory reactions (McCollom & Shock 1997, Amend & Shock 2001, Akerman et al. 2011, Shibuya et al. 2016), metals act as cofactors in the functioning of several key enzymes in assimilatory reactions (Ferry 1993, Vadas et al. 1999, Dupont et al. 2006, Nitschke & Russell 2009), and metals may exert a toxic stress leading to a detrimental impact on microbial growth (Holden & Adams 2003, Edgcomb et al. 2004). In many

cases, an essential metal for a microbe may be toxic at higher concentration – for example, zinc plays a crucial role in the activation of coenzyme M, a key enzyme in the production of methane by methanogens (Sauer & Thauer 2001). However, at higher concentrations or without ligand complexation, zinc has proven to be lethal in methanogens (Edgcomb 2004). Thus, the response elicited by a metal is a direct function of the concentration of the bioavailable forms of the metal. While only a few of all the chemical forms of a metal may be bioavailable (Morel et al. 1979, Poldoski et al. 1979, Pärt & Wikmark 1984, Daly et al. 1990, Zhang et al. 2016, Levina et al. 2017), it is well established that the concentration of these forms (i.e. the chemical speciation) is governed by the total concentration of dissolved metal, total concentration of metal-complexing ligands (inorganic and organic) and pH along with the associated logK values at the corresponding temperature and pressure.

Geochemical modeling of hydrothermal fluid mixing with seawater has shown that organic complexation plays a significant role in the metal transport around hydrothermal vents (Sander and Koschinsky 2007, Sander and Koschinsky 2011). The high value of stability constants (log K ~ 21-22 for iron and logK ~12-14 for copper) used in these simulations suggest the presence of siderophores for iron and thiol compounds for copper. Siderophores are known to be biotic in origin and Reeves et al. attributed the presence of methanthiol in unsedimented hydrothermal vent fields to biotic degradation (Reeves et al. 2014). Alternately, abiotic synthesis of O⁻ ligands like formate in hydrothermal fields has been validated (McDermott et al. 2015) in line with theoretical predictions (Shock & Schulte 1998). While production of longer carboxylic acids has also been predicted, kinetic and analytical limitations have been attributed to their absence.

Therefore, to elucidate the influence of O⁻ ligands on metal speciation in a hydrothermal system, we have simulated metal speciation in two hypothetical hydrothermal mixing fluids consisting of only one O⁻ ligand – hexanoic acid. Hexanoic acid was chosen its abiotic synthesis in hydrothermal fluids has been predicted previously at elevated temperatures and all thermodynamic data for metal-hexanoate complexes was obtained through our estimation methods due to the absence of such data in the literature (except for logK at 25°C for Cu⁺²). Rainbow and Lau hydrothermal systems were chosen as the model hydrothermal systems due to the high abundance of metals in these fluids (Fouquet et al. 1991, Douville et al. 2002, Haalboom et al. 2020, Cohen et al. 2021).

The concentration of all metals and ligands along with temperature and pH used in the calculations are described in Table 1. Thermodynamic data for all associated metal-ligand complexation reactions were obtained from the literature if available, or estimated as described in Table 2. Mixing at 125°C was obtained using a linear model as described in McCollom & Shock 1997 Table 1. The total concentration of hexanoic acid was taken as 1 µmolal based on the analytical detection limit (McDermott et al. 2015). The speciation of hexanoic acid and the main biologically relevant metals is provided in the following sections as a function of pH in the pH range of 4 to 8. Speciation calculations were performed using the geochemical software EQ3/6 (Wolery 2010).

5.2.1 Speciation of hexanoic acid

As per our speciation model for Rainbow mixing fluid (Fig. 29(a)), hexanoic acid is the dominant species at pH below 4.8 and hexanoate is the dominant species at pH above 4.8 that is explained by its pK_a value of ~5.0. Among metals, sodium dominates hexanoic acid speciation

Table 1- Selected composition of bottom seawater (BWS), the hydrothermal vent fluids at Rainbow and Lau and their mixing zones

	BSW	Rainbow	Rainbow mixing	Lau	Lau mixing
Temperature	2	350	125.00	334	124.97
pН	7.8	2.8	4-8	2	4-8
O ₂	0.1	0	64.66	0	62.96
H ₂	0	16	5655.04	0.5	185.20
Σ H ₂ S	0	1.2	424.13	13.1	4852.24
CH ₄	0.0000003	2.5	883.60	0.06	22.22
$\sum CO_2$	2.3	16	7142.128	20	8856.08
sigma SO ₄	27.9	0	18039.024	0	17565.84
sigma PO ₄	0.00075	0	0.4849200	0	0.47
NO ₃ -	0.0003	0	0.1939680	0	0.19
NH ₃ ⁺	0	0.1	35.344	5	1852.00
SiO ₂	0.16	6.9	2542.186	14.5	5471.54
Na ⁺	464	533	488387.360	590	510670.40
Cl	546	750	618101.760	489	524887.20
Br ⁻	0.84	1.18	960.170	1.14	951.12
K ⁺	9.8	20.4	13546.464	79	35431.68
Al ⁺³	0.00002	0	0.013	0.006	2.23
Ca ⁺²	10.2	66.6	30134.016	41.3	21719.44
Mg ⁺²	52.7	0	34073.712	0	33179.92
Fe ⁺³	0.0000015	0	0.0009698	0	0.00094440
Fe ⁺²	0	24.1	8517.904	2.5	926.00
Ba ⁺²	0.00014	0.008	2.918	0.04	14.90
Mn ⁺²	0	2.25	795.240	7.1	2629.84
Cu ⁺²	0.000007	0.16	56.555	0.034	12.60
Zn ⁺²	0.000007	0.185	65.391	3	1111.20
Pb ⁺²	0	0	0.0000000	0.0039	1.44

All concentrations in µmolal. Bottom Seawater (BSW), Mid-Atlantic Ridge (MAR), East Pacific Rise (EPR), Central Indian Ridge (CIR), mid-ocean ridge (MOR), back-arc basin (BAB). BSW composition from Bruland (1983) and McCollom (2007, 2008). Rainbow data from Charlou et al. (2002). Guaymas data from Von Damm et al. (1985b, 2005) and Campbell et al. (1988b), and from compilation by Gamo (1995) where original sources are: Piepgras & Wasserburg (1985), Lupton (1983), Campbell et al. (1988b), Welhan & Lupton (1987) and Gieskes et al. (1988). Endeavour vent fluid from Lilley et al. (1993) and Butterfield et al. (1994) in Gamo (1995) and Seewald et al. (2003); Al⁺³, Ba⁺² and Pb⁺² from Juan de Fuca Ridge S. Cleft Segment, used in the absence of readily available data for Endeavour, are from Hinkley & Tatsumoto (1987), Trefrey et al. (1994), Philpotts et al. (1987), Von Damm & Bischoff (1987) and Evans et al. (1988). Lau Basin vent fluid composition from Fouquet et al. (1991a,b, 1993), and Charlou et al. (1991); methane, ΣCO_2 . H₂ (aq), ΣH_2S from maximum values presented in Tivey (2007) for back-arc basins; Al3+ from White Lady vent in north Fiji back-arc basin (Ishibashi et al. 1994a,b). EPR 9N compositions from Von Damm et al. (1991, 1997), Shanks et al. (1991), Lilley et al. (1991) and Lupton et al. (1991); Al⁺³, Ba⁺², Zn⁺², Pb⁺², NH₄⁺, Cu⁺² concentrations from EPR 21N OBS (Von Damm et al. 1985a) used in the absence of readily available data. TAG data from Campbell et al. (1988a), Douville et al. (2002) and Charlou et al. (1996, 2002); NH₄⁺ from maximum values presented in Tivey (2007) for mid-ocean ridges. Kairei data from Gallant & Von Damm (2006) and Kumagai et al. (2008). Mixing at 125°C was obtained using a linear model as described in McCollom & Shock 1997.

Table 2- Thermodynamic data of stability constant and complexation entropy for the reactions used in speciation simulations

Note: Data for first, second and third order metal-ligand complexation reactions: $M^{i+} + nL^{j-} = ML_n^{i-nj}$ (n=1, 2 or 3) has been provided. These stability constant values represent the standard state value at ionic strength of zero extrapolated from the values reported in the references using the Bdot equation

Table 2a- Thermodynamic data for silicate[†] complexes at 25°C and 1 bar

Metal Ion	$log \beta_1$	Reference	ΔS ₁ ° (cal/mol/K)	Reference
Al^{+3}	7.93	This work	38.4	This work
Ba ⁺²	2.19	This work	9.3	This work
Ca ⁺²	1.04	Santschi & Schindler 1974	13.5	This work
Cu ⁺²	5.88	This work	11.6	This work
Fe ⁺²	4.87	This work	18.8	This work
Fe ⁺³	9.7	Porter & Weber 1971	39.5	Olson & O'Melia 1973
H^+	9.82	Busey & Mesmer 1977	24.43	Busey & Mesmer 1977
K^+	1.52	This work	NA	Reference data not available
Mg ⁺²	1.16	Santschi & Schindler 1974	17.4	This work
Mn ⁺²	4.13	This work	20.1	This work
Na ⁺	1.25	Huang & Sverjensky 2019	-9	This work
Pb ⁺²	6.08	This work	NA	Reference data not available
Zn ⁺²	5.23	This work	24.4	This work

[†]Higher order complexes were assumed to be absent due to lack of data

Table 2b- Thermodynamic data for bicarbonate†‡ complexes at 25°C and 1 bar

Metal Ion	$log \beta_1$	Reference
Al ⁺³	3.28	This work
Ba ⁺²	0.982	Busenberg & Plummer 1986
Ca ⁺²	1.25	Nakayama 1968
Cu ⁺²	1.8	Byrne & Miller 1985
Fe ⁺²	1.2	Millero et al. 1995
Fe ⁺³	4.42	This work
H^+	6.35	Harned & Davis 1943
K ⁺	-0.59	This work
Mg^{+2}	1.067	Siebert & Hostetler 1977
Mn ⁺²	1.97	Morgan 1965
Na ⁺	-0.161	Nakayama 1971
Pb ⁺²	2.59	Neher-Neumann 1992
Zn ⁺²	1.4	Ryan & Bauman 1978

[†]Higher order complexes were assumed to be absent due to lack of data

[‡]Stability constants were assumed to be constant over the temperature range of 25°C to 125°C due to lack of data

Table 2c- Thermodynamic data for hexanoate complexes at 25°C and 1 bar

Metal Ion	logβ1	Reference	ΔS ₁ ° (cal/mol/K)	Reference	logβ2	logβ3	ΔS ₂ ° (cal/mol/K)	ΔS ₃ ° (cal/mol/K)	Reference
A1 ⁺³	2.73	This work	31.7	This work	5.30	7.32	54.68	60.04	Estimated as per methodology outlined in SI-1
Ba ⁺²	0.89	This work	12.5	This work	1.93	2.79	21.56	23.67	Estimated as per methodology outlined in SI-1
Ca ⁺²	0.99	This work	12.4	This work	2.11	3.04	21.39	23.48	Estimated as per methodology outlined in SI-1
Cu ⁺²	1.9	Israeli & Pettit 1975	14.6	This work	3.78	5.27	25.19	27.65	Estimated as per methodology outlined in SI-1
Fe ⁺²	1.39	This work	3.9	This work	2.84	4.02	6.73	7.39	Estimated as per methodology outlined in SI-1
Fe ⁺³	3.62	This work	35.2	This work	6.92	9.51	60.72	66.67	Estimated as per methodology outlined in SI-1
H^{+}	4.879	Christensen et al. 1970	24.5	Christensen et al. 1970	NA	NA	NA	NA	Data not available
K ⁺	-0.27	This work	3.5	This work	-0.19	-0.06	6.04	6.63	Estimated as per methodology outlined in SI-1
Mg ⁺²	0.91	This work	12.5	This work	1.97	2.84	21.56	23.67	Estimated as per methodology outlined in SI-1
Mn ⁺²	1.19	This work	18.1	This work	2.48	3.53	31.22	34.28	Estimated as per methodology outlined in SI-1
Na ⁺	-0.11	This work	8.1	This work	0.10	0.33	13.97	15.34	Estimated as per methodology outlined in SI-1
Pb ⁺²	2.55	This work	13.5	This work	4.97	6.87	23.29	25.57	Estimated as per methodology outlined in SI-1
Zn ⁺²	1.49	This work	18.1	This work	3.03	4.27	31.22	34.28	Estimated as per methodology outlined in SI-1

Table 2d- Thermodynamic data for carbonate†\$ complexes at 25°C and 1 bar

Metal Ion	logβ1	Reference	
A1 ⁺³	NA	Data not available	
Ba ⁺²	2.71	Busenberg & Plummer 1986	
Ca ⁺²	4.48	Nakayama 1968	
Cu ⁺²	6.82	Byrne & Miller 1985	
Fe ⁺²	5.45	Millero et al. 1995	
Fe ⁺³	NA	Data not available	
H^+	10.33	Harned & Scholes 1941	
\mathbf{K}^{+}	NA	Data not available	
Mg ⁺²	2.98	Siebert & Hostetler 1977	
Mn ⁺²	5.69	Morgan 1965	
Na ⁺	0.55	Nakayama 1971	
Pb ⁺²	6.6	Bilinski & Schindler 1982	
Zn ⁺²	4.75	Powell et al. 2013	

[†]Higher order complexes were assumed to be absent due to lack of data

Table 2e- Thermodynamic data for sulfate $^{\dagger \S}$ complexes at 25°C and 1 bar

Metal Ion	logβ ₁	Reference
Al ⁺³	3.17	Tagirov & Schott 2001
Ba ⁺²	2.31	Monnin 2019
Ca ⁺²	2.30	Smith & Martell 1985
Cu ⁺²	2.36	Owen & Gurry 1938
Fe ⁺²	2.44	St Clair et al. 2019
Fe ⁺³	4.04	Mattoo 1959
H ⁺	1.92	Hamer 1934
K ⁺	0.88	Smith & Martell 1976
Mg ⁺²	2.23	Smith & Martell 1985
Mn ⁺²	2.36	Smith & Martell 1976
Na ⁺	0.703	Righellato & Davies 1930
Pb ⁺²	2.69	Smith & Martell 1985
Zn ⁺²	2.31	Owen & Gurry 1938

[†]Higher order complexes were assumed to be absent due to lack of data

[§]Temperature dependence of stability constants was obtained by methods outlined by Sverjensky et al. 1997

[§]Temperature dependence of stability constants was obtained by methods outlined by Sverjensky et al. 1997

Table 2f- Thermodynamic data for phosphate (PO₄-3) †‡ complexes at 25°C and 1 bar

Metal Ion	logβ1	Reference
Al ⁺³	9.19	Ramamoorthy & Manning 1974
Ba ⁺²	NA	Data not available
Ca ⁺²	6.46	Chughtai et al. 1968
Cu ⁺²	NA	Data not available
Fe ⁺²	NA	Data not available
Fe ⁺³	NA	Data not available
H^+	11.9	Pitzer 1937
K ⁺	1.39	Daniele et al. 1983
Mg ⁺²	NA	Data not available
Mn ⁺²	NA	Data not available
Na ⁺	1.53	Daniele et al. 1983
Pb ⁺²	NA	Data not available
Zn ⁺²	NA	Data not available

[†]Higher order complexes were assumed to be absent due to lack of data

Table 2g- Thermodynamic data for monohydrogen phosphate (HPO₄-²) †‡ complexes at 25°C and 1 bar

Metal Ion	logβ1	Reference		
Al^{+3}	NA	Data not available		
Ba ⁺²	NA	Data not available		
Ca ⁺²	2.27	Childs 1970		
Cu ⁺²	4.27	Childs 1970		
Fe ⁺²	3.6	Nriagu 1972a		
Fe ⁺³	9.83	Galal-Gorchev & Stumm 1963		
H^+	7.2	Pitzer 1937		
K^+	1.01	Daniele et al. 1983		
Mg ⁺²	2.71	Childs 1970		
Mn ⁺²	NA	Data not available		
Na ⁺	1.17	Daniele et al. 1983		
Pb ⁺²	3.1	Nriagu 1972b		
Zn^{+2}	3.37	Childs 1970		

[†]Higher order complexes were assumed to be absent due to lack of data

[‡]Stability constants were assumed to be constant over the temperature range of 25°C to 125°C due to lack of data

[‡]Stability constants were assumed to be constant over the temperature range of 25°C to 125°C due to lack of data

Table 2h- Thermodynamic data for dihydrogen phosphate (H2PO4) † complexes at 25°C and 1 bar

Metal Ion	logβ1	Reference & Comments
Al ⁺³	3.15	This work
Ba ⁺²	0.53	This work
Ca ⁺²	1.04	Childs 1970
Cu ⁺²	1.74	Childs 1970
Fe ⁺²	2.7	Nriagu 1972a
Fe ⁺³	3.94	Galal-Gorchev & Stumm 1963
H^+	2.16	Griffith & McKeown 1940
K ⁺	0.13	Daniele et al. 1983
Mg ⁺²	1.09	Childs 1970
Mn ⁺²	1.42	This work
Na ⁺	0.41	Daniele et al. 1983
Pb ⁺²	1.50	Nriagu 1972b
Zn ⁺²	1.64	Childs 1970

[†]Higher order complexes were assumed to be absent due to lack of data

Table 2i- Thermodynamic data for nitrate†‡ complexes at 25°C and 1 bar

Metal Ion	logβ1	Reference
Al^{+3}	NA	Data not available
Ba ⁺²	0.917	Righellato & Davies 1930
Ca ⁺²	0.283	Righellato & Davies 1930
Cu ⁺²	0.54	Fedorov et al. 1973
Fe ⁺²	NA	Data not available
Fe ⁺³	1.0	Mattoo 1959
H^+	-1.3	Shock et al. 1997
K ⁺	-0.15	Smith & Martell 1976
Mg^{+2}	NA	Data not available
Mn ⁺²	0.204	Fedorov et al. 1974
Na ⁺	-0.55	Smith & Martell 1985
Pb ⁺²	NA	Data not available
Zn ⁺²	0.42	Fedorov et al. 1973

[†]Higher order complexes were assumed to be absent due to lack of data

[‡]Stability constants were assumed to be constant over the temperature range of 25°C to 125°C due to lack of data

[‡]Stability constants were assumed to be constant over the temperature range of 25°C to 125°C due to lack of data

Table 2j- Thermodynamic data for bisulfide (HS-) ‡ complexes at 25°C and 1 bar

Metal Ion	logβ ₁	Reference	logβ2	Reference	
A1 ⁺³	NA	Data not available	NA	Data not available	
Ba ⁺²	NA	Data not available	NA	Data not available	
Ca ⁺²	NA	Data not available	NA	Data not available	
Cu ⁺²	7.6	Zhang & Millero 1994	14.0	Zhang & Millero 1994	
Fe ⁺²	5.9	Zhang & Millero 1994	9.35	Dyrssen 1985	
Fe ⁺³	NA	Data not available	NA	Data not available	
H ⁺	7.05	Ellis & Mileston 1967	NA	Data not available	
K ⁺	NA	Data not available	NA	Data not available	
Mg ⁺²	NA	Data not available	NA	Data not available	
Mn ⁺²	7.3	Zhang & Millero 1994	6.4	Dyrssen 1985	
Na ⁺	NA	Data not available	NA	Data not available	
Pb ⁺²	7.7	Zhang & Millero 1994	14.5	Zhang & Millero 1994	
Zn ⁺²	6.0	Zhang & Millero 1994	14.7	Zhang & Millero 1994	

[‡]Stability constants were assumed to be constant over the temperature range of 25°C to 125°C due to lack of data

Table 2k- Thermodynamic data for chloride§ complexes at 25°C and 1 bar

Metal Ion	logβı	Reference	logβ2	Reference	logβ3	Reference	logβ4	Reference
Al ⁺³	NA	Data not available	NA	Data not available	NA	Data not available	NA	Data not available
Ba ⁺²	NA	Data not available	NA	Data not available	NA	Data not available	NA	Data not available
Ca ⁺²	NA	Data not available	NA	Data not available	NA	Data not available	NA	Data not available
Cu ⁺²	0.4	Ramette & Fan 1983	-0.69	Sverjensky et al. 1997	2.29	Sverjensky et al. 1997	4.59	Sverjensky et al. 1997
Fe ⁺²	NA	Data not available	NA	Data not available	NA	Data not available	NA	Data not available
Fe ⁺³	1.48	Rabinowitch & Stockmayer 1942	NA	Data not available	NA	Data not available	NA	Data not available
H^{+}	-0.67	Ruaya & Seward 1987	NA	Data not available	NA	Data not available	NA	Data not available
K ⁺	NA	Data not available	NA	Data not available	NA	Data not available	NA	Data not available
Mg ⁺²	NA	Data not available	NA	Data not available	NA	Data not available	NA	Data not available
Mn ⁺²	NA	Data not available	NA	Data not available	NA	Data not available	NA	Data not available
Na ⁺	-0.77	Eigen & Wicke 1954	NA	Data not available	NA	Data not available	NA	Data not available
Pb ⁺²	NA	Data not available	NA	Data not available	NA	Data not available	NA	Data not available
Zn ⁺²	0.38	Sverjensky et al. 1997	0.45	Sverjensky et al. 1997	0.51	Sverjensky et al. 1997	-0.42	Sverjensky et al. 1997

[§]Temperature dependence of stability constants was obtained by methods outlined by Sverjensky et al. 1997

Table 21- Thermodynamic data for bromide†\$ complexes at 25°C and 1 bar

Metal Ion	logβ1	Reference	
Al ⁺³	NA	Data not available	
Ba ⁺²	NA	Data not available	
Ca ⁺²	NA	Data not available	
Cu ⁺²	NA	Data not available	
Fe ⁺²	NA	Data not available	
Fe ⁺³	NA	Data not available	
H ⁺	NA	Data not available	
K ⁺	-1.73	Sverjensky et al. 1997	
Mg ⁺²	NA	Data not available	
Mn ⁺²	NA	Data not available	
Na ⁺	-1.36	Sverjensky et al. 1997	
Pb ⁺²	NA	Data not available	
Zn ⁺²	NA	Data not available	

[†]Higher order complexes were assumed to be absent due to lack of data

[§]Temperature dependence of stability constants was obtained by methods outlined by Sverjensky et al. 1997

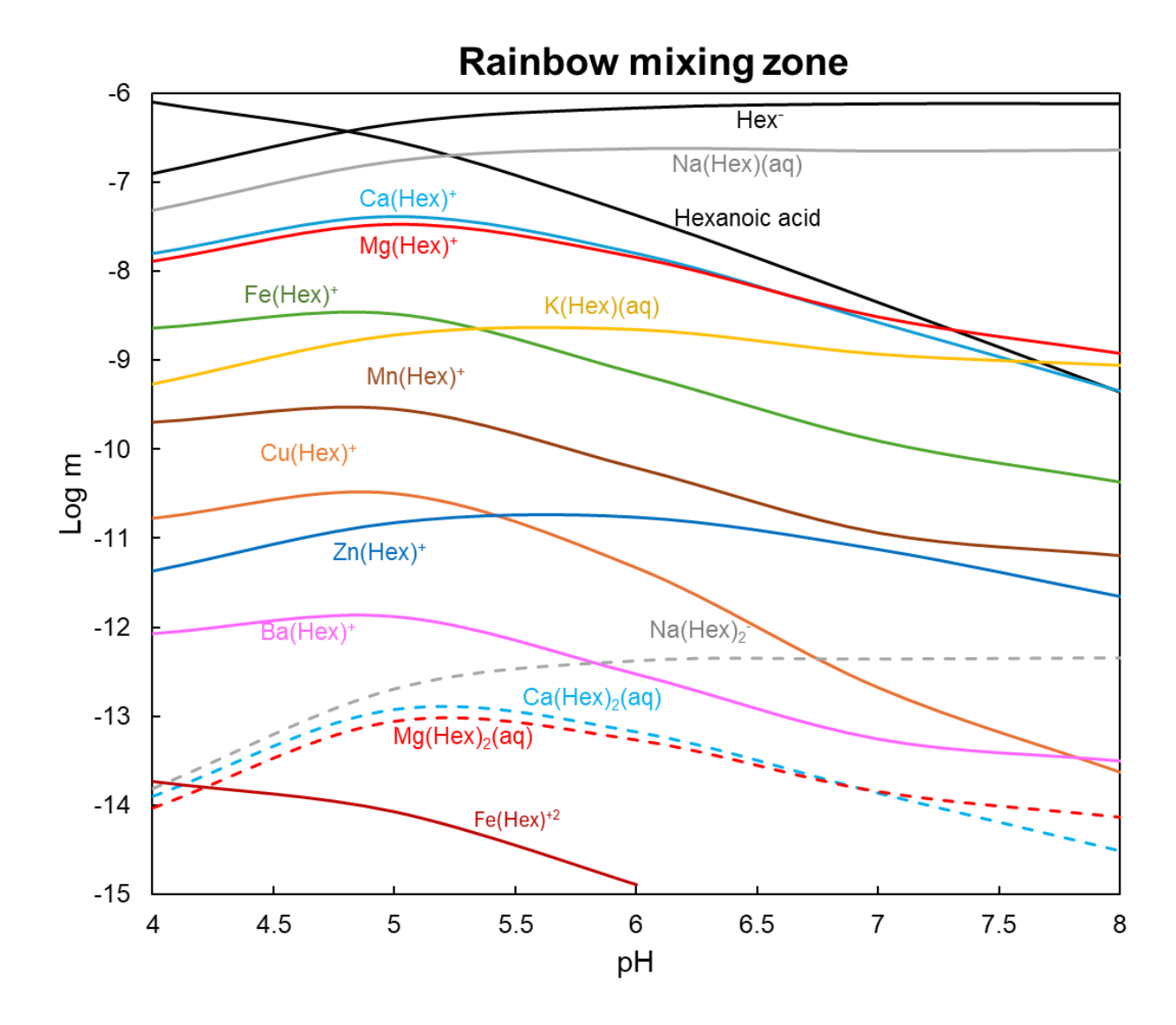


Fig 29(a). Log molal concentrations of metal hexanoate complexes in a hypothetical mixing zone at Rainbow consisting of 1µmolal total hexanoic acid at 125 °C as a function of pH at equilibrium. The black curves correspond to hexanoic acid and hexanoate (Hex), grey correspond to Na-hexanoate complexes, light blue to Ca-hexanoate complexes, red to Mghexanoate complexes, green to Fe(II)-hexanoate complexes, yellow to K-hexanoate complexes, brown to Mn-hexanoate complexes, orange to Cu(II)-hexanoate complexes, dark blue to Zn-hexanoate complexes, pink to Ba-hexanoate complex and maroon to Fe(III)-hexanoate complex. The first and second complexes of hexanoate have been shown by the solid and dashed lines, respectively. The stability constant at 125 °C for all metal complexes used in this figure were calculated using the van't Hoff equation with estimated values of stability constant and entropies at 25 °C from this work.

Zn speciation in Rainbow

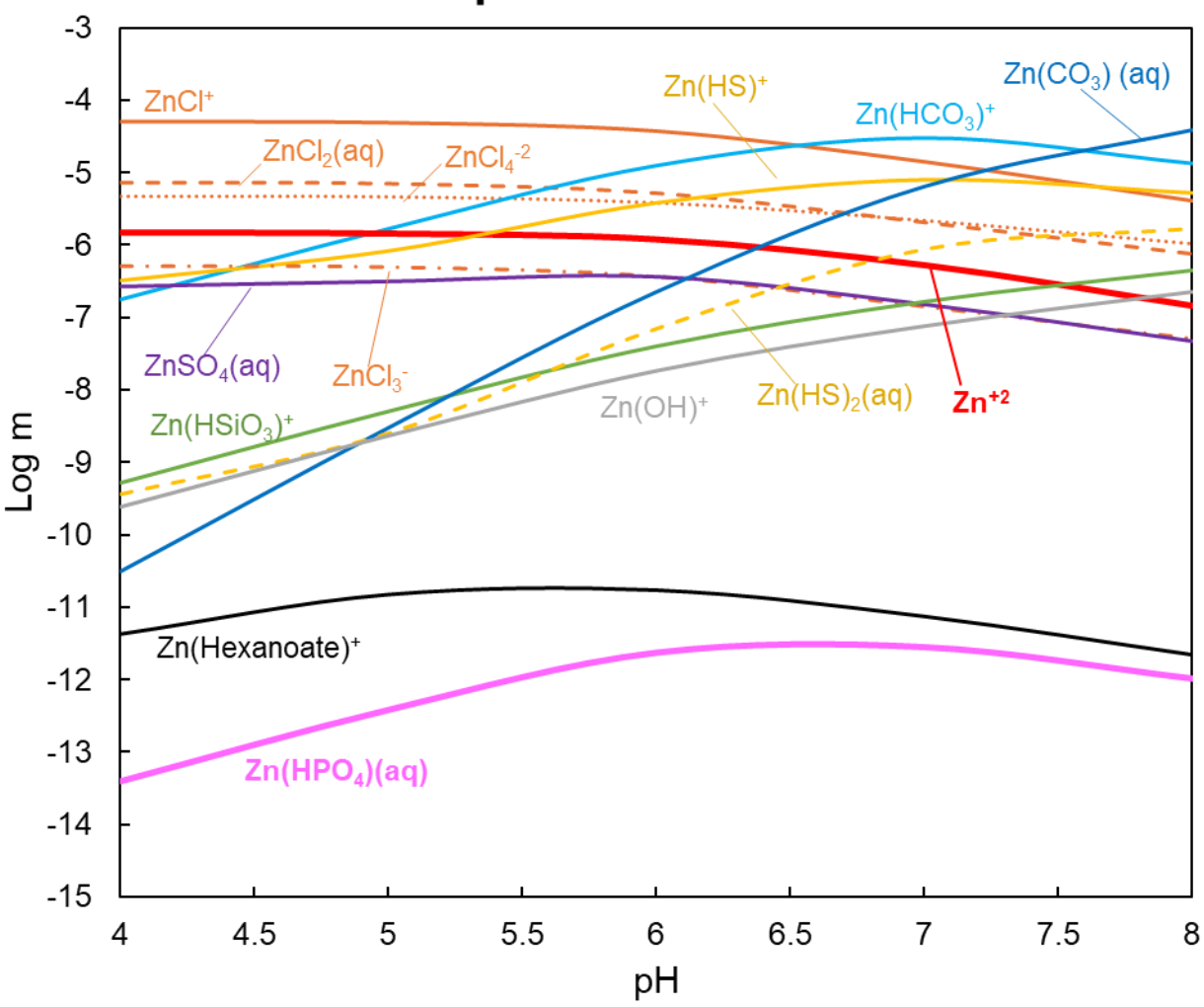


Fig 29(b). Log molal concentrations of zinc complexes in a hypothetical mixing zone at Rainbow hydrothermal field consisting of 1µmolal total hexanoic acid at 125 °C as a function of pH at equilibrium. First, second, third and fourth complexes with a ligand are depicted with solid, dashed, dashed & dotted and dotted curves, respectively. The orange curves correspond to chloride complexes, light blue to bicarbonate complex, dark blue to carbonate complex, yellow to bisulfide complexes, red to free metal ion, purple to sulfate complex, green to silicate complex, grey to hydroxide complex, maroon to bromide complex, light pink to monohydrogen phosphate complex, dark pink to phosphate complex and black to hexanoate complex. The bioavailable forms are depicted in bolded curves and labels. The stability constant at 125°C for all complexes used in this figure were obtained from the literature if available or calculated using the van't Hoff equation with estimated values of stability constant and entropies at 25 °C from this work.

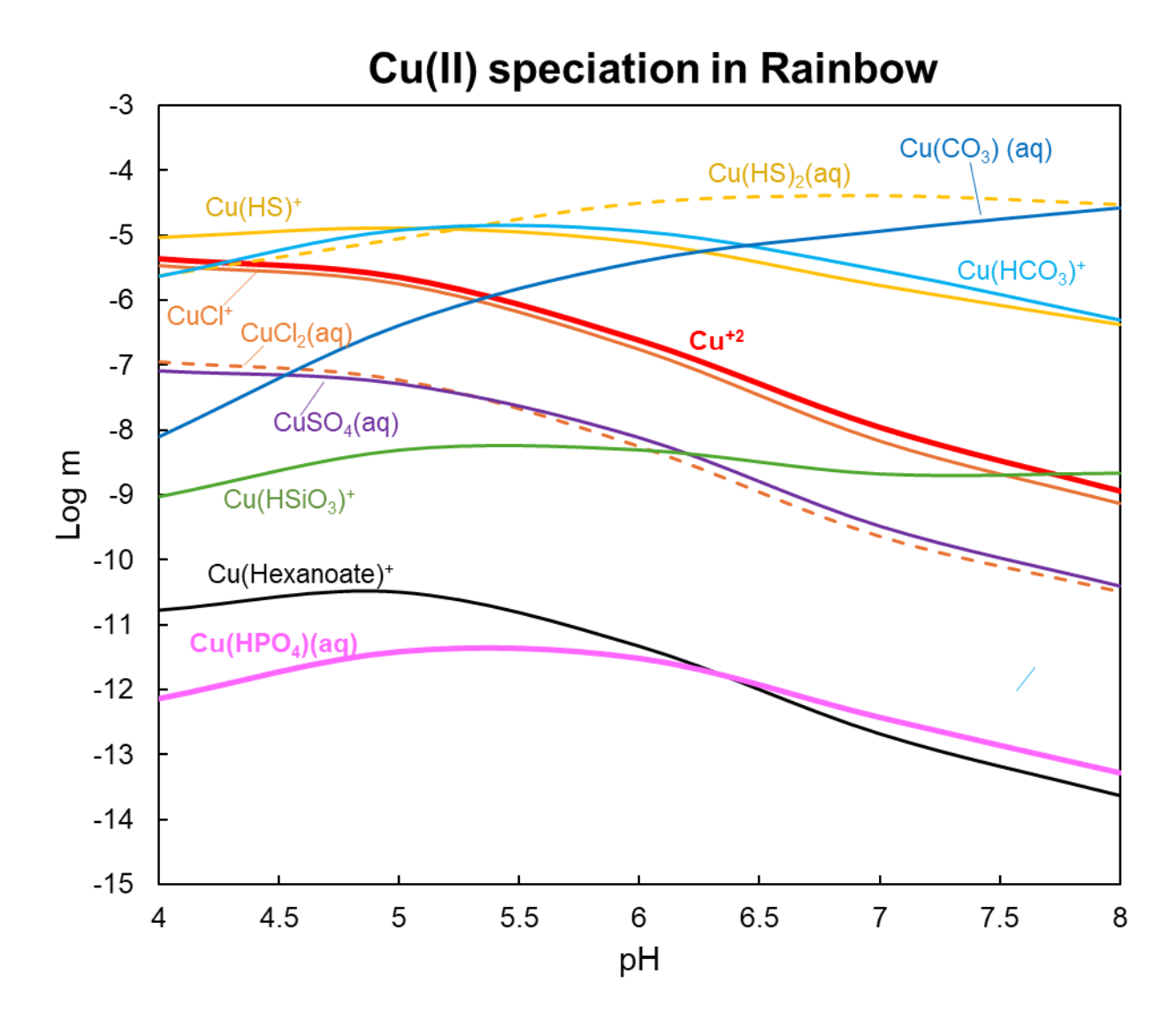


Fig 29(c). Log molal concentrations of copper complexes in a hypothetical mixing zone at Rainbow hydrothermal field consisting of 1μmolal total hexanoic acid at 125 °C as a function of pH at equilibrium. First, second, third and fourth complexes with a ligand are depicted with solid, dashed, dashed & dotted and dotted curves, respectively. The orange curves correspond to chloride complexes, light blue to bicarbonate complex, dark blue to carbonate complex, yellow to bisulfide complexes, red to free metal ion, purple to sulfate complex, green to silicate complex, light pink to monohydrogen phosphate complex, dark pink to phosphate complex and black to hexanoate complex. The bioavailable forms are depicted in bolded curves and labels. The stability constant at 125 °C for all complexes used in this figure were obtained from the literature if available or calculated using the van't Hoff equation with estimated values of stability constant and entropies at 25 °C from this work.

Fe(II) speciation in Rainbow 0 -1 FeCI+ Fe⁺² Fe(HCO₃)⁴ -2 Fe(CO₃)(aq) -3 Fe(HS)+ -4 Fe(SO₄)(aq) -5 eCl₂(aq) -6 -7 $Fe(HSiO_3)^{+2}$ Fe(HS)₂(aq) -8 Fe(HPO₄)(aq) -9 -10 Fe(Hexanoate)+ -11 Fe(H₂PO₄ -12 -13 -14 4 4.5 5 5.5 6 6.5 7 7.5 8 pΗ

Fig 29(d). Log molal concentrations of Fe(II) complexes in a hypothetical mixing zone at Rainbow hydrothermal field consisting of 1µmolal total hexanoic acid of Rainbow hydrothermal vent system at 125 °C as a function of pH at equilibrium. First, second, third and fourth complexes with a ligand are depicted with solid, dashed, dashed & dotted and dotted curves, respectively. The orange curves correspond to chloride complexes, light blue to bicarbonate complex, dark blue to carbonate complex, yellow to bisulfide complexes, red to free metal ion, purple to sulfate complex, green to silicate complex, light pink to monohydrogen phosphate complex, dark pink to phosphate complex and black to hexanoate complex. The bioavailable forms are depicted in bolded curves and labels. The stability constant at 125°C for all complexes used in this figure were obtained from the literature if available or calculated using the van't Hoff equation with estimated values of stability constant and entropies at 25 °C from this work.

Fe(III) speciation in Rainbow -8 Fe(HCO₃)+2 -9 Fe(CO₃)+ Fe(HSiO₃)+2 -10 FeCl₂⁺ -11 FeCI+2 -12 E -12 Bo₋₁₃ Fe⁺³ -14 Fe(Hexanoate)+2 -15 -16

-17

4

4.5

5

5.5

Fig 29(e). Log molal concentrations of Fe(III) complexes in a hypothetical mixing zone at Rainbow hydrothermal field consisting of 1µmolal total hexanoic acid at 125 °C as a function of pH at equilibrium. First, second, third and fourth complexes with a ligand are depicted with solid, dashed, dashed & dotted and dotted curves, respectively. The orange curves correspond to chloride complexes, light blue to bicarbonate complex, dark blue to carbonate complex, red to free metal ion, purple to sulfate complex, green to silicate complex, light pink to monohydrogen phosphate complex, dark pink to phosphate complex and black to hexanoate complex. The bioavailable forms are depicted in bolded curves and labels. The stability constant at 125°C for all complexes used in this figure were obtained from the literature if available or calculated using the van't Hoff equation with estimated values of stability constant and entropies at 25 °C from this work.

6

pΗ

6.5

7

7.5

8

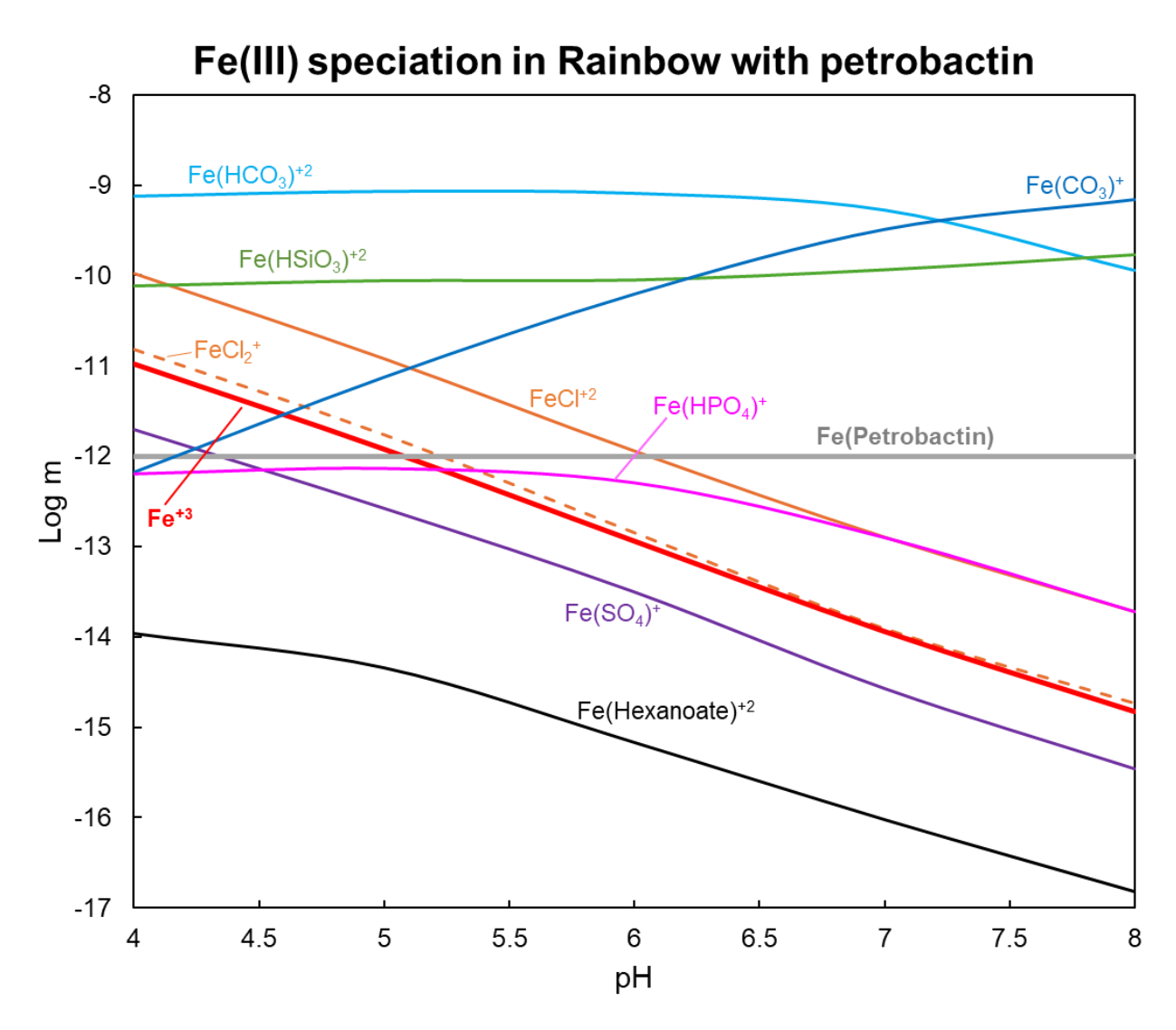


Fig 29(f). Log molal concentrations of Fe(III) complexes in a hypothetical mixing zone at Rainbow hydrothermal field consisting of 1µmolal total hexanoic acid and 1pmolal total petrobactin at 100 °C as a function of pH at equilibrium. First, second, third and fourth complexes with a ligand are depicted with solid, dashed, dashed & dotted and dotted curves, respectively. The orange curves correspond to chloride complexes, light blue to bicarbonate complex, dark blue to carbonate complex, red to free metal ion, purple to sulfate complex, green to silicate complex, light pink to monohydrogen phosphate complex, dark pink to phosphate complex and black to hexanoate complex. The bioavailable forms are depicted in bolded curves and labels. The stability constant at 125°C for all complexes used in this figure were obtained from the literature if available or calculated using the van't Hoff equation with estimated values of stability constant and entropies at 25 °C from this work.

owing to its high concentration and lack of competing ligands. The order of dominance of the remaining metals can largely be explained by total metal concentration in the mixing fluid and the stability constant. The second hexanoate complexes of sodium, calcium and magnesium are prevalent owing to the high concentration of these metals and those for remaining metals fall under the fmolal threshold.

The speciation of hexanoic acid at Lau (Fig. 30(a)) is largely similar to the speciation at Rainbow with minor variations that can be explained by the difference in the total metal concentration in the two fluids. Lead, which is absent at Rainbow is present at picomolal concentration at Lau. The higher concentration of Fe(III)-hexanoate complex at Lau may be explainable by the low total Fe(II) and Cu concentrations.

5.2.2 Speciation of zinc

Zinc speciation at Rainbow (Fig. 29(b)) is dominated by chloride complexes at low pH and bicarbonate and carbonate complexes at high pH that may be explained by the concentration of bicarbonate and carbonate over the pH range. Bisulfide, sulfate and silicate complexes are present in the μ molal to nmolal range while Zn-hexanoate complex is present in pmolal amounts. The dominant bioavailable form of zinc is Zn⁺² that ranges from 0.2 – 2 μ molal. The other known bioavailable form of zinc in this system is Zn(HPO₄) (Zhao et al. 2016) that is present at pmolal concentration.

In contrast to Rainbow, zinc speciation at Lau (Fig. 30(b)), is dominated by bisulfide complexes that may be explained by the high abundance (~5 mmol) of dissolved H₂S. This result is consistent with other observations such as amelioration of metal toxicity due to the addition of sulfide (Edgcomb et al. 2004). Zn-hexanoate concentration at Lau is slightly higher than that at

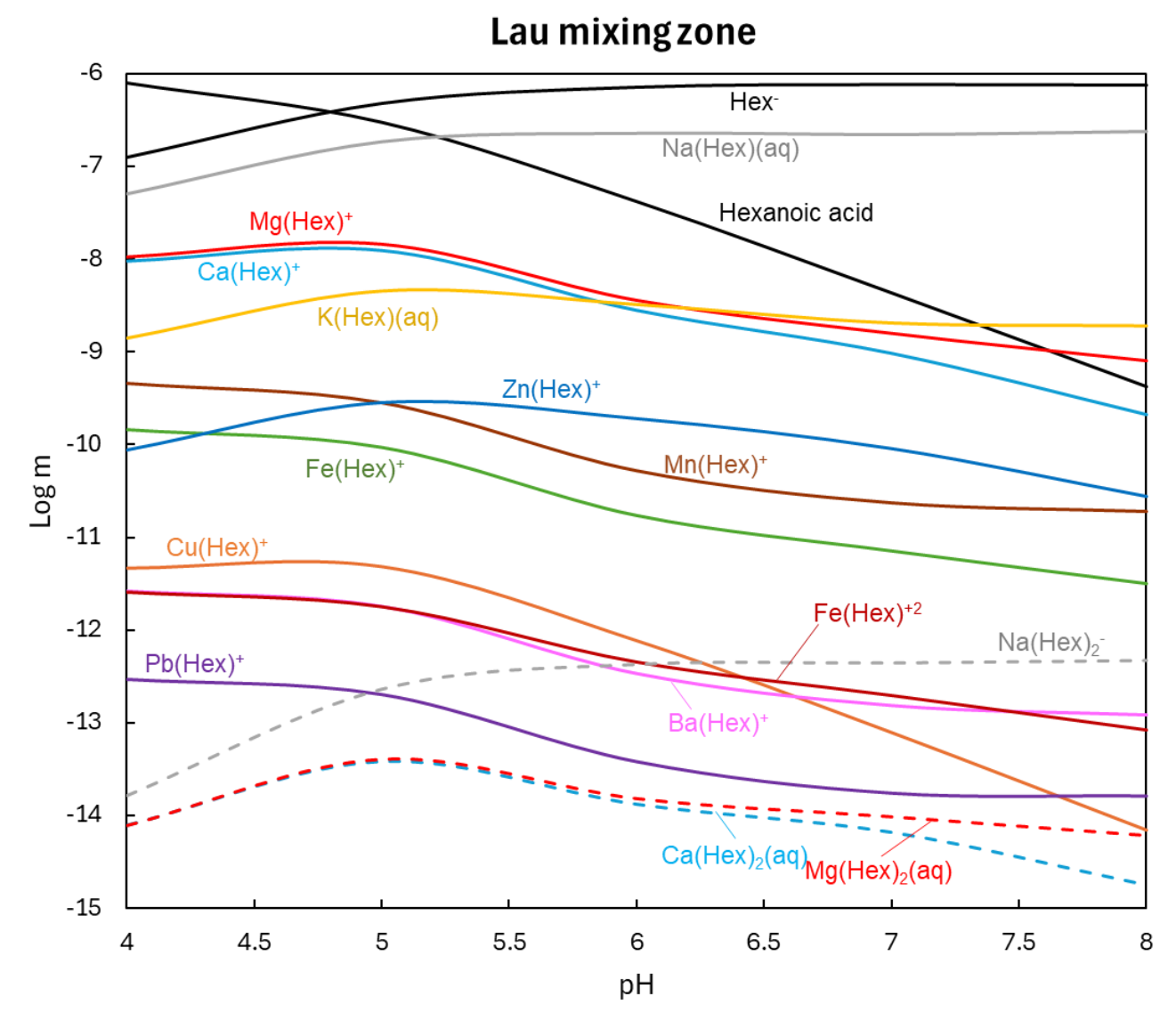


Fig 30(a). Log molal concentrations of metal hexanoate complexes in a hypothetical mixing zone at Lau hydrothermal field consisting of 1µmolal total hexanoic acid at 125 °C as a function of pH at equilibrium. The black curves correspond to hexanoic acid and hexanoate (Hex), grey correspond to Na-hexanoate complexes, light blue to Ca-hexanoate complexes, red to Mg-hexanoate complexes, green to Fe(II)-hexanoate complexes, yellow to K-hexanoate complexes, brown to Mn-hexanoate complexes, orange to Cu(II)-hexanoate complexes, dark blue to Zn-hexanoate complexes, pink to Ba-hexanoate complexes and maroon to Fe(III)-hexanoate complex. The first and second complexes of hexanoate have been shown by the solid and dashed lines, respectively. The stability constant at 125°C for all metal complexes used in this figure were calculated using the van't Hoff equation with estimated values of stability constant and entropies at 25 °C from this work.

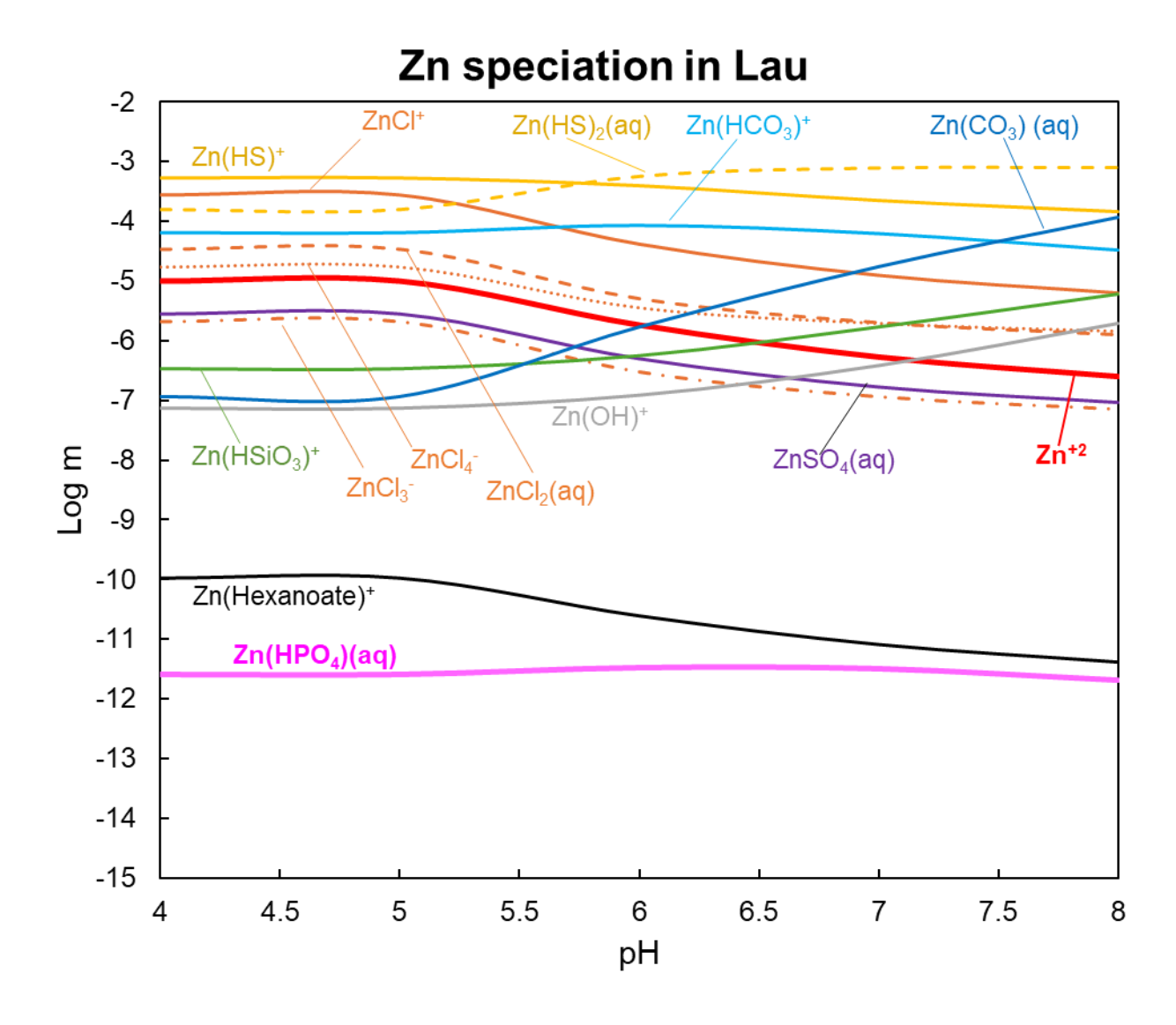


Fig 30(b). Log molal concentrations of zinc complexes in a hypothetical mixing zone at Lau hydrothermal field consisting of 1µmolal total hexanoic acid at 125 °C as a function of pH at equilibrium. First, second, third and fourth complexes with a ligand are depicted with solid, dashed, dashed & dotted and dotted curves, respectively. The orange curves correspond to chloride complexes, light blue to bicarbonate complex, dark blue to carbonate complex, yellow to bisulfide complexes, red to free metal ion, purple to sulfate complex, green to silicate complex, grey to hydroxide complex, maroon to bromide complex, light pink to monohydrogen phosphate complex, dark pink to phosphate complex and black to hexanoate complex. The bioavailable forms are depicted in bolded curves and labels. The stability constant at 125°C for all complexes used in this figure were obtained from the literature if available or calculated using the van't Hoff equation with estimated values of stability constant and entropies at 25 °C from this work.

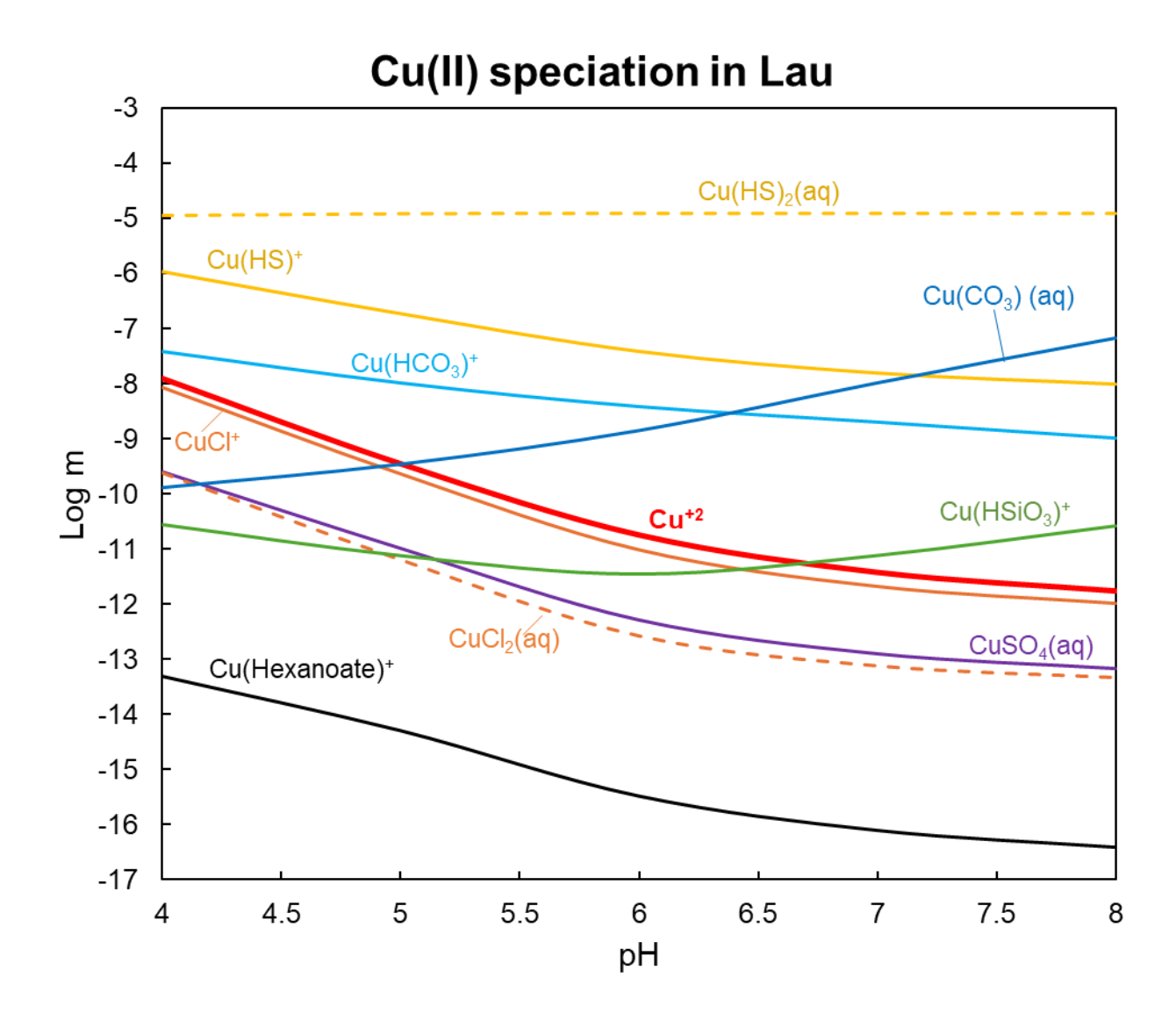


Fig 30(c). Log molal concentrations of copper complexes in a hypothetical mixing zone at Lau hydrothermal field consisting of 1µmolal total hexanoic acid at 125 °C as a function of pH at equilibrium. First, second, third and fourth complexes with a ligand are depicted with solid, dashed, dashed & dotted and dotted curves, respectively. The orange curves correspond to chloride complexes, light blue to bicarbonate complex, dark blue to carbonate complex, yellow to bisulfide complexes, red to free metal ion, purple to sulfate complex, green to silicate complex, light pink to monohydrogen phosphate complex, dark pink to phosphate complex and black to hexanoate complex. The bioavailable forms are depicted in bolded curves and labels. The stability constant at 125°C for all complexes used in this figure were obtained from the literature if available or calculated using the van't Hoff equation with estimated values of stability constant and entropies at 25 °C from this work.

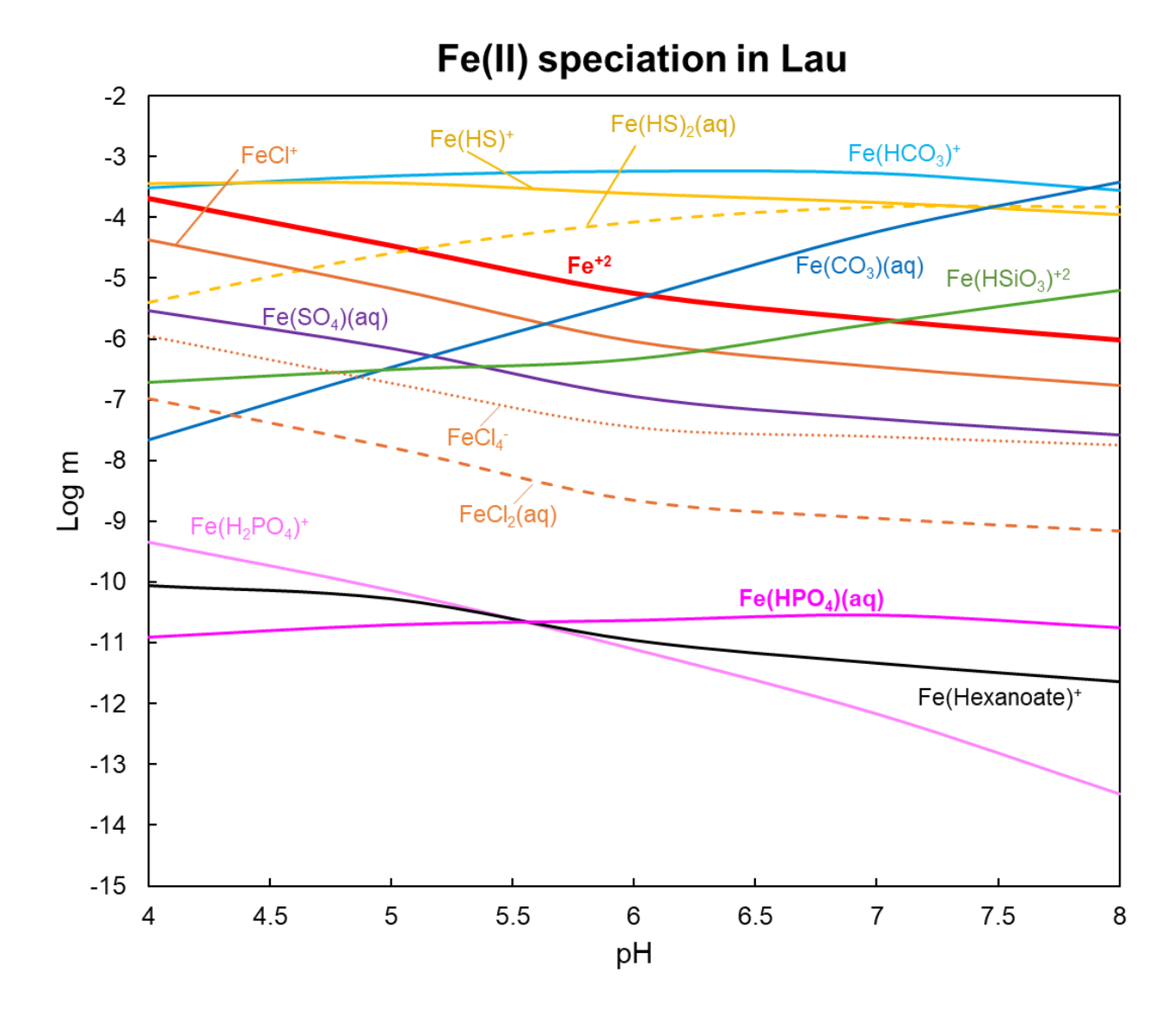


Fig 30(d). Log molal concentrations of Fe(II) complexes in a hypothetical mixing zone at Lau hydrothermal field consisting of 1μM total hexanoic acid of Rainbow hydrothermal vent system at 125 °C as a function of pH at equilibrium. First, second, third and fourth complexes with a ligand are depicted with solid, dashed, dashed & dotted and dotted curves, respectively. The orange curves correspond to chloride complexes, light blue to bicarbonate complex, dark blue to carbonate complex, yellow to bisulfide complexes, red to free metal ion, purple to sulfate complex, green to silicate complex, light pink to monohydrogen phosphate complex, dark pink to phosphate complex and black to hexanoate complex. The bioavailable forms are depicted in bolded curves and labels. The stability constant at 125°C for all complexes used in this figure were obtained from the literature if available or calculated using the van't Hoff equation with estimated values of stability constant and entropies at 25 °C from this work.

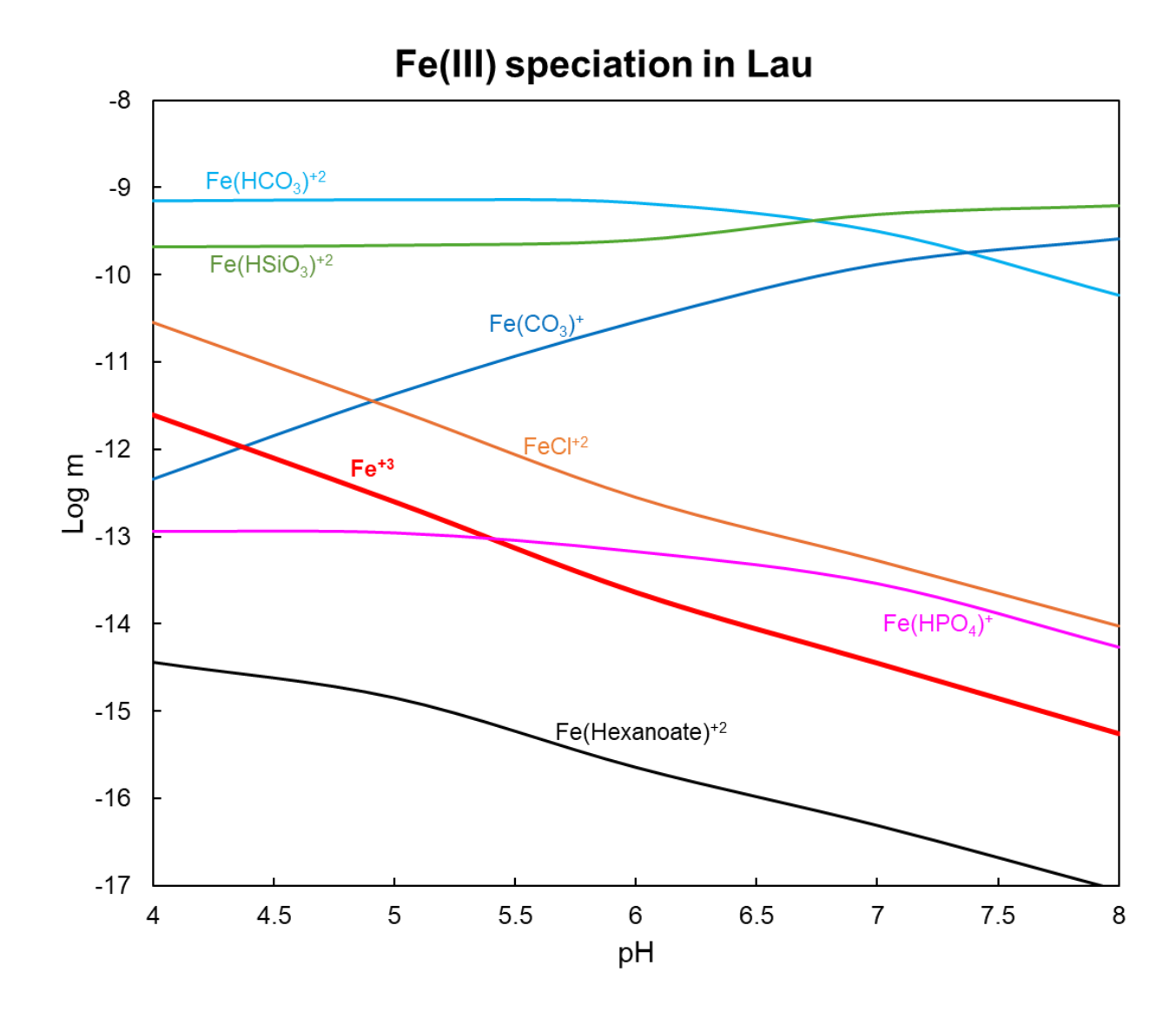


Fig 30(e). Log molal concentrations of Fe(III) complexes in a hypothetical mixing zone at Lau hydrothermal field consisting of 1µmolal total hexanoic acid at 125 °C as a function of pH at equilibrium. First, second, third and fourth complexes with a ligand are depicted with solid, dashed, dashed & dotted and dotted curves, respectively. The orange curves correspond to chloride complexes, light blue to bicarbonate complex, dark blue to carbonate complex, red to free metal ion, purple to sulfate complex, green to silicate complex, light pink to monohydrogen phosphate complex, dark pink to phosphate complex and black to hexanoate complex. The bioavailable forms are depicted in bolded curves and labels. The stability constant at 125°C for all complexes used in this figure were obtained from the literature if available or calculated using the van't Hoff equation with estimated values of stability constant and entropies at 25 °C from this work.

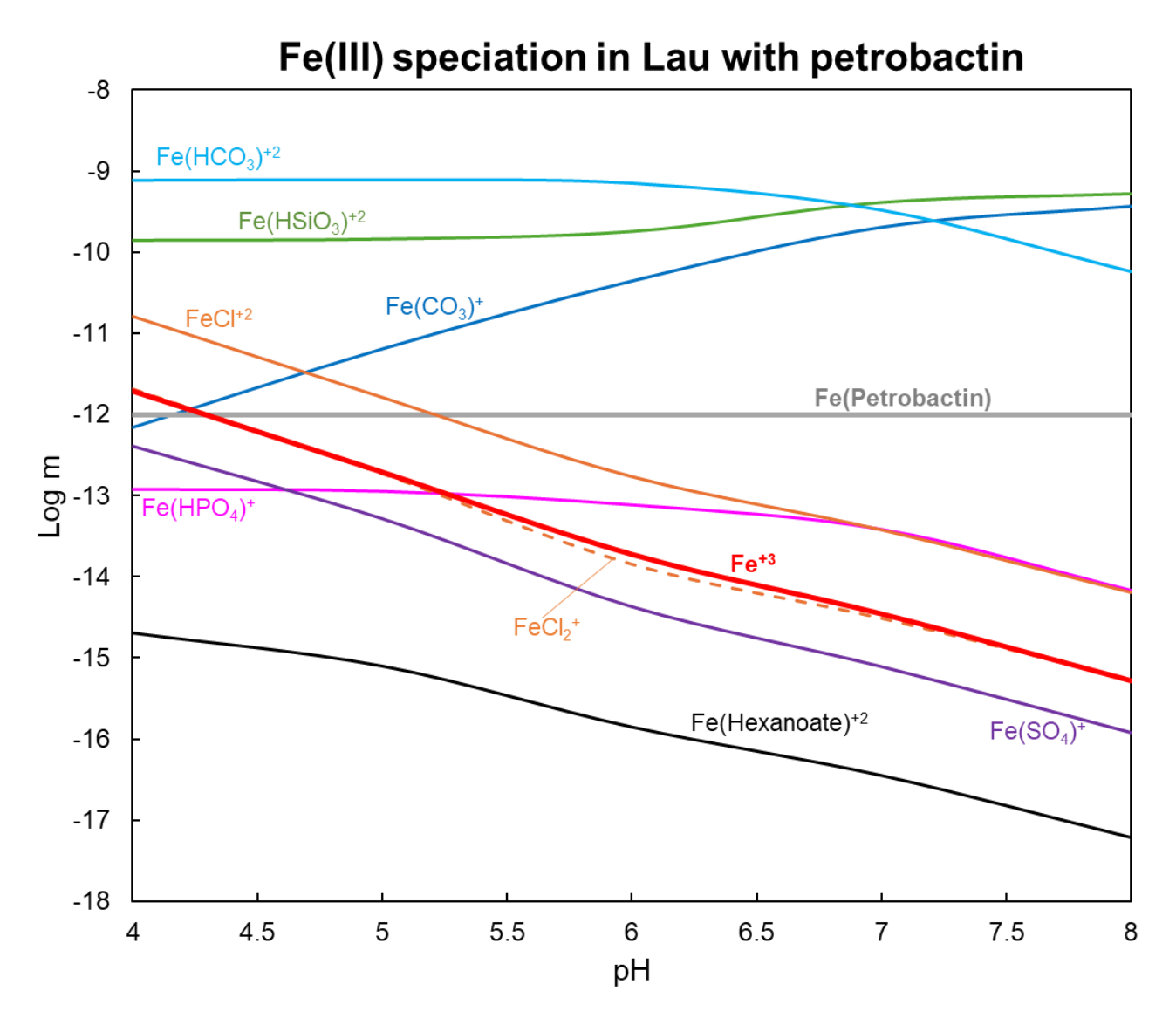


Fig 30(f). Log molal concentrations of Fe(III) complexes in a hypothetical mixing zone at Lau hydrothermal field consisting of 1µmolal total hexanoic acid and 1pmolal total petrobactin at 100 °C as a function of pH at equilibrium. First, second, third and fourth complexes with a ligand are depicted with solid, dashed, dashed & dotted and dotted curves, respectively. The orange curves correspond to chloride complexes, light blue to bicarbonate complex, dark blue to carbonate complex, red to free metal ion, purple to sulfate complex, green to silicate complex, light pink to monohydrogen phosphate complex, dark pink to phosphate complex and black to hexanoate complex. The bioavailable forms are depicted in bolded curves and labels. The stability constant at 125°C for all complexes used in this figure were obtained from the literature if available or calculated using the van't Hoff equation with estimated values of stability constant and entropies at 25 °C from this work.

Rainbow due to the higher concentration of total zinc at Lau. The same reason may be attributed to the $\sim 10x$ higher concentration of the bioavailable forms Zn^{+2} and $Zn(HPO_4)$.

5.2.3 Speciation of copper

The dominant form of copper at both Rainbow (Fig. 29(c)) and Lau (Fig. 30(c)) is dominated by bisulfide complexes that may be explained by the high stability constants of these complexes and the high concentration of dissolved H_2S . While bicarbonate complexes compete with the sulfide complexes around pH 5.2 at Rainbow, bisulfide complexes outcompete these complexes by almost two orders of magnitude at Lau owing to the 20x higher concentration of hydrogen sulfide. The rest of the speciation directly follows from this: chloride, sulfate and silicate complexes are present in the μ molal to nmolal range at Rainbow while hexanoate and monohydrogen phosphate complexes are present in pmolal amounts at Rainbow. The concentration of the corresponding complexes at Lau is \sim 3 orders of magnitude lower at Lau owing to the dominance of the bisulfide complexes of copper. A similar pattern is seen in the concentration of the free copper ion Cu^{+2} at the two sites.

5.2.4 Speciation of iron (II)

When calculating speciation of redox-sensitive metals, EQ3/6 has the provision of constraining redox transformation and keeping the total concentration of metal in a particular oxidation state constant. Thus, the total concentration of Fe(II) at Rainbow in our calculations stays constant at 8517 μ molal while the concentration of Fe(III) stays constant at ~1 nmolal. The speciation of iron has been depicted separately for both mixing fluids.

At Rainbow (Fig. 29(d)), the free ion Fe⁺² dominates the Fe(II) speciation at pH range of 4 – 4.5 while the bicarbonate complex leads speciation at remaining pH. The first chloride complex is one of the dominant species at low pH but it decreases in abundance at higher pH. A similar trend is seen for the higher complexes of chloride albeit at lower concentrations. The first iron-bisulfide complex stays relatively constant at ~ 30 μmolal across pH while the concentration of the second complex increases with pH. A contrasting trend is seen between the sulfate and the silicate complexes in the μmolal range with sulfate complex decreasing in concentration with pH as the silicate concentration increases with pH. The concentration of the hexanoate and monohydrogen phosphate complexes mildly fluctuate in the nmolal range. The concentration of dihydrohen phosphate decreases with pH as governed by the corresponding pK_a values.

Fe(II) speciation at Lau (Fig. 30(d)) is largely similar to the speciation profile seen at Rainbow except for the higher influence of bisulfide complexes that may be explainable due to the much higher concentration of sulfide at Lau, and the lower concentration of the free Fe⁺² ion that may be explained by the lower concentration of total Fe(II) at Lau.

5.2.5 Speciation of iron (III)

Fe(III) speciation at Rainbow (Fig. 29(e)) is largely governed by bicarbonate, silicate and chloride complexes at lower pH and bicarbonate, carbonate and silicate at higher pH. Chloride, sulfate and hexanoate complexes decrease drastically over pH due to the extremely low concentration of total Fe(III). Fe(III) speciation at Lau is largely similar to that at Rainbow except that silicate complex has higher abundance due to an additional 3 mmolal concentration of silicate at Lau which pushes the concentration of the non-dominant forms by ~ 1 order of magnitude

Recently, Hoffman et al. reported the observation of Fe(III)-chelating siderophores at several sites along the Mid-Atlantic ridge including high temperature black smokers (Hoffman et al. 2023). As the concentration of siderophores observed was on the order of pmolal concentration, we calculated Fe(III) speciation in the presence of 1 pmolal petrobactin, one of the siderophores that was identified with high confidence at multiple sites. As siderophores are biotic in origin, these calculations were conducted at 100°C but the overall fluid composition was kept the same as only slight compositional changes are expected in this temperature difference. The resulting speciation calculations are depicted in Fig. 29(f) and Fig. 30(f) for Rainbow and Lau, respectively. While Fe-petrobactin complex is still a non-dominant form of Fe(III), it is worth noticing that petrobactin consumes Fe(III) to its maximum capacity owing to its exceptionally high stability constant (logK = 43).

In summary, the addition of 1 μ molal hexanoic acid to two metal-replete hydrothermal mixing fluids does not seem to significantly impact metal speciation which is understandable due to its low values of stability constants of metal-hexanoate complexes vis-à-vis other ligands. However, the purpose of this analysis was to provide an example of how the estimation of logK and ΔS_{ML} values can be applied to a geochemically relevant test case when no thermodynamic data except pK_a is available. This analysis may be expanded to add all possible O⁻ ligands that have been predicted to be synthesized in such hydrothermal systems such as octanoic acid, nonanoic acid and dodecanoic acid along with other classes of ligands and guide future discussions of metal speciation and bioavailability.

5.2.3 Other applications

As mentioned earlier in the Discussion, metal-ligand complexation is an area of deep interest in various scientific disciplines. Here, we would like to highlight some areas of scientific inquiry where our findings may directly be applied.

Our work has direct applications on investigations of metal flux and transport around terrestrial hydrothermal vents that is an active area of interest (Sander and Koschinsky 2011, Haalboom et al. 2020, Cohen et al. 2021). Till now, the general practice in many studies has been to clump all metal-ligand complexes into broad categories such as (metal-inorganic)_{seawater}, (metal-organic)_{seawater}, (metal-inorganic)_{hydrothermal} or (metal-organic)_{hydrothermal} (Bennett et al. 2008, Sarradin et al. 2009, Toner et al. 2009, Sander and Koschinsky 2011). We believe that our estimates for metal complexes of bicarbonate, silicate and carboxylic acids will allow future investigators to use specific compounds in their speciation calculations of hydrothermal fluids under 125°C and hence achieve more high-resolution results. These estimates may also be extended to extra-terrestrial hydrothermal systems Enceladus where organic molecules consisting of phenol and carboxyl groups has either been observed (Postberg et al. 2018, Cable et al. 2021, Khawaja et al. 2023), or Mars where carboxylic acids have been suggested to be present (Benner et al. 2000, Stockton et al. 2011, Millan et al. 2022a, Millan et al. 2022b, Ansari 2023, McIntosh et al. 2024).

A related area of research where our results can have a direct application is the field of deep-sea biology, especially life associated with hydrothermal systems. As pointed earlier, the biological response to metals can largely be classified as dissimilatory, assimilatory and toxic. Our stability constant estimates for Fe(II), Fe(III) and Mn(II) complexes can be used to obtain the available metabolic energy of corresponding redox reactions (McCollom & Shock 1997, Amend & Shock 2001) that can guide future geomicrobiology explorations. Our stability

constant estimates for Ni complexes can be used to guide the minimum total nickel abundance required for the microbial growth of several archaea and bacteria like methanogens, anaerobes and sulfate reducers that require Ni as an essential cofactor for enzymes like Ni-Fe hydrogenases, carbon monoxide dehydrogenase, methyl CoM reductase and urease (Bini 2010). Similarly, our estimates for Co and Zn complexes can be used to guide the minimum abundance requirement of these metals that are involved in essential biological activities (Schönheit et al. 1979, Sauer & Thauer 2000, Bini 2010), and also the maximum tolerance of these metals that are known to produce a toxic response (Holden & Adams 2003, Edgcomb et al. 2004). Similar calculations can be extended to surface ocean microbiology and elemental cycling of biologically essential and toxic metals like iron and copper even though metal speciation in these systems is mostly dictated by high stability constant ligands like siderophore and chalkophores or highly abundant macromolecular complexes like humic acids and fulvic acids (Shaked & Lis 2012, Gledhill & Buck 2012, Heller & Croot 2015, Whitby et al. 2015).

Our are also of direct relevance to the study of origin and evolution of life on Earth.

Metals have for time been closely associated with origin of life research (Banin & Navrot 1975,
Navarro-González & C. Ponnamperuma 1995, Nitschke & Russell 2009, Nitschke et al. 2013).

As summarized by Aulakh et al. (Aulakh et al. 2022), several recent discoveries have pointed to metal ion catalysis as the driver for origin of the earliest metabolic pathways such as glycolysis, pentose phosphate pathway and tricarboxylic acid cycle (Keller et al. 2014, Keller et al. 2016,
Muchowska et al. 2017). In addition to the necessity of metals for methanogensis and sulfate reduction discussed earlier, several key biological reactions such as CO₂ fixation, N₂ fixation and aerobic respiration require metal-binding proteins or metal atoms like Fe, Mo, V, Mn, Ca, and Cu as cofactors (Einsle et al. 2002, Brunori et al. 2005, Rehder 2015, Gong et al. 2016, Paul et

al. 2017, Sanchez-Andrea et al. 2020). These arguments in addition to the recent finding (Bromberg et al. 2022) of the availability of biologically functional metallopeptides before the assembly of fully functional proteins over 3.8 billion years ago suggests that these metallopeptides serve as a reasonable starting point for the evolution of metabolic enzymes. Many of these reactions have been shown to be catalyzed by the reduced form of a metal such as Fe⁺² that was the dominant form iron in the Archaean ocean but is no longer so due to major biogeological events like the Great Oxygenation Event (GOE) and the Neoproterozoic Oxidation Event (NOE). The presence of these reduced forms in modern mitochondrial respiratory chain along with metal reductases, metal transporters and metallochaperones indicates the necessity for intracellular metal ion homeostasis. We believe our estimates of bicarbonate, silicate and carboxylate complexes of transition metals like Fe, Cu, Zn and Ni will aid in the speciation and bioavailability assessment of these metals as Earth's oceanic composition changed over time. Additionally, the lactate, pyruvate, formate, ascorbate, bicarbonate and silicate complexes of redox metals like Fe and Cu will facilitate scalable investigations in the exploration of interactions between metals, metabolites and proteins in the intracellular environment.

Yet another area of application of our research is the field of environmental chemistry and biology. Over the last few decades, equilibrium speciation modeling has been used to study the environmental behavior, fate and bioavailability of metals (Di Bonito et al. 2024). Speciation modeling has facilitated prediction of metal transport in groundwaters and surface waters (Runkel et al. 1999, Davis et al. 2004, Miller et al. 2010), assessment of contamination remediation options (Runkel & Kimball 2002, Derakhshan Nejad et al. 2018), and prediction of toxic effects of metals as a function of environmental chemistry (Smith et al., 2015). In these modeling techniques, interactions of metal ions with inorganic ligands like bicarbonate,

monomeric organic ligands like carboxylic acids and polymeric organic ligands like humic acids and fulvic acids play a major role. We believe our estimates for bicarbonate and silicate complexes, and carboxylic acid Lewis bases like formate and acetate for 75 metal ions will be useful in modeling interactions with inorganic ligands and a relevant fraction of monomeric organic ligands. Additionally, a lot of research has been performed on building linear free energy estimates for metal-organic stability constants as a model to parameterize metal ion interaction with polymeric organic ligands (Carbonaro & Di Toro 2007, Carbonaro et al. 2011, Atalay et al. 2013). Much of the existing work in this regard is limited to a small subset of cations ranging from 6-25. Our estimates will allow the extension of such LFER estimates to 75 metal ions, thereby increasing the existing thermodynamic database by several fold.

6. Conclusions

From catalysis of fundamental biological reactions like TCA-cycle to exertion of toxic stress, metal-ligand interactions have proven to play a fundamental role in biology as we know it. At the same time, models of metal speciation and bioavailability have proven to be very successful in recent years (Davis et al. 2004, Smith et al. 2015, Di Bonito et al. 2024). Since metal speciation depends directly on metal-ligand thermodynamics, methods to estimate these properties, especially the stability constants, are increasingly in demand. Rigorous analytical measurement of these properties requires time and investment, leading to an inevitable inability to keep up with the rising diversity of metals and ligands. As a step toward addressing this problem, we have developed estimation strategies to estimate metal-ligand stability constants over the biologically relevant temperature range of 0 to 125°C for a large class of metals and ligands.

In addition to estimating stability constants that fill gaps in the available experimental data for well- and lesser-studied monovalent oxygen ligands, our methods allow estimating logK_{ML} values for ligands with no thermodynamic data except for the ligand pK_a. The total number of estimated metal-ligand stability constants at 25°C and 1 bar amounts to 16,629 covering 69 metal ions and 241 ligands. This increases the currently available experimentally measured logK_{ML} values (417) by almost a factor of 40. We predict that most of these stability constants are accurate within ± 0.5 log units and thus are unlikely to affect speciation calculations adversely. Since metal-ligand complexation entropy measurements are scarcer, the total number of estimated ΔS°_{ML} values at 25°C and 1 bar are much fewer: 4992 complexes of 156 carboxylic acids with 32 metal ions and 1848 metal complexes for 66 phenols with 28 metal ions. We predict that the estimates for carboxylic acids are accurate within ± 2 cal mol⁻¹K⁻¹, which keeps predictions of log K_{ML} over the range of 0 to 125°C within ± 0.5 log units. These estimates for phenols and inorganic ligands are accurate within ± 5 cal mol⁻¹K⁻¹, which keeps log K_{ML} predictions over 0-125°C within ±1 log units. We suspect that the lower accuracy for phenols and inorganic ligands can be attributed to the lack of experimental data advocate subsequent researchers to conduct additional analyses of thermodynamic properties of these metal complexes. However, as these values are low in magnitude, they are not likely to affect van't Hoff extrapolations of the corresponding stability constants substantially.

Such estimation exercises are challenged by two potentially contradictory goals: high accuracy and extensive applicability. In this study we assembled an extensive database of experimentally obtained thermodynamic values, which permitted a search for the closest proxy ligands for building correlations. As a consequence, we believe we have achieved these goals simultaneously. Multiple correlations among structurally related ligands suggest that these

patterns reflect properties of the ligand molecular structures and provide a foundation for further extension of methods to predict metal-ligand thermodynamics.

Declaration of competing interest

The authors declare that they have no known competing financial interests or personal relationships that could have appeared to influence the work reported in this paper.

Acknowledgements

This work was supported by Deep Carbon Observatory. The authors would like to thank Arizona State University (ASU) and all the past and current members of Group Exploring Organic Processes In Geochemistry (GEOPIG) at ASU for helpful discussions.

Appendix A. Supplementary material

The supplementary material for this paper includes two files. 'Supplementary Table' includes all experimental and estimated stability constants (log K_{ML}) and standard entropy changes (ΔS°_{ML}) at 25°C and 1 bar for all metal-ligand complexation reactions mentioned in the paper. 'Supplementary Information' includes details on how thermodynamic data was estimated for higher order complexes of hexanoate.

References

Adamson, A. W. (1954). A Proposed Approach to the Chelate Effect. *Journal of the American Chemical Society*, 76(6), 1578–1579.

Amend, J. P., Rogers, K. L., Shock, E. L., Gurrieri, S., & Inguaggiato, S. (2003). Energetics of chemolithoautotrophy in the hydrothermal system of Vulcano Island, southern Italy. *Geobiology*, *I*(1), 37–58.

- Amend JP, Shock EL. (2001) Energetics of overall metabolic reactions of thermophilic and hyperthermophilic Archaea and bacteria. *FEMS Microbiol Rev.* 25(2):175-243. doi: 10.1111/j.1574-6976.2001.tb00576.x. PMID: 11250035.
- Ansari AH (2023) Detection of organic matter on Mars, results from various Mars missions, challenges, and future strategy: A review. *Front. Astron. Space Sci.* 10:1075052. doi: 10.3389/fspas.2023.1075052
- Atalay, Y. B., Di Toro, D. M., & Carbonaro, R. F. (2013). Estimation of stability constants for metalligand complexes containing neutral nitrogen donor atoms with applications to natural organic matter. *Geochimica et Cosmochimica Acta*, 122, 464–477.
- Aulakh, S. K., Varma, S. J., & Ralser, M. (2022). Metal ion availability and homeostasis as drivers of metabolic evolution and enzyme function. *Current opinion in genetics & development*, 77, 101987. https://doi.org/10.1016/j.gde.2022.101987
- Banin A, Navrot J. (1975) Origin of life: clues from relations between chemical compositions of living organisms and natural environments. Science. 189(4202):550-1. doi: 10.1126/science.1170640. PMID: 1170640.
- Başaran, B., Avşar, E., Göçmen, A., & Erim, F. B. (1994). The thermodynamics of benzoate complexes of copper(II) and iron(III) in aqueous solution. *Thermochimica Acta*, 247(2), 407–413.
- Benner SA, Devine KG, Matveeva LN, Powell DH. (2000) The missing organic molecules on Mars. Proc Natl Acad Sci USA, 14;97(6):2425-30. doi: 10.1073/pnas.040539497. PMID: 10706606; PMCID: PMC15945.
- Bennett, Sarah & Achterberg, E. & Connelly, Douglas & Statham, P.J. & Fones, Gary & German, Christopher. (2008). The distribution and stabilisation of dissolved Fe in deep-sea hydrothermal plumes. *Earth and Planetary Science Letters*. 270. 157-167. 10.1016/j.epsl.2008.01.048.
- Berthon, G. (1995). The stability constants of metal complexes of amino acids with polar side chains. *Pure and Applied Chemistry*, 67(7), 1117–1240.
- Bini E. (2010) Archaeal transformation of metals in the environment. FEMS Microbiol Ecol. 73(1):1-16. doi: 10.1111/j.1574-6941.2010.00876.x. Epub 2010 Mar 30. PMID: 20455933.
- Bromberg, Y., Aptekmann, A. A., Mahlich, Y., Cook, L., Senn, S., Miller, M., Nanda, V., Ferreiro, D. U., & Falkowski, P. G. (2022). Quantifying structural relationships of metal-binding sites suggests origins of biological electron transfer. *Science advances*, 8(2), eabj3984. https://doi.org/10.1126/sciadv.abj3984
- Brunori, M., Giuffrè, A., & Sarti, P. (2005). Cytochrome c oxidase, ligands and electrons. *Journal of inorganic biochemistry*, 99(1), 324–336. https://doi.org/10.1016/j.jinorgbio.2004.10.011
- Cable, Morgan & Porco, Carolyn & Glein, Christopher & German, Christopher & MacKenzie, Shannon & Neveu, Marc & Hoehler, Tori & Hofmann, Amy & Hendrix, A. & Eigenbrode, Jennifer & Postberg, Frank & Spilker, Linda & Mcewen, Alfred & Khawaja, Nozair & Waite, J. & Wurz, Peter

- & Helbert, J. & Anbar, Ariel & de Vera, Jean-Pierre & Núnez, Jorge. (2021). The Science Case for a Return to Enceladus. *The Planetary Science Journal*. 2. 132. 10.3847/PSJ/abfb7a.
- Carbonaro, R. F., & Di Toro, D. M. (2007). Linear free energy relationships for metal-ligand complexation: Monodentate binding to negatively-charged oxygen donor atoms. *Geochimica et Cosmochimica Acta*, 71(16), 3958–3968.
- Carbonaro, R. F., Atalay, Y. B., & Di Toro, D. M. (2011). Linear free energy relationships for metalligand complexation: Bidentate binding to negatively-charged oxygen donor atoms. *Geochimica et Cosmochimica Acta*, 75(9), 2499–2511.
- Cobble, J. W. (1953a). Empirical considerations of entropy. I. The entropies of the oxy-anions and related species. *The Journal of Chemical Physics*, 21(9), 1443–1445.
- Cobble, J. W. (1953b). Empirical considerations of entropy. II. The entropies of inorganic complex ions. *The Journal of Chemical Physics*, 21(9), 1446–1450.
- Cohen, N. R., Noble, A. E., Moran, D. M., McIlvin, M. R., Goepfert, T. J., Hawco, N. J., German, C. R., Horner, T. J., Lamborg, C. H., McCrow, J. P., Allen, A. E., and Saito, M. A.: Hydrothermal trace metal release and microbial metabolism in the northeastern Lau Basin of the South Pacific Ocean, *Biogeosciences*, 18, 5397–5422, https://doi.org/10.5194/bg-18-5397-2021, 2021
- Davies, C. W. (1951). 280. The electrolytic dissociation of metal hydroxides. *Journal of the Chemical Society (Resumed)*, 1256–1258.
- Davis, J.A., Meece, D.E., Kohler, M., & Curtis, G.P. (2004). Approaches to surface complexation modeling of Uranium(VI) adsorption on aquifer sediments. *Geochimica et Cosmochimica Acta*, 68, 3621-3641.
- Derakhshan Nejad, Z., Jung, M. C., & Kim, K. H. (2018). Remediation of soils contaminated with heavy metals with an emphasis on immobilization technology. *Environmental Geochemistry and Health*, 40(3), 927-953. https://doi.org/10.1007/s10653-017-9964-z
- Di Bonito, M., Lofts, S., & Groenenberg, J. E. (2024). Models of geochemical speciation: Structure and applications. In B. de Vivo, H. E. Belkin, & A. Lima (Eds.), *Environmental Geochemistry: Site Characterization, Data Analysis, Case Histories, and Associated Health Issues* (3 ed., pp. 329-419). Elsevier. https://doi.org/10.1016/B978-0-443-13801-0.00017-7
- Dieleman, J. L., Baral, R., Birger, M., Bui, A. L., Bulchis, A., Chapin, A., ... Murray, C. J. L. (2016). US spending on personal health care and public health, 1996-2013. *JAMA Journal of the American Medical Association*, 316(24), 2627–2646.
- Edgcomb VP, Molyneaux SJ, Saito MA, Lloyd K, Böer S, Wirsen CO, Atkins MS, Teske A. (2004) Sulfide ameliorates metal toxicity for deep-sea hydrothermal vent archaea. Appl Environ Microbiol. 70(4):2551-5. doi: 10.1128/AEM.70.4.2551-2555.2004. PMID: 15066859; PMCID: PMC383022.

- Einsle, O., Tezcan, F. A., Andrade, S. L., Schmid, B., Yoshida, M., Howard, J. B., & Rees, D. C. (2002). Nitrogenase MoFe-protein at 1.16 A resolution: a central ligand in the FeMo-cofactor. *Science (New York, N.Y.)*, 297(5587), 1696–1700. https://doi.org/10.1126/science.1073877
- Gledhill M and Buck KN (2012) The organic complexation of iron in the marine environment: a review. *Front. Microbio.* **3**:69. doi: 10.3389/fmicb.2012.00069
- Gong, F., Cai, Z. & Li, Y. Synthetic biology for CO₂ fixation. *Sci. China Life Sci.* **59**, 1106–1114 (2016). https://doi.org/10.1007/s11427-016-0304-2
- Gordon, R. B., Bertram, M., & Graedel, T. E. (2006). Metal stocks and sustainability. *Proceedings of the National Academy of Sciences of the United States of America*, 103(5), 1209–1214.
- Hancock, R. D. (1997). Approaches to predicting stability constants. A critical review. *Analyst*, 122, (51R-58R)
- Hancock, R. D., & Marsicano, F. (1976). The chelate effect: A simple quantitative approach. *Journal of the Chemical Society, Dalton Transactions*, (12), 1096–1098.
- Haalboom, S., Price, D. M., Mienis, F., van Bleijswijk, J. D. L., de Stigter, H. C., Witte, H. J., Reichart, G.-J., and Duineveld, G. C. A.: Patterns of (trace) metals and microorganisms in the Rainbow hydrothermal vent plume at the Mid-Atlantic Ridge, *Biogeosciences*, 17, 2499–2519, https://doi.org/10.5194/bg-17-2499-2020, 2020.
- Hancock, R. D., & Marsicano, F. (1978). Parametric Correlation of Formation Constants in Aqueous Solution. 1. Ligands with Small Donor Atoms. *Inorganic Chemistry*, 17(3), 560–564.
- Helgeson, H. C. (1969). Thermodynamics of hydrothermal systems at elevated temperatures and pressures. *American Journal of Science*, 267(7), 729–804.
- Heller, M. I., & Croot, P. L. (2015). Copper speciation and distribution in the Atlantic sector of the Southern Ocean. *Marine Chemistry*, *173*, 253-268. https://doi.org/10.1016/j.marchem.2014.09.017
- Hinchey, R. J., & Cobble, J. W. (1970). Standard-State Entropies for the Aqueous Trivalent Lanthanide and Yttrium Ions1,2. *Inorganic Chemistry*, *9*(4), 917–921.
- Holden JF, Adams MW. (2003) Microbe-metal interactions in marine hydrothermal environments. Curr Opin Chem Biol. 7(2):160-5. doi: 10.1016/s1367-5931(03)00026-7. PMID: 12714047.
- Irving H & Rossotti, H. (1956). Some relationships among the stabilities of metal complexes. *Recueil Des Travaux Chimiques Des Pays-Bas*, 10, 72–93.
- Jackson, G. E., & Byrne, M. J. (1996). Metal ion speciation in blood plasma: Gallium-67-citrate and MRI contrast agents. *Journal of Nuclear Medicine*, *37*(2), 379–386.
- Keller, M. A., Turchyn, A. V., & Ralser, M. (2014). Non-enzymatic glycolysis and pentose phosphate pathway-like reactions in a plausible Archean ocean. *Molecular systems biology*, 10(4), 725. https://doi.org/10.1002/msb.20145228

- Keller, M. A., Zylstra, A., Castro, C., Turchyn, A. V., Griffin, J. L., & Ralser, M. (2016). Conditional iron and pH-dependent activity of a non-enzymatic glycolysis and pentose phosphate pathway. *Science advances*, 2(1), e1501235. https://doi.org/10.1126/sciadv.1501235
- Khawaja, N., O'Sullivan, T. R., Klenner, F., Sanchez, L. H., & Hillier, J. (2023). Discriminating aromatic parent compounds and their derivative isomers in ice grains from Enceladus and Europa using a laboratory analogue for spaceborne mass spectrometers. *Earth and Space Science*, 10, e2022EA002807. https://doi.org/10.1029/2022EA002807
- Kim, Y. J., Eom, H. J., Seo, E. Y., Lee, D. Y., Kim, J. H., & Han, N. S. (2012). Development of a chemically defined minimal medium for the exponential growth of Leuconostoc mesenteroides ATCC8293. *Journal of Microbiology and Biotechnology*, 22(11), 1518–1522.
- Kiss, T., Enyedy, É. A., & Jakusch, T. (2017, December 1). Development of the application of speciation in chemistry. *Coordination Chemistry Reviews*. Elsevier B.V.
- Kiss, T., Tamás & Gergeley, A.. (1991). Critical survey of stability constants of complexes of glycine. Pure and Applied Chemistry *Pure and Applied Chemistry*, 63. 597-638.
- Lentner, C., & CIBA-GEIGY Limited. (1981). Geigy scientific tables. Basle, Switzerland: Ciba-Geigy.
- Levina, A., Crans, D. C., & Lay, P. A. (2017, December 1). Speciation of metal drugs, supplements and toxins in media and bodily fluids controls in vitro activities. *Coordination Chemistry Reviews*. Elsevier B.V, *352*, 473-498.
- Martell, A. E., & Smith, R. M. (1974). Critical stability constants: Volume 1. New York: Plenum Press.
- Martell, A. E., & Smith, R. M. (1977). Critical stability constants: Other organic ligands.
- Martell, A. E., Hancock, R. D., Martell, A. E., & Hancock, R. D. (1996). Chelating Ligands. In *Metal Complexes in Aqueous Solutions*. Springer US.
- McIntosh, O. & Freissinet, Caroline & Buch, A. & Lewis, J.M.T. & Millan, Maëva & Williams, Amy & Fornaro, Teresa & Eigenbrode, J.L. & Brucato, John & Szopa, Cyril. (2024). Analysis of aromatic carboxylic acid and calcium salt couples with gas chromatography-mass spectrometry: Implications and comparison with in situ measurements at Mars' surface. *Icarus*. 413. 116015. 10.1016/j.icarus.2024.116015.
- McCollom TM, Shock EL. (1997) Geochemical constraints on chemolithoautotrophic metabolism by microorganisms in seafloor hydrothermal systems. Geochim Cosmochim Acta. Oct;61(20):4375-91. doi: 10.1016/s0016-7037(97)00241-x. PMID: 11541662.
- Millan, M., Teinturier, S., Malespin, C.A. *et al.* (2022a) Organic molecules revealed in Mars's Bagnold Dunes by Curiosity's derivatization experiment. *Nat Astron* **6**, 129–140. https://doi.org/10.1038/s41550-021-01507-9
- Millan, M., Williams, A. J., McAdam, A. C., Eigenbrode, J. L., Steele, A., Freissinet, C., et al. (2022b). Sedimentary organics in Glen Torridon, Gale Crater, Mars: Results from the SAM

- instrument suite and supporting laboratory analyses. *Journal of Geophysical Research: Planets*, 127, e2021JE007107. https://doi.org/10.1029/2021JE007107
- Miller, A. W., Rodriguez, D. R., & Honeyman, B. D. (2010). Upscaling sorption/desorption processes in reactive transport models to describe metal/radionuclide transport: a critical review. *Environmental science & technology*, 44(21), 7996–8007. https://doi.org/10.1021/es101822v
- Muchowska, K. B., Varma, S. J., Chevallot-Beroux, E., Lethuillier-Karl, L., Li, G., & Moran, J. (2017). Metals promote sequences of the reverse Krebs cycle. *Nature ecology & evolution*, *1*(11), 1716–1721. https://doi.org/10.1038/s41559-017-0311-7
- Nancollas, G. H. (1956). Thermodynamics of ion association. Part II.Alkaline earth acetates and formates. *Journal of the Chemical Society (Resumed)*, 735–743.
- Navarro-González, R., & Ponnamperuma, C. (1995). Role of trace metal ions in chemical evolution. The case of free-radical reactions. *Advances in space research*, *15*(3), 357–364. https://doi.org/10.1016/s0273-1177(99)80107-0
- Nitschke, W., McGlynn, S. E., Milner-White, E. J., & Russell, M. J. (2013). On the antiquity of metalloenzymes and their substrates in bioenergetics. *Biochimica et biophysica acta*, *1827*(8-9), 871–881. https://doi.org/10.1016/j.bbabio.2013.02.008
- Nitschke, W., Russell, M.J. Hydrothermal Focusing of Chemical and Chemiosmotic Energy, Supported by Delivery of Catalytic Fe, Ni, Mo/W, Co, S and Se, Forced Life to Emerge. *J Mol Evol* **69**, 481–496 (2009). https://doi.org/10.1007/s00239-009-9289-3
- Paul, S., Neese, F., & Pantazis, D.A. (2017). Structural models of the biological oxygen-evolving complex: achievements, insights, and challenges for biomimicry. *Green Chemistry*, 19, 2309-2325.
- Pettit, L. D. (1984). International union of pure and applied chemistry: Analytical chemistry division commission on equilibrium data critical evaluation of equilibrium constants in solution part a: Stability constants of metal complexes critical survey of formation constants of complexes of histidine, phenylalanine, tyrosine, 1-dopa and tryptophan. *Pure and Applied Chemistry*, 56(2), 247–292.
- Postberg, F., Khawaja, N., Abel, B. *et al.* (2018) Macromolecular organic compounds from the depths of Enceladus. *Nature* **558**, 564–568. https://doi.org/10.1038/s41586-018-0246-4
- Prapaipong, P., Shock, E. L., & Koretsky, C. M. (1999). Metal-organic complexes in geochemical processes: Temperature dependence of the standard thermodynamic properties of aqueous complexes between metal cations and dicarboxylate ligands. *Geochimica et Cosmochimica Acta*, 63(17), 2547–2577.
- Prapaipong, P., & Shock, E. L. (2001). Estimation of standard-state entropies of association for aqueous metal-organic complexes and chelates at 25°C and 1 bar. *Geochimica et Cosmochimica Acta*, 65(21), 3931–3953.

- Rehder D. (2015). The role of vanadium in biology. *Metallomics*, 7(5), 730–742. https://doi.org/10.1039/c4mt00304g
- Runkel, R.L., & Kimball, B.A. (2002). Evaluating remedial alternatives for an acid mine drainage stream: application of a reactive transport model. *Environmental science & technology*, *36 5*, 1093-101.
- Runkel, Robert & Kimball, Briant & Mcknight, Diane & Bencala, Ken. (1999). Reactive Solute Transport in Streams: A Surface Complexation Approach for Trace Metal Sorption. Water Resources Research WATER RESOUR RES. 35. 3829-3840. 10.1029/1999WR900259.
- Sánchez-Andrea, I., Guedes, I.A., Hornung, B. *et al.* The reductive glycine pathway allows autotrophic growth of *Desulfovibrio desulfuricans*. *Nat Commun* **11**, 5090 (2020). https://doi.org/10.1038/s41467-020-18906-7
- Sander, S., Koschinsky, A. (2011) Metal flux from hydrothermal vents increased by organic complexation. *Nature Geosci* **4**, 145–150. https://doi.org/10.1038/ngeo1088
- Sarradin PM, Waeles M, Bernagout S, Le Gall C, Sarrazin J, Riso R. (2009) Speciation of dissolved copper within an active hydrothermal edifice on the Lucky Strike vent field (MAR, 37 degrees N). *Sci Total Environ*. 407(2):869-78. doi: 10.1016/j.scitotenv.2008.09.056.
- Sauer, K. and Thauer, R.K. (2000), Methyl-coenzyme M formation in methanogenic archaea. European Journal of Biochemistry, 267: 2498-2504. https://doi.org/10.1046/j.1432-1327.2000.01245.x
- Schönheit P, Moll J, Thauer RK. (1979) Nickel, cobalt, and molybdenum requirement for growth of Methanobacterium thermoautotrophicum. Arch Microbiol. 123(1):105-7. doi: 10.1007/BF00403508. PMID: 120728.
- Shaked Y and Lis H (2012) Disassembling iron availability to phytoplankton. *Front. Microbio.* **3**:123. doi: 10.3389/fmicb.2012.00123
- Sheldon, R. A., & Woodley, J. M. (2018, January 24). Role of Biocatalysis in Sustainable Chemistry. *Chemical Reviews*. American Chemical Society, *118*, 801-838.
- Shock, E.L., & Canovas, P. (2010). The Potential for Abiotic Organic Synthesis and Biosynthesis at Seafloor Hydrothermal Systems. In *Frontiers in Geofluids* (pp. 161–192). Wiley-Blackwell.
- Shock, E. L., & Koretsky, C. M. (1993). Metal-organic complexes in geochemical processes: Calculation of standard partial molal thermodynamic properties of aqueous acetate complexes at high pressures and temperatures. *Geochimica et Cosmochimica Acta*, 57(20), 4899–4922.
- Shock, E. L., & Koretsky, C. M. (1995). Metal-organic complexes in geochemical processes: Estimation of standard partial molal thermodynamic properties of aqueous complexes between metal cations and monovalent organic acid ligands at high pressures and temperatures. *Geochimica et Cosmochimica Acta*, 59(8), 1497–1532.
- Smith, K.S., Balistrieri, L.S., & Todd, A.S. (2015). Using biotic ligand models to predict metal toxicity in mineralized systems. *Applied Geochemistry*, *57*, 55-72.

- Smith, R. M., & Martell, A. E. (1975). *Critical Stability Constants: Volume 2: Amines*. Boston, MA: Springer US.
- Smith, R. M., & Martell, A. E. (1976). Critical stability constants: Volume 4. New York: Plenum Press.
- Smith, R. M., & Martell, A. E. (1982). *Critical stability constants. Volume 5. First supplement.* New York, N.Y: Plenum.
- Smith, R. M., & Martell, A. E. (1989). Critical stability constants: Volume 6. New York: Plenum Press.
- Stockton, Amanda & Tjin, Caroline & Chiesl, Thomas & Mathies, Richard. (2011). Analysis of Carbonaceous Biomarkers with the Mars Organic Analyzer Microchip Capillary Electrophoresis System: Carboxylic Acids. Astrobiology. 11. 519-28. 10.1089/ast.2011.0634.
- Sunda, W., & Guillard R. R. L. (1976). The relationship between cupric ion activity and the toxicity of copper to phytoplankton. *Journal of Marine Research*, *34*, 511-529.
- Sverjensky, D. A., Shock, E. L., & Helgeson, H. C. (1997). Prediction of the thermodynamic properties of aqueous metal complexes to 1000°C and 5 kb. *Geochimica et Cosmochimica Acta*, 61(7), 1359–1412.
- Tansel, B. (2017). From electronic consumer products to e-wastes: Global outlook, waste quantities, recycling challenges. *Environment International*. Elsevier Ltd. 98, 35-45.
- Tipping, E. (2002). *Cation Binding by Humic Substances* (Cambridge Environmental Chemistry Series). Cambridge: Cambridge University Press.
- Toner, B., Fakra, S., Manganini, S. *et al.* (2009) Preservation of iron(II) by carbon-rich matrices in a hydrothermal plume. *Nature Geosci* **2**, 197–201. https://doi.org/10.1038/ngeo433
- Van Uitert, L. G., Fernelius, W. C., & Douglas, B. E. (1953). Studies on Coordination Compounds. V. A Comparison of the Chelating Tendencies of β-Diketones toward Divalent Metals. *Journal of the American Chemical Society*, 75(11), 2739–2741.
- Whitby H, Hollibaugh JT and van den Berg CMG (2017) Chemical Speciation of Copper in a Salt Marsh Estuary and Bioavailability to Thaumarchaeota. *Front. Mar. Sci.* 4:178. doi: 10.3389/fmars.2017.00178
- Willey, L. M., Kharaka, Y. K., Presser, T. S., Rapp, J. B., & Barnes, I. (1975). Short chain aliphatic acid anions in oil field waters and their contribution to the measured alkalinity. *Geochimica et Cosmochimica Acta*, 39(12), 1707–1711.
- Wolery, T. J. (2010, December 13). EQ3/6 A Software Package for Geochemical Modeling (Version 05) [Computer software].